Durham E-Theses

Plasma metallization

Crowther, Jonathan Mark

How to cite:

Crowther, Jonathan Mark (1997) *Plasma metallization*, Durham theses, Durham University. Available at Durham E-Theses Online: http://etheses.dur.ac.uk/5032/

Use policy

The full-text may be used and/or reproduced, and given to third parties in any format or medium, without prior permission or charge, for personal research or study, educational, or not-for-profit purposes provided that:

- a full bibliographic reference is made to the original source
- a link is made to the metadata record in Durham E-Theses
- the full-text is not changed in any way

The full-text must not be sold in any format or medium without the formal permission of the copyright holders.

Please consult the full Durham E-Theses policy for further details.

Academic Support Office, Durham University, University Office, Old Elvet, Durham DH1 3HP
e-mail: e-theses.admin@dur.ac.uk Tel: +44 0191 334 6107
http://etheses.dur.ac.uk

PLASMA METALLIZATION

Jonathan Mark Crowther

Ph.D. Thesis

Department of Chemistry

University of Durham

September 1997

The copyright of this thesis rests with the author. No quotation from it should be published without the written consent of the author and information derived from it should be acknowledged.

1 2 MAR 1999

For Mum and Dad

DECLARATION

STATEMENT OF COPYRIGHT

The copyright of this thesis rests with the author. No quotation from it should be published without his written consent and information derived from it should be acknowledged.

The work described within this thesis was performed in the Department of Chemistry at the University of Durham between October 1994 and September 1997. It is the original work of the author except where otherwise acknowledged or where specific reference is made to other sources.

Work in this thesis has formed all or part of the following publications:

"Non-Isothermal Plasma Metallization of Polymer Supported Gold(III) Complexes", J. M. Crowther, J. P. S. Badyal, submitted for publication.

"Cold Plasma Metallization of Supported Silver & Palladium Salt Layers", J. M. Crowther, J. P. S. Badyal, submitted for publication.

ACKNOWLEDGEMENTS

I would like to acknowledge my supervisor Professor Jas Pal Badyal, for his guidance over the last three years. Also everyone in Lab 98 (and I suppose now Lab 96) with whom it has been my pleasure to work with during my time here. Special thanks must go to Colin 'Waffa' Campbell for his lengthy chats about the nature of the interactions of plasmas with metal surfaces, and the intricacies of the rules of American football.

A big thank you to my mother and father for their frequent trips to Durham, and for providing me with many excellent Sunday lunches at The Avenue.

My condolences go out to Paula who has had to put up with sharing a house with me during this last year. Never mind P., at least you've managed to escape now.

Of course I could not possibly go without acknowledging Jim and Neil in the mechanical workshop, George, Kelvin and Barry in the electrical workshop, and also Gordon and Ray - the glassblowers, who have all put up with my constant demand for attention and indecipherable designs.

And to all the unknown minions, who have not been named here but have helped me over the course of my Ph.D., I give you my heartiest thanks.

ABSTRACT

Many methods are currently used for the production of thin metal films. However, all of these have drawbacks associated with them, for example the need for UHV conditions, high temperatures, exotic metal precursors, or the inability to coat complex shaped objects. Reduction of supported metal salts by non-isothermal plasma treatment does not suffer from these drawbacks.

In order to produce and analyse metal films before they become contaminated, a plasma chamber which could be attached directly to a UHV chamber with XPS capability was designed and built. This allowed plasma treatment of supported metal salts and surface analysis by XPS to be performed without exposure of the metal film to the atmosphere.

Non-equilibrium plasma treatment of Nylon 66 supported gold(III) chloride using hydrogen as the feed gas resulted in a 95% pure gold film, the remaining 5% of the film being carbon. If argon or helium were used as the feed gases during plasma treatment the resultant gold films were 100% pure. Some degree of surface contamination of the films due to plasma treatment was observed but was easily removed by argon ion cleaning.

Hydrogen plasma reduction of glass supported silver(I) nitrate and palladium(II) acetate films reveals that this metallization technique is applicable to a wide variety of metal salts and supports, and has also shown the ability of plasma reduction to retain the complex 'fern-like' structures seen for spin coated silver(I) nitrate layers.

Some metal salts are susceptible to decomposition by X-rays. The reduction of Nylon 66 supported gold(III) chloride films by soft X-rays to produce nanoscopic gold particles has been studied. The spontaneous reduction of these X-ray irradiated supported gold(III) chloride films on exposure to the atmosphere to produce gold rich metallic films has also been reported.

SOME CHOICE QUOTES

So distinct are these phenomena from anything which occurs in air or gas at the ordinary tension, that we are led to assume that we are here brought face to face with Matter in a Fourth state or condition, a condition so far removed from the State of gas as a gas is from a liquid.

In studying this Fourth state of Matter we seem at length to have within our grasp and obedient to our control the little indivisible particles which with good warrant are suppose to constitute the physical basis of the universe. . . We have actually touched the border land where Matter and Force seem to merge into one another, the shadowy realm between Known and Unknown, which for me has always had peculiar temptations. I venture to think that the greatest scientific problems of the future will find their solution in this Border Land, and even beyond; here it seems to me, lie Ultimate Realities, subtle, far-reaching, wonderful.

Sir William Crookes, in a lecture on 'Radiant Matter' for the British Association for the Advancement of Science, Sheffield, August 22nd, 1879.

Good science does not always involve being right - at least not in every detail. It is far more important to paint the broad outlines of a subject, to discover entirely new phenomena, and to point the way to new and fruitful investigations.

From *Frozen Star*, by George Greenstein, Macdonald and Co. (Publishers) Ltd., Great Britain, 1984.

... a scientist must be absolutely like a child. If he sees a thing, he must say that he sees it, whether it was what he thought he was going to see or not. See first, think later, then test. But always see first. Otherwise you will only see what you were expecting. Most scientists forget that.

John Watson speaking to Arthur Dent from *So Long, And Thanks For All The Fish*, by Douglas Adams, William Heinemann Ltd., Great Britain, 1992.

I hate mondays.

Garfield, Jim Davis, Ravette Books Ltd..

CONTENTS

CHAPTER 1 : THIN METAL FILMS, PLASMAS, AND EXPERIMENTAL TECHNIQUES

1.1 THIN METAL FILMS 2

1.1.1 Methods of producing thin metal films 2

1.1.1.1 Sputter deposition 3

1.1.1.2 Evaporation 3

1.1.1.3 Chemical vapour deposition 3

1.1.1.4 Variants of CVD 4

1.1.1.5 Electrodeposition 4

1.1.1.6 Electroless deposition 5

1.1.2 Properties of thin films 5

1.2 PLASMAS 5

1.2.1 The Glow Discharge 6

1.2.2 Radio Frequency Discharges 8

1.2.3 Electron Energy Distribution Function 8

1.2.4 Plasma Potential 10

1.2.5 Floating Potential 10

1.2.6 Plasma Sheath 11

1.2.7 Plasma Chemistry 11

1.2.8 Hydrogen Plasmas 14

1.3 EXPERIMENTAL TECHNIQUES 16

1.3.1 X-ray Photoelectron Spectroscopy (XPS) 16

1.3.1.1 Instrumentation 18

1.3.1.2 Spectral Interpretation 19

1.3.2 Attenuated Total Reflectance Fourier Transform Infra-Red Spectroscopy (ATR-FTIR) 20

1.3.3 X-ray Diffraction (XRD) 22

1.3.4 Raman Spectroscopy 23

1.3.5 Electrical Resistivity 24

1.4 REFERENCES 25

CHAPTER 2 : NON-ISOTHERMAL HYDROGEN PLASMA METALLIZATION OF POLYMER SUPPORTED GOLD(III) COMPLEXES

2.1 INTRODUCTION 32
2.2 EXPERIMENTAL 34
2.3 RESULTS 37
2.4 DISCUSSION 44
2.5 CONCLUSIONS 46
2.6 REFERENCES 47

CHAPTER 3 : NON-ISOTHERMAL NOBLE GAS PLASMA METALLIZATION OF POLYMER SUPPORTED GOLD(III) COMPLEXES

3.1 INTRODUCTION 51
3.2 EXPERIMENTAL 52
3.3 RESULTS 53
3.4 DISCUSSION 60
3.5 CONCLUSIONS 62
3.6 REFERENCES 62

CHAPTER 4 : X-RAY ASSISTED METALLIZATION OF SUPPORTED GOLD COMPLEXES

4.1 INTRODUCTION 66
4.2 EXPERIMENTAL 67
4.3 RESULTS 68
4.4 DISCUSSION 78
4.5 CONCLUSIONS 83
4.6 REFERENCES 83

CHAPTER 5 : COLD HYDROGEN PLASMA METALLIZATION OF SUPPORTED SILVER & PALLADIUM SALT LAYERS

5.1 INTRODUCTION 88
5.2 EXPERIMENTAL 89
5.3 RESULTS 90
5.4 DISCUSSION 103
5.5 CONCLUSIONS 103
5.6 REFERENCES 103

CHAPTER 6 : COLD HYDROGEN PLASMA METALLIZATION OF SUPPORTED METAL BI-SALT LAYERS

6.1 INTRODUCTION 108
6.2 EXPERIMENTAL 109
6.3 RESULTS 109
6.4 DISCUSSION 114
6.5 CONCLUSIONS 119
6.6 REFERENCES 119

CHAPTER 7 : CONCLUSIONS
7.1 CONCLUSIONS 122
7.2 FUTURE WORK 123
7.2.1 Optimisation of Noble Gas Plasma Treatment Conditions 123
7.2.2 X-ray Degradation of Other Metal Salts 124
7.2.3 Deposition of Plasma Polymer Layers to Enable Metallization of PTFE 124

APPENDIX 125

CHAPTER 1

THIN METAL FILMS, PLASMAS, AND EXPERIMENTAL TECHNIQUES

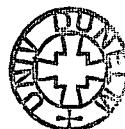

CHAPTER 1

THIN METAL FILMS, PLASMAS, AND EXPERIMENTAL TECHNIQUES

The use of plasma processing of materials has increased in the last 30 years. Until now no attempt has been made to produce thin metal films through the action of a non-isothermal plasma on a metal salt layer deposited on a substrate. This chapter introduces some of the uses, methods for the deposition, and properties of thin metal films. A brief overview of plasmas and the analytical techniques used during the preparation of this thesis is also presented.

1.1 THIN METAL FILMS

Metal films have an immensely diverse range of uses in the world today, including; jewellery, electrical contacts and printed circuit boards, diffusion barriers, optical mirrors, architectural glazing, corrosion resistant coatings, solar cells, gas sensors, and catalytic surfaces and membranes.[1] The use of only small amounts of metal in the deposition of a thin film allows the lowering of production costs due to a reduction in the use of expensive raw materials.

1.1.1 Methods of Producing Thin Metal Films

The methods utilised for the production of thin metal films are, like their uses, diverse, each with its own advantages and disadvantages. It would be impossible to give a complete review of all the techniques used for their deposition here as such an undertaking would require several volumes alone. However, some of the more widely utilised deposition techniques are briefly outlined below.

1.1.1.1 Sputter Deposition

Sputter deposition involves the removal of particles from a target during bombardment by energetic projectile species.[2] These ejected particles are then deposited on a substrate forming a film. This process is capable of forming films of metals, alloys, compounds, and polymers by varying the method of sputtering, for example DC or RF discharges or ion beam sources, and by altering the gas present in the vacuum chamber. Sputter deposition requires the use of high or ultra high vacuum conditions (10^{-6} to 10^{-10} torr) depending upon the material being sputtered and is essentially a line of sight deposition technique, which is incapable of coating complex shaped objects without object rotation.

1.1.1.2 Evaporation

Evaporation involves the heating of a sample until it evaporates. The vaporised sample then condenses out on a substrate to form a film.[3] This process is usually carried out under vacuum (10^{-5} to 10^{-6} torr) so that the evaporated atoms undergo collision-less line-of-sight transport. The sample to be vaporised is either held in a crucible or coated onto a wire. Heating of the sample is achieved by various methods, including electrical resistance, arc evaporation, electron beam, or induction heating. Evaporation can be used for the deposition of various materials including metals, alloys, compounds (for example borides, oxides, nitrides, and carbides), and intermetallic compounds. Due to the high temperatures involved it is unsuitable for the deposition of heat sensitive compounds, such as polymers.

1.1.1.3 Chemical Vapour Deposition

Chemical vapour deposition (CVD) produces films of material on a heated substrate by the chemical breakdown of a gaseous precursor.[4] Breakdown of the species in the vapour phase may occur by purely thermal decomposition, e.g. the deposition of nickel from nickel(0) tetracarbonyl, through the action of a reducing agent, e.g. the production of tungsten films from the reaction of tungsten(VI) fluoride with hydrogen, or by the use of a coupled reaction, e.g. the production of aluminium oxide from aluminium(III) chloride, hydrogen and carbon dioxide. By varying the temperatures used for CVD, films consisting of different microstructures can be deposited, such as platelets, whiskers, dendrites, polycrystallites, and amorphous deposits. CVD processes are based upon chemistry occurring at the interface between the vapour and substrate. Consequently,

they are very sensitive to the effects of contaminants in the feed gases or from the reactor, which can be deposited within the film. Various materials can be deposited by the use of CVD including, elements, oxides, carbides, and nitrides. The lack of suitable volatile precursors can be a problem for the deposition of certain metals such as silver.[5] Also there is a need for reasonably high temperatures that precludes the use of heat sensitive substrates.

1.1.1.4 Variants of CVD

There are other variants involving the principles of CVD, but which do not rely on high temperatures for the breakdown of the volatile precursor. These methods include: plasma enhanced CVD (PECVD) in which a low pressure RF discharge is used to lower the operating temperatures required for some reactions to occur.[6] For example the thermal deposition of titanium(IV) nitride from titanium(IV) chloride in nitrogen and hydrogen would require temperatures of the order of 1000 °C, however by the use of PECVD the reaction can be carried out at 400 °C. Laser promoted CVD (LCVD)[7] uses a laser to photolytically or pyrolytically decompose a precursor species in the gas phase and therefore deposit a film, e.g. the production of gold films by the irradiation of dimethylgold(III) hexafluoroacetylacetonate using xenon chloride and Ar^+ lasers.[8, 9]

1.1.1.5 Electrodeposition

Electrodeposition requires the use of a direct current (DC) source connected to electrodes placed in an electrolyte.[10] When a current passes through the circuit positive ions, e.g. metal ions, present in the electrolyte are attracted to the cathode, where they accept electrons and are reduced. The reduced species are then deposited on the cathode. This process requires an electrically conducting electrode, so it is very difficult to coat polymers and ceramics without pre-seeding the surface with some metal. It is technically demanding to obtain a plating solution that is totally free of impurities. As a result of this impurities can be incorporated into the growing film. As electrodeposition is a wet chemical process, there is a need for large quantities of solvents, which must be disposed of after the treatment. Electrodeposition can be used to deposit any conducting film, e.g. metals and alloys.

1.1.1.6 Electroless Deposition

Electroless deposition, unlike electrodeposition requires no external source of electrical current.[11] This process is used for the deposition of metal coatings through the reaction of a metal salt in solution with electrons supplied by a reducing agent also present in the solution. The reactions tend to be catalysed by certain metals in the solution and so proceed in a controlled manner. The reaction becomes autocatalytic as the deposit builds up. In order to prevent spontaneous reduction of the metal salt coating everything, including the inside surface of the bath as well as substrate, various stabilisers and other additives are placed in the solution. This results in the need for careful disposal of the solvent and additives. The unstable plating solutions can also be a problem. However, unlike electroplating which requires a conducting substrate, electroless deposition can be used to produce deposits on polymers, ceramics and glasses.

1.1.2 Properties of Thin Films

In the process of thin film formation the material is reduced from being three dimensional down to two dimensions. This reduction in dimension can produce different electrical properties for the film when compared to the bulk material. Electrical resistivity for thin metal films increases as the film thickness becomes comparable to the mean free path of electrons within the metal,[12] and very thin films of insulating materials can show conduction by the process of electron tunnelling.[13] Also some mechanical properties of thin films can vary according to their method of production, e.g. stresses induced during the production of the film[14] can be either tensile or compressive depending upon their method of manufacture.

1.2 PLASMAS

Plasmas constitute more than 99.9% of the mass of the known universe, being the principal ingredient of stars. However, on earth they are less common; they can be seen as lightning,[15] the Aurorae Borealis and Australis,[16] and recently a theory has been put forward using them to account for one type of UFO sighting.[17] The term plasma was first applied to them by Langmuir. They are often referred to as the fourth state of matter, and contain a multitude of species including electrons, neutrals, ions and electromagnetic radiation.[18] They are quasi-neutral, possessing roughly equal numbers of negative and positively charged species. In order to satisfy this criterion the Debye

length, λ_D, (the distance over which a charge imbalance can exist) has to be much less than the physical size of the plasma.[19] The equation for the Debye length is;

$$\lambda_D = \sqrt{(\varepsilon_0 k T_e / n e^2)} \qquad \text{Equation 1.1}$$

where ε_0 is the permittivity of free space, k is the Boltzmann constant, n is the electron density, e the charge on the electron, and T_e the electron temperature.

There are two main types of plasma characterised by the temperature of their constituent particles. In *equilibrium plasmas* T_e is roughly equal to the gas temperature T_g.[20] Examples of this type are plasma arcs and plasma jets. These types of plasmas generally require high temperatures to produce them (around 30,000K) and as such are not used for the chemical modification of heat sensitive substrates. *Non-equilibrium plasmas* are characterised by having an electron temperature T_e >> gas temperature T_g.[20] This difference in temperatures is explained by the much smaller mass of the electron compared to atoms and molecules in the gas. The electrons being much lighter acquire a greater kinetic energy when subjected to an electric field.

$$\text{Work done by electric field} = \text{Eed} = \frac{(\text{Eet})^2}{2M_e} \qquad \text{Equation 1.2}$$

where E is the applied electric field, e the charge on the electron, d the distance travelled, t the time, and M_e the mass of the electron. Typically such non-equilibrium plasmas possess T_e around 10^4-10^5 K whereas T_g is around room temperature (300K). The glow discharge is one example of a non-equilibrium plasma.

1.2.1 The Glow Discharge

A glow discharge is created by applying electric field to a gas at low pressure. Free electrons are required to initiate the discharge (e.g. from cosmic rays or radioactivity, photoionization or field emission[21]). The free electrons are accelerated by electric field and gain kinetic energy. Energy is transferred to atoms and molecules by these accelerated electrons. For low kinetic energy electrons collisions are pseudo-elastic resulting in only a small energy transference (typically 10^{-5} as the energy loss for elastic

collisions is given by $\Delta E/E = -2M_e/M$ where $\Delta E/E$ is the energy loss, M_e and M the electron and target mass respectively). However, electrons continue to gain kinetic energy between collisions until they have enough to ionise or excite atoms and molecules in the gas. The former situation leads to formation of more electrons and so a cascade process ensues.

The processes that occur in a gas as a function of the applied voltage are often described in terms of the function of the applied voltage, V, on the discharge current, I. A typical I-V curve is shown in Figure 1.1.[21]

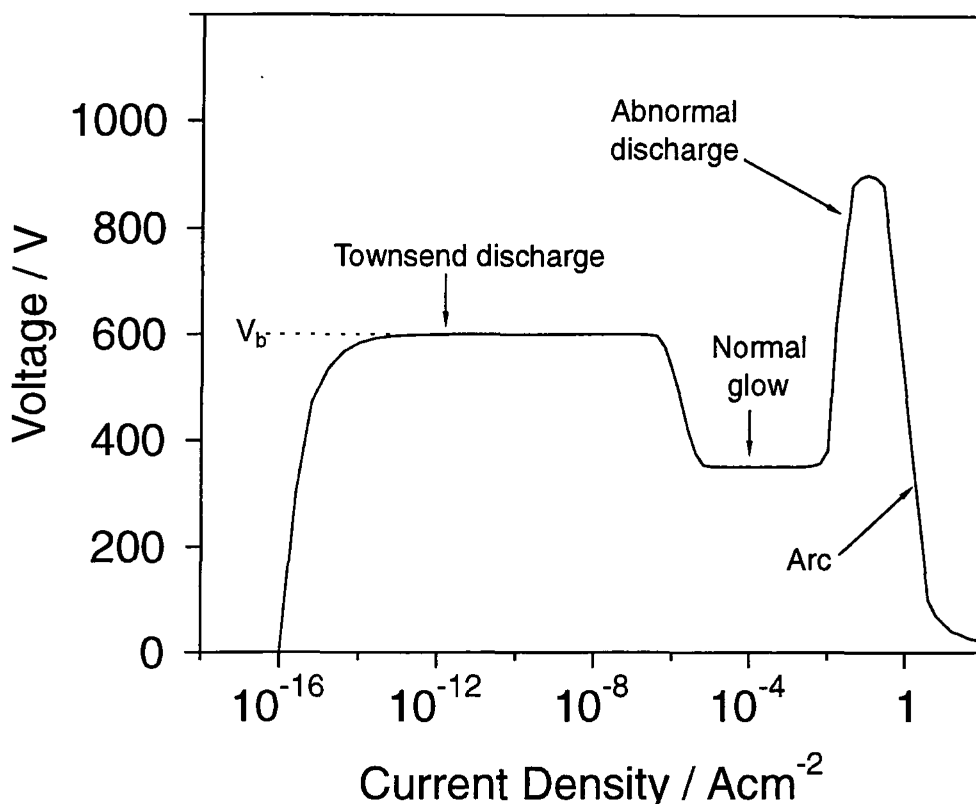

Figure 1.1. I-V characteristics of a dc discharge.

At low potentials only a small number charge carriers are present and consequently the current is low. Increasing the voltage results in more charged species being produced by ionisation of the gas. The voltage rises to a limit which is determined by the output impedance of the power generator. This region of the I-V curve is known as the *Townsend discharge*. At a critical voltage (Breakdown voltage V_b) there is an abrupt

rise in current as an avalanche of electrons are produced. Here the number of free electrons produced is enough to compensate for their loss rate, e.g. by recombination with ions and diffusion. At this point the plasma becomes self sustaining and a *glow discharge* is produced. The characteristic glow derives from the relaxation of excited species within the plasma. Electromagnetic radiation is produced ranging in energy from radio frequency to vacuum ultra violet. As the current density is increased further the *abnormal discharge* region is reached, where the current density is controlled by the area of the electrodes and the resistance of the circuit. At still higher current densities the voltage drops as the gas breaks down and *arcing* occurs.

1.2.2 Radio Frequency Discharges.

There are various ways to produce glow discharges, including; DC, AC, microwave, ECR, corona, and radio frequency (rf). Rf plasmas can be run with the electrodes outside the reactor, thereby reducing contamination. They are homogeneous if the wavelength used is greater than the length of the reactor, and are similar to the DC discharge if the collision frequency is higher than the applied frequency. For rf plasmas power can be coupled to the plasma either inductively or capacitively. Rf plasmas work well at low pressure (e.g. glow discharge) and also at atmospheric pressure (e.g. silent discharge). The use of a fixed frequency and variable power is preferred. A frequency of 13.56 MHz is used for the discharge process so that it does not interfere with radio communications.[22] A matching network is connected between the rf generator and the coil around the glow discharge. This enables the impedance of the plasma reactor to be adjusted so that it matches the 50 Ω output from the rf generator, and allowing the maximum power dissipation in the discharge.[22] A Faraday cage is placed around the plasma reactor to shield radio and other electronic equipment from interference caused by the electromagnetic radiation produced by the plasma.

1.2.3 Electron Energy Distribution Function.

Because electrons are lighter than ions they are more easily accelerated by the electric field and absorb the largest amount of energy from it. The electrons then pass on their energy to other species (e.g. atoms and/or molecules) through collisions.[19] These collisions also results in dissociation and ionisation of species in the plasma and the release of more electrons. The velocity distribution of electrons within a plasma can be

derived by solving the Boltzmann equation.[20] However, no exact solution to this equation exists and so approximations are needed. The basic solution to the Boltzmann distribution assumes the absence of an external electric field and no inelastic energy loss.[20] This is a *Maxwellian distribution* and is characterised by having the electrons in equilibrium with the gas molecules at gas temperature i.e. $T_e = T_g$.[19] The equation for the Maxwellian distribution is given below.

$$f(E) = 2.07E_{av}^{-3/2}E^{1/2}\exp\left(\frac{-1.5E}{E_{av}}\right) \qquad \text{Equation 1.2}$$

where E_{av} is the average energy of electrons, and f(E) the fraction of electrons possessing energy E. However, this approximation is not accurate for low pressure plasmas, and the following assumptions need to be made in order to produce a more accurate model; i) the electric field strength is low enough to neglect inelastic collisions, but high enough to ensure $T_e \gg T_g$ ii) the frequency of the electric field is lower than the frequency of collisions, and iii) the collision frequency is independent of the electron energy.[19] If these assumptions are used then the electron distribution in the plasma can be given by the *Druyvesteyn distribution.* The equation for the Druyvesteyn distribution is given below.

$$f(E) = 1.04E_{av}^{-3/2}E^{1/2}\exp\left(-\frac{0.55E^2}{E_{av}^2}\right) \qquad \text{Equation 1.3}$$

The Druyvesteyn distribution is a more accurate model for low temperature non-equilibrium plasmas than the Maxwellian distribution, and indicates a shift towards higher electron temperatures.[19] Figure 1.2 shows the Maxwellian and Druyvesteyn electron energy distributions for an average electron temperature of 1eV.

As can be seen both models predict a tail of high energy electrons, which have a large impact on the chemistry occurring in the plasma.

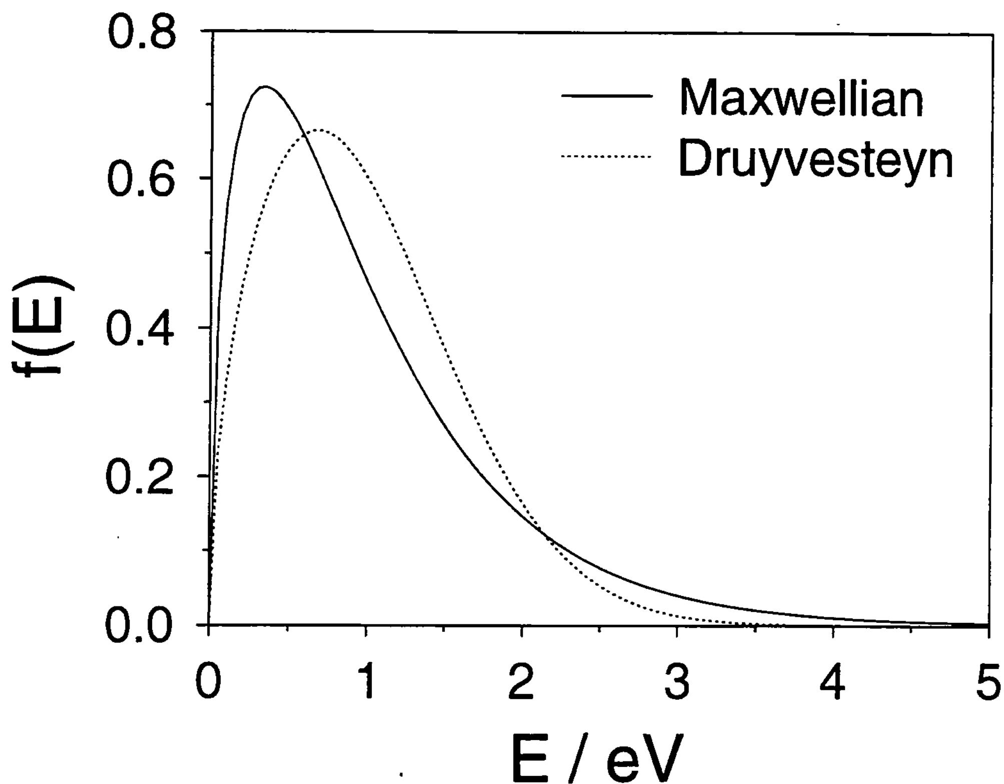

Figure 1.2. Maxwellian and Druyvesteyn electron energies distributions.

1.2.4 Plasma Potential.

As previously mentioned electrons within a plasma possess a greater kinetic energy (and also velocity) with respect to the ions. As a result of this the rate of collision between electrons and the reactor wall will be higher than that for ions, and the plasma will build up a net positive charge with respect to the walls of the reactor.[23, 24] This increase in positive charge within the bulk of the plasma will then reduce the flux of electrons to the walls. Eventually a steady state situation will be established between the bulk plasma and the walls of the reactor. Under these conditions ions and electrons are lost to the walls of the reactor at equal rates. The resulting plasma potential is roughly several volts more positive than the potential of the reactor walls.

1.2.5 Floating Potential.

Due to the greater mobility of electrons compared to ions within the plasma, when an electrically isolated substrate is placed within the plasma it will become negatively charged.[23] Within a relatively short period of time the build up of negative charge on the substrate, with respect to the quasi-neutral plasma bulk will repel the influx of further

electrons. When this occurs the substrate will be subjected to an equal flux of ions and electrons. The sample is now referred to as having reached the *floating potential*, which is typically negative with respect to the *plasma potential*.

1.2.6 Plasma Sheath.

The build up of the net negative charge on a substrate within a plasma results in a reduction in the electron density and therefore an increase in the net positive charge near to the surface. This region of positive space charge is known as the *plasma sheath*.[24] The lowering of electron density in this region leads to a low degree of gas excitation and consequently little emission of electromagnetic radiation. For obvious reasons this sheath is often referred to as the dark region, or dark space.

1.2.7 Plasma Chemistry.

Plasmas are a reactive media consisting of atoms, molecules, metastables, electrons, ions, neutrals and photons ranging in energy from radio frequency (rf) to vacuum ultra violet (VUV). Reactions initiated by them may be classified as homogeneous (occurring within the gas phase) or heterogeneous (between the plasma and reactor wall/sample).[25] In this section the wide range of reactions that occur within a plasma will be summarised, and displayed in Figure 1.3. A, B and C denote atoms, e^- electrons, M a third body, hv photons, S a surface, X any moiety capable of absorbing and/or polymerizing on the surface, and P a polymeric species.

Homogeneous reactions result from inelastic collisions in the plasma occurring between electrons and heavier species, and between heavy species themselves.

a) *Excitation*: Excited states of atoms and molecules are formed by the impact of electrons with heavy targets.

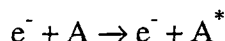

$$e^- + A \rightarrow e^- + A^*$$

b) *Dissociative attachment*: Low energy electrons may attach to molecules, resulting in dissociation and production of a negative ion.

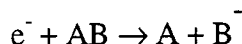

$$e^- + AB \rightarrow A + B^-$$

c) *Ion Pair Formation*: Dissociative ionisation caused by electron impact.

$$e^- + AB \rightarrow A^+ + B^- + e^-$$

d) *Dissociation*: Inelastic collision of an electron with a molecule without the formation of ions.

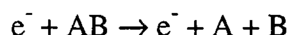

$$e^- + AB \rightarrow e^- + A + B$$

e) *Ionisation*: Ionisation induced by electron impact.

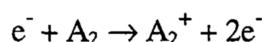

$$e^- + A_2 \rightarrow A_2^+ + 2e^-$$

f) *Recombination*: Recombination of charged particles.

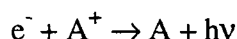

$$e^- + A^+ \rightarrow A + h\nu$$

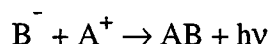

$$B^- + A^+ \rightarrow AB + h\nu$$

g) *Charge transfer*: Transfer of positive charge through collision.

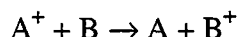

$$A^+ + B \rightarrow A + B^+$$

h) *Transfer of heavy reactants*: Formation of new compound through ion-molecule reaction.

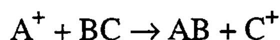

$$A^+ + BC \rightarrow AB + C^+$$

i) *Associative detachment*: Electron production and new compound formation resulting from collision with negative ions.

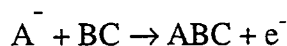

$$A^- + BC \rightarrow ABC + e^-$$

j) *Electron transfer*: Formation of new ions by the transfer of an electron between colliding species.

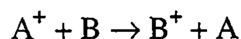

$$A^+ + B \rightarrow B^+ + A$$

k) *Ionisation*: Collisions between two energetic neutral species can result in the ionisation of one of them.

$$A + B \rightarrow A^+ + B + e^-$$

l) *Penning ionisation/dissociation*: Transfer of energy from excited metastable species to a target.

$$A + B^* \rightarrow A^+ + B + e^-$$

m) *Attachment of atoms*: Attachment of an atom to a molecule requiring the participation of third body (M) to allow conservation of momentum.

$$A + BC + M \rightarrow ABC + M$$

n) *Disproportionation*: Similar to the ion-molecule reaction (h) but occurring between two neutral species.

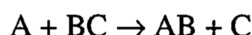

$$A + BC \rightarrow AB + C$$

o) *Recombination of radicals*: Formation of molecular species by the recombination of radicals. For this to occur between two atomic radicals a third body must be present to conserve momentum.

$$A + A \rightarrow A_2$$

p) *Chemiluminescence*: Relaxation of an excited species resulting in the emission of a photon.

$$AB^* \rightarrow AB + h\nu$$

Heterogeneous reactions

q) *Adsorption*: Adsorption of species within the plasma on to a surface. $X_{(g)}$ and $X_{(s)}$ represent species in the plasma and on the surface respectively.

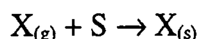

$$X_{(g)} + S \rightarrow X_{(s)}$$

r) *Recombination or compound formation*: Formation of compounds between species in the plasma and adsorbed on the surface.

$$S\text{-}A + A \rightarrow S + A_2$$

s) *Metastable de-excitation*: Quenching of metastables by energy loss to the surface.

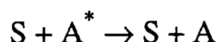

$$S + A^* \rightarrow S + A$$

t) *Sputtering*: Removal of atoms from the surface by ions in the plasma with sufficient energy.

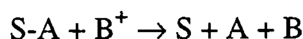

$$S\text{-}A + B^+ \rightarrow S + A + B$$

u) *Polymerisation*: Reaction between radicals in the plasma and on the surface.

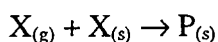

$$X_{(g)} + X_{(s)} \rightarrow P_{(s)}$$

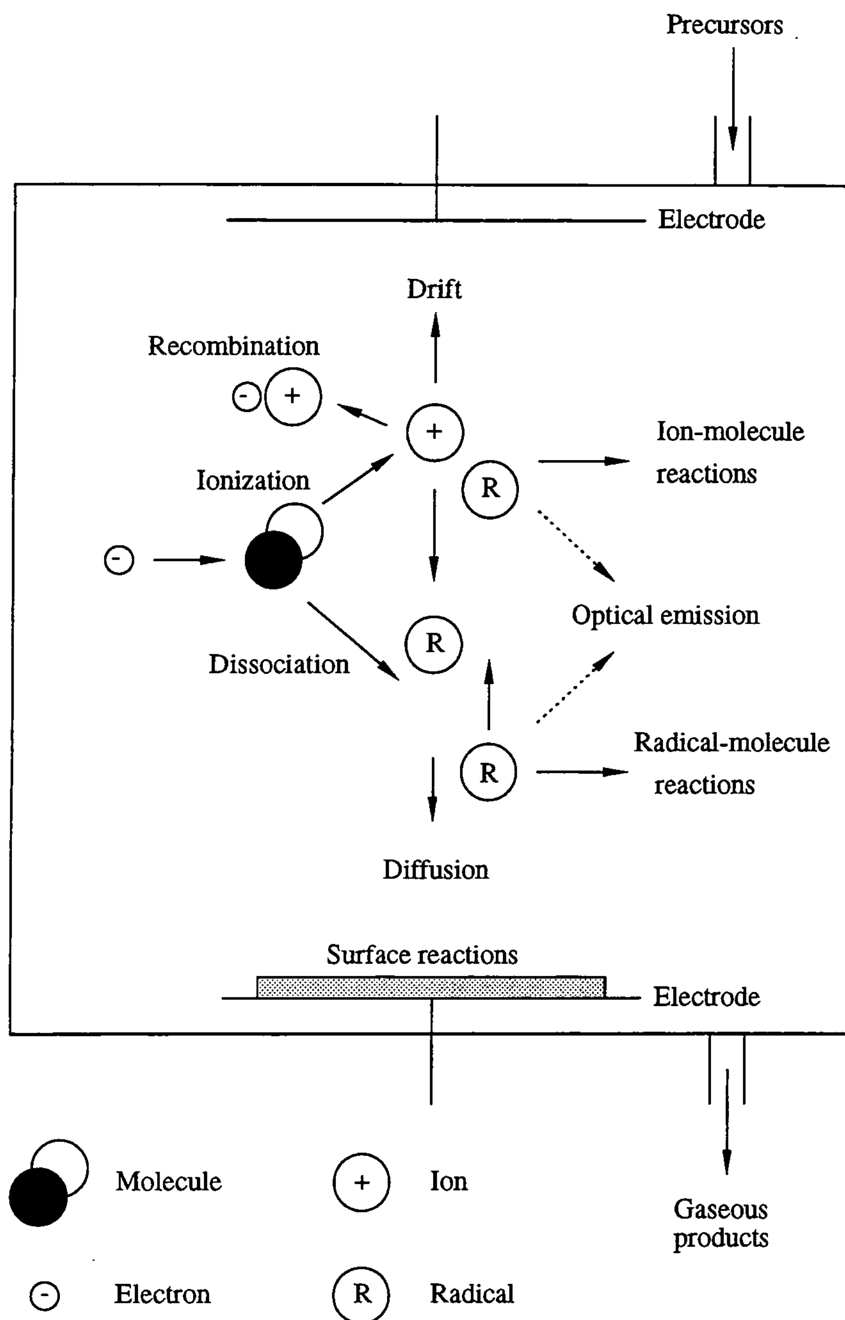

Figure 1.3. Summary of reactions occurring within a plasma.

1.2.8 Hydrogen Plasmas.

Wood showed in 1922 that a low frequency discharge through hydrogen could be used for the generation of high concentrations of hydrogen atoms.[26] Due to the low mass of hydrogen atoms they are unable to undergo simple recombination on collision. They need a third body to remove the excess energy, e.g. at the walls of the reactor, or from another species in the gas phase.

The effects of hydrogen atoms on various compounds are given below.

Hydrocarbons : addition of hydrogen atoms (as well as breakage of the carbon backbone at higher temperatures) is seen in their reaction with unsaturated hydrocarbons, resulting in the formation of saturated hydrocarbon moieties.[27] In their reactions with compounds containing carbon, hydrogen and oxygen, hydrogen abstraction and again breaking down of the molecule into smaller fragments occurs.[27] This ability of hydrogen plasmas to break down organic groups has lead to their use for the non destructive cleaning of materials.[28] It is even thought that electrical discharges through gas mixtures containing hydrogen along with methane, ammonia and other gases were responsible for the beginning of life itself.[29]

Carbon monoxide : reaction of carbon monoxide with hydrogen atoms leads mainly to the formation of formaldehyde and some polymerised material.[30] However, some other compounds are also produced including methanol, ethanol, methane and water.

Elements : reaction of hydrogen with many elements leads to the formation of hydrides, i.e. phosphorus, antimony, sulphur, arsenic, germanium, tin, tellurium, selenium, carbon, oxygen, chlorine and other halides.[31, 32, 33, 34] Even metals such as silver, beryllium, gallium, indium, and tantalum gave surface films exhibiting hydride like properties.[35]

Inorganic halides : reaction of hydrogen atoms with inorganic halides results in halide removal, and reduction of the oxidation state of the metal.[36] The inorganic halide is usually present in the gas phase, mixed with hydrogen and then passed through the discharge. One example of this type of reduction is the formation of Group I, II and III metals through the action of a hydrogen microwave discharge on their halides in the gaseous phase.[37]

Metal oxides : hydrogen atoms have been reported to reduce some metal oxides down to the metal or to lower valency forms.[38, 39, 40] For example lithium niobate crystals have been exposed to a microwave hydrogen discharge at high temperatures resulting in a low resistivity layer of uncertain composition.[41]

Metals : atomic hydrogen tends to penetrate into bulk metals. There has been an interest in studying this phenomena due to the use of metals in Tokamak fusion systems. Amongst others, studies of hydrogen permeation into stainless steel,[42] molybdenum,[43] vanadium,[44] palladium,[45, 46] titanium,[47] and intermetallic compounds[48] have been reported.

1.3 EXPERIMENTAL TECHNIQUES.

Various experimental techniques were used to analyse the spin coated metal salt and resultant metal films prepared in this thesis. Some techniques are surface sensitive (X-ray Photoelectron Spectroscopy), whereas some have been used to perform bulk analysis, e.g. X-ray diffraction.

1.3.1 X-ray Photoelectron Spectroscopy (XPS).

The principal behind X-ray photoelectron spectroscopy is very simple; the sample is irradiated with high energy photons, resulting in the emission of electrons from the surface due to the photoelectric effect. The kinetic energy of these electrons is then measured, and the binding energy of the emitted photoelectron can be calculated,

$$E_B = h\nu - E_K - \Phi \qquad \text{Equation 1.4}$$

where E_B and E_K are the binding and kinetic energies of the emitted photoelectron respectively, $h\nu$ energy of the incident photon, and Φ the work function of the system. The work function is normally determined by referencing to known element. The binding energy is unique for a given element and is also dependant upon the oxidation state of that element. Upon emission of a photoelectron, another electron from a higher energy level within the atom may fall down to fill the hole. This leads to the emission of another electron and is known as Auger emission. Electrons emitted by the Auger process are also used for surface analysis in Auger Emission Spectroscopy (AES). In theory it is possible to use any photon source which has $h\nu$ greater than the work function, i.e. UV and shorter wavelength radiation. The most common sources are narrow wavelength range X-ray sources, although UV sources are employed for

ultraviolet photoelectron spectroscopy which is used to obtain information about valence band structure. The transitions involved in XPS, AES and UPS are shown in Figure 1.4.

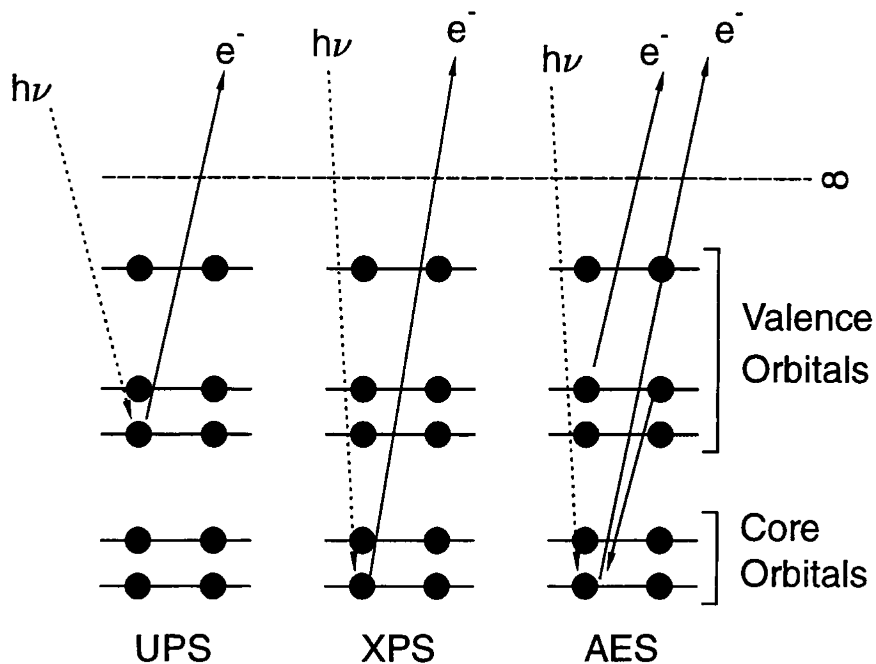

Figure 1.4. XPS, AES, and UPS transitions.

The surface sensitivity of XPS comes from the energy dependence on the escape depth of the photoelectrons. There are three processes of energy loss that can occur in a solid; lattice vibrations (phonons), excitation of collective density fluctuations (plasmons), and excitation of particles. Low kinetic energy (KE) electrons are not able to produce these effects and their escape depth is large. For high KE electrons the cross section for these interactions is again low and so their escape depth is large. However, medium KE electrons have a high cross section for these effects and their escape depth is much smaller. A graph of escape depth against energy is shown in Figure 1.5.[49]

The escape depth goes through minimum of 1 nm at an electron KE of approximately 100 eV. The KE's of photoelectrons produced by excitation from a X-ray source are about 100-1000 eV. The corresponding escape depth for these photoelectrons are about 1-3 nm, hence this is a surface sensitive technique.

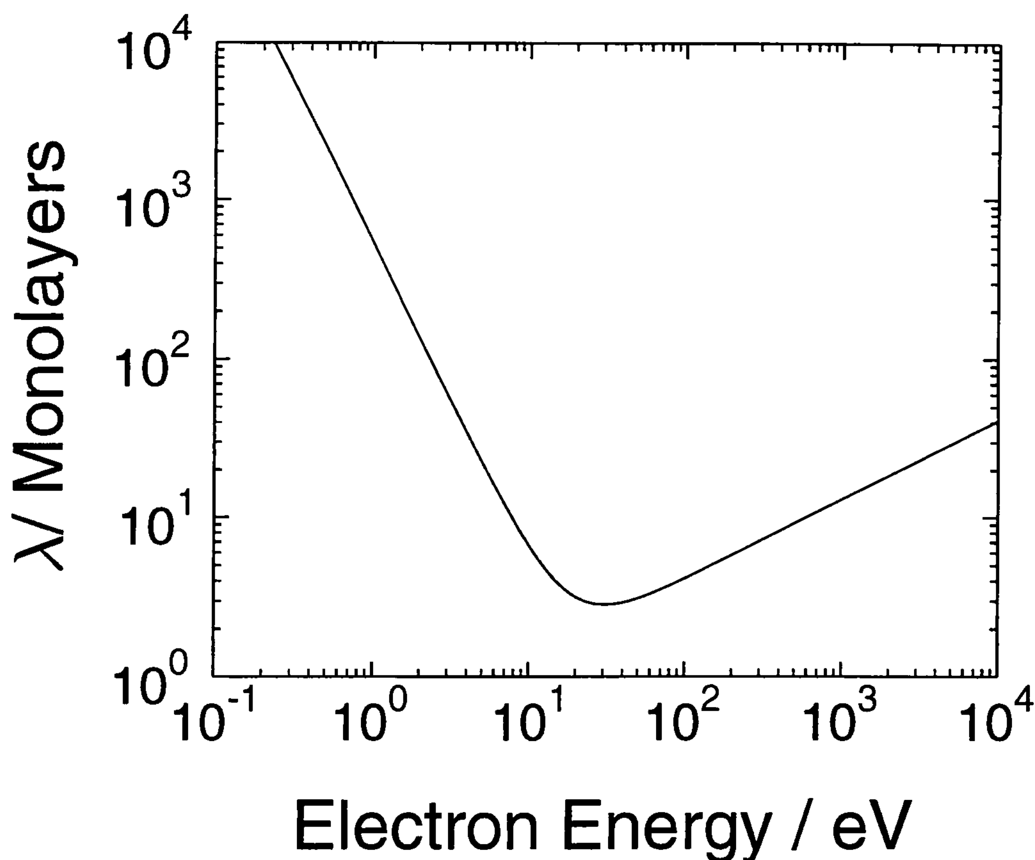

Figure 1.5. Escape depth curve.

1.3.1.1 Instrumentation.

Ultra high vacuum (UHV) conditions are required to perform XPS. A pressure of < 10^{-6} torr is needed to prevent electrons scattering from the gas present.[50] However, the necessity of UHV conditions arises from the need to reduce surface contamination of the sample due to background gases in the chamber. For most experiments base pressures in the region of 2×10^{-10} torr are adequate.

XPS analysis of a sample requires three main components; an X-ray source, an electron energy analyser, and an electron detector. The X-ray source contains a filament surrounding a central anode. Electrons emitted from the filament are accelerated towards the anode and cause the production of X-rays upon collision with it. The energy of the resultant X-rays is dependant upon the material with which the anode is coated. This coating is usually magnesium or aluminium (resulting in main X-ray lines at 1253.6 eV or 1486.6 eV respectively).[50] An aluminium window is placed between the X-ray source and the sample to reduce contamination, and screen the sample from electrons

produced by the X-ray source.[51] Photoelectrons emitted from the sample are collected by a lens, and have their energies retarded before passing into the analyser. There are two main types of analyser used for XPS; the Concentric Hemispherical Analyser (CHA) and the Cylindrical Mirror Analyser (CMA).[52] The CMA is most often used for Auger electron spectroscopy (AES) and so its operation will not be discussed further. A CHA consists of two hemispherical plates positioned concentrically. A voltage is applied between these plates, and only electrons of a certain energy can pass between them and reach the electron detector. In XPS the analyser can be run in two modes; Constant Analyser Energy CAE and Constant Retard Ratio CRR. Each of these two modes of operation have different resolutions. In CAE the energy of the incoming electrons is reduced to a value designated by the operator. This voltage is defined as the *pass energy*. CAE provides good resolution at low kinetic energies, but low signal to noise ratios, and as such is the preferred method of operation for XPS. In CRR mode the pass energy (ΔE) varies as a function of the kinetic energy (E), such that;

$$\frac{\Delta E}{E} = \text{constant} \qquad \text{Equation 1.5}$$

As a consequence of this the sensitivity is improved at higher kinetic energies, but the resolution is poorer (at these higher kinetic energies) than for CAE. CRR is the preferred mode of operation for AES.

1.3.1.2 Spectral interpretation.

X-ray photoelectron spectra are usually displayed as a function of counts against binding energy. The signal intensity is related to elemental abundance, and the ionisation cross-section for the particular core level of the element being analysed. In order to produce quantitative surface composition measurements the measured signal intensities need to be corrected by a sensitivity factor.[53]

Non-equivalent atoms of the same element have different binding energies.[54] This effect is called *chemical shift*. As a simple model the binding energy is determined by the effective charge on the nucleus.[54] If an atom is surrounded by a more electronegative environment, then its outer shell electrons will be pulled away, resulting in the core electrons experiencing a greater (effective) nuclear charge and so being held more

tightly. The binding energy of these core level electrons will therefore increase. This model does not take into account *final state effects* such as the polarization of the surrounding electrons by the core hole.[54]

Spectral interpretation is also complicated by several other effects. Due to the fact that standard X-ray sources are non-monochromatic, not only photoelectrons produced by the $K\alpha_{1,2}$ line are seen for magnesium and aluminium, but also from the $K\alpha_{3,4}$ line as well as other lower intensity *X-ray satellites*. The presence of this $K\alpha_{3,4}$ line leads to a secondary signal about 8% of the intensity, and at 8.4 eV lower BE, than the primary signal produced by the $K\alpha_{1,2}$ line.[55] The fitting of a monochromator to the X-ray source removes these satellite lines as well as the Bremsstrahlung background radiation. *Ghosts* result from the presence of contamination on the X-ray anode.[54] These produce X-rays of different energies to those of the material coating the anode, and weak ghost signals in the XP spectra. *Shake-up* can result as a consequence of restructuring of the valence electrons after photoemission, and may result in the promotion of one of them to a higher unfilled level.[56] This leads to the formation of a satellite a few eV higher BE than the main peak. An example of this would be the π-π^* transition in aromatic systems. *Shake-off* satellites are produced when valence electrons are completely excited to an unbound continuum state.[54] *Multiplet splitting* occurs when photoionization takes place from an orbital with non zero angular momentum, i.e. p, d, or f orbital. The effect of this is to split the peak into two components, the ratios of which are determined by their respective degeneracies (2j+1), i.e. the Au(4f) line is split into Au($4f_{7/2}$) and Au($4f_{5/2}$) with relative areas of 4 : 3. Photoemission lines in metals become broadened to higher BE sides, resulting in the formation of an *asymmetric peak*, caused by the excitation of e-hole pairs in the fermi surface.[54, 57] The greater the density of states (DOS) in the metal the more this effect is likely to occur. *Auger peaks* also occur in the XP spectra further complicating peak assignment.

1.3.2 Attenuated Total Reflectance Fourier Transform Infra-Red Spectroscopy (ATR-FTIR).

Infra-red spectroscopy is concerned with the excitation of molecular vibrations by photons in 100 μm - 1 μm region.[58] An alternating electric field from the changing charge distribution during the vibration, couples the molecular vibrations with the

oscillating field of the electromagnetic radiation. In order for a transition to be *infra-red active* there has to be change in the dipole moment of the group being excited. Totally symmetric transitions are IR inactive because there is no change in the dipole moment during motion. Strong signals are produced by groups with a strong dipole moment.

Attenuated total reflectance fourier transform infra-red spectroscopy (ATR FTIR) is used to obtain IR spectra of opaque materials. The sample is placed on top of a crystal (e.g. KRS-5, silver chloride, germanium, or diamond) which is transparent in the region of the IR being used. The refractive index of the sample has to be much less than that of the crystal. Due to the differences in refractive indices between the optically more dense crystal, and more rare sample, internal reflection occurs at the interface for angles of incidence greater than the critical angle. The critical angle is defined by,

$$\Theta_c = \sin^{-1}\frac{n_2}{n_1} \qquad \text{Equation 1.6}$$

where Θ_c is the critical angle of incidence, and n_2 and n_1 are the refractive indices of the sample and crystal respectively. The beam is not completely reflected at the interface but propagates a short distance (a few µm into the surface), Figure 1.6.

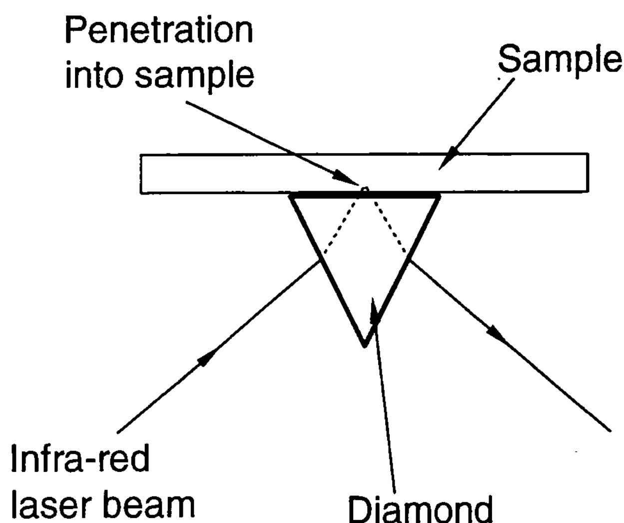

Figure 1.6. Reflection at the interface between the ATR crystal and sample.

This beam can interact with the groups present in this region and be absorbed, resulting in an absorption spectra of the surface of the sample. The depth of penetration into the sample is dependant upon the wavelength, and is about 10^{-3} to 10^{-4} cm for infra red radiation,[59] so good contact between sample and the crystal is necessary. The strength of the signal can be improved by allowing multiple passes of the beam through the crystal thereby increasing the effective path length.

1.3.3 X-ray Diffraction (XRD).

Due to the similarity between the wavelength of X-rays and the interplanar separation inside a crystal, X-rays are diffracted on passing through a crystal.[60] This phenomena can be explained by considering crystals as stacks of planes of separation d, with lattice planes acting as mirrors. In order for constructive interference to occur, the path length difference between the incident and reflected beams must be an integral number of wavelengths, Figure 1.7.

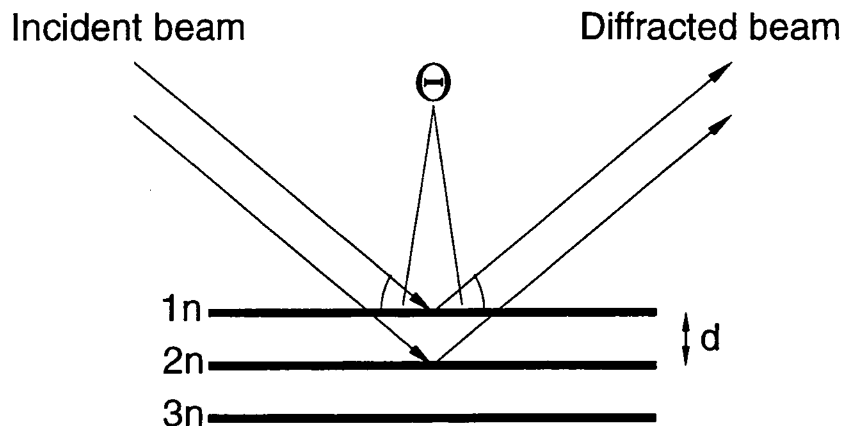

Figure 1.7. Reflection of radiation at lattice planes.

A bright spot, caused by constructive interference, is produced when the glancing angle satisfies the *Bragg Law*. The Bragg Law equation is,

$$n\lambda = 2d \sin \theta \qquad \text{Equation 1.7}$$

where λ is the wavelength of the incident radiation, d is the interplanar spacing and θ is the angle between the incident radiation and the plane.

Laues original method used broad band of X-rays which were projected through a single crystal. *Powder X-ray techniques* do not require single crystals. The *Debye-Scherrer* method was used to obtain the results given within this work. Ideally this method needs an infinite number of randomly orientated crystallites. Each set of *hkl* lattice planes in these crystallites will scatter at a particular 2θ value. A cone of scattering then results as all possible crystallite orientations are present. Originally the sample was placed within a capillary tube which could be rotated, thus ensuring random orientation of the crystallites present within the sample. The intercept of the diffraction cones on a film allowed values to be measured. In modern powder diffraction equipment the sample is mounted on a flat plate and a computer is used to record the location of the 2θ values at which diffraction occurs.[61]

X-ray diffraction is a bulk analysis technique and has many applications including; identification of materials by fingerprinting, precise determination of lattice parameters, elucidation of phase diagrams, and qualitative analysis of mixtures.[61]

1.3.4 Raman Spectroscopy.

The passage of light through a sample will result in a fraction of that light being scattered.[62] This scattering is usually elastic, i.e. *Rayleigh scattering*. However, a small proportion of the light will be scattered inelastically, i.e. *Raman scattering*. Raman scattering results in a change in the frequency of the light. This change comes about from the energy transfer between the incident photon and intermediate virtual states of the sample, Figure 1.8.[63] If some energy is given up by the photon to the sample then this is referred to as *Stokes Raman scattering*, which is the most common type of Raman scattering. However, if energy is given to the photon from the sample then *Anti-Stokes Raman scattering* occurs. The ratio of the intensities of Stokes to Anti-Stokes scattering is governed by the temperature of the sample.[63]

Unlike IR spectroscopy which requires a change in the dipole moment for the transition to occur, Raman scattering needs a change in the polarizability.[63] This is why IR and Raman are often used as complementary techniques.

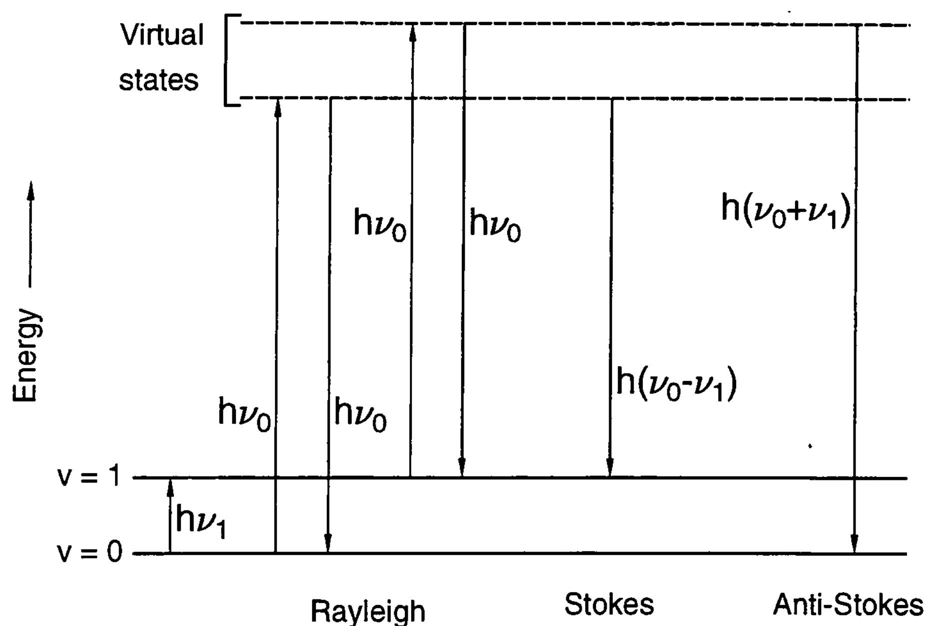

Figure 1.8. The fundamental processes involved in Raman scattering.

As the probability of Raman scattering occurring is very low, an intense light source is required. Also a monochromatic source is needed as the shifts in frequency are quite small. Due to these requirements lasers have become the usual source of incident radiation.[64]

Raman spectroscopy can be applied to many different types of samples such as, metal salts, polymers, liquids, fibres, powers, and single crystals. Fluorescence of the sample can be a problem. However, sometimes this can be solved by leaving the laser on for long time.[65] Problems with fluorescence can also be eliminated by using incident radiation with a different frequency, i.e. using a different laser.[65] Coloured samples can sometimes cause problems when trying to obtain Raman spectra (i.e. heating of the sample can result in thermal decomposition). This is alleviated by cooling the sample, or by reducing the intensity of the laser.[66]

1.3.5 Electrical Resistivity.

The electrical resistivity of a sample can be calculated from knowledge of its resistance, cross-sectional area and length, and is defined as;[67]

$$\rho = R \times \frac{A}{l} \qquad \text{Equation 1.8}$$

where ρ and R are the resistivity and resistance of the sample, and A and l its cross-sectional area and length respectively. There are various factors that can contribute to the electrical resistivity of thin metallic films including: temperature, the presence of point defects and impurities, and imperfections in the structural lattice.

The thickness of the film will also affect its resitivity;[68] the resistivity of a metal is dependant upon the mean free path of its conduction electrons. When an electron reaches the edges of the metal it will under go some form of reflection. As the thickness of the metal film is decreased these reflections will account for a greater fraction of the total number of collisions. If the collisions with the edges of the metal are nonspecular, i.e. the direction that the electron travels after the collision is not dependant on its direction before collision, then an increase in the resistivity of the metal film as compared to the bulk metal will be observed. This effect only becomes important for most pure metals at thickness below about 30 nm at room temperature.[68]

1.4 REFERENCES

1 *Handbook of Depositional Technologies for Films and Coatings* (Ed. R. F. Bunshah) Noyes Publications, USA, **1994**, Chapter 1.

2 *Handbook of Depositional Technologies for Films and Coatings* (Ed. R. F. Bunshah) Noyes Publications, USA, **1994**, Chapter 5.

3 *Handbook of Thin Film Technology* (Eds. L. I. Maissel, R. Glang) McGraw-Hill, USA, **1983**, Chapter 1.

4 *Handbook of Depositional Technologies for Films and Coatings* (Ed. R. F. Bunshah) Noyes Publications, USA, **1994**, Chapter 7.

5 Z. Yuan, N. H. Dryden, J. J. Vittal, R. J. Puddephatt, *Chem. Mater.* **1995**, *7*, 1696.

6 *Handbook of Depositional Technologies for Films and Coatings* (Ed. R. F. Bunshah) Noyes Publications, USA, **1994**, Chapter 8.

7 *Laser Microfabrication Thin Film Processes and Lithography* (Eds. D. J. Ehrlich, J. Y. Tsao) Academic Press, USA, **1989**, Chapter 7.

8 D. Wexler, J. I. Zink, L. W. Tutt, S. R. Lunt, *J. Phys. Chem.* **1993**, *97*, 13563.

9 T. H. Baum, C. R. Jones, *Appl. Phys. Lett.* **1985**, *47*, 538.

10 *Handbook of Depositional Technologies for Films and Coatings* (Ed. R. F. Bunshah) Noyes Publications, USA, **1994**, Chapter 10.

11 *Handbook of Thin Film Technology* (Eds. L. I. Maissel, R. Glang) McGraw-Hill, USA, **1983**, Chapter 5.

12 *Handbook of Thin Film Technology* (Eds. L. I. Maissel, R. Glang) McGraw-Hill, USA, **1983**, Chapter 13.

13 *Handbook of Thin Film Technology* (Eds. L. I. Maissel, R. Glang) McGraw-Hill, USA, **1983**, Chapter 14.

14 *Handbook of Thin Film Technology* (Eds. L. I. Maissel, R. Glang) McGraw-Hill, USA, **1983**, Chapter 12.

15 G. Francis in *Ionization Phenomena in Gases* Butterworths Publications Ltd., Great Britain, **1960**, Chapter 5.

16 F. M. Penning in *Electrical Discharges in Gases* Philips Technical Library, Netherlands, **1957**, Chapter 1.

17 P. Brovetto, V. Maxia, *Nuovo Cimento Della Societa Italiana di Fisica D - Condensed Matter Atomic Molecular and Chemical Physics Fluids Plasma Biophysics* **1995**, *17*, 169.

18 J. Coburn, *IEEE Trans. Plas. Sci.* **1991**, *19*, 1048.

19 A. Grill in *Cold Plasmas in Materials Technology* IEEE Press, USA, **1994**, Chapter 1.

20 *Techniques and Applications of Plasma Chemistry* (Eds. J. R. Hollahan, A. T. Bell) John Wiley and Sons, USA, **1974**, Chapter 1.

21 A. Grill in *Cold Plasmas in Materials Technology* IEEE Press, USA, **1994**, Chapter 2.

22 B. Chapman in *Glow Discharge Processes* John Wiley and Sons, USA, **1980**, Chapter 5.

23 B. Chapman in *Glow Discharge Processes* John Wiley and Sons, USA, **1980**, Chapter 3.

24 *Thin Film Processes II* (Eds. J. L. Vossen, W. Kern) Academic Press, USA, **1991**, Part II.

25 A. Grill in *Cold Plasmas in Materials Technology* IEEE Press, USA, **1994**, Chapter 3.

26 R. W. Wood, *Proc. Royal Soc. A* **1922**, *102*, 1.

27 F. K. McTaggart in *Plasma Chemistry in Electrical Discharges* Elsevier Publishing Company, Netherlands, **1967**, Chapter 6.

28 *Techniques and Applications of Plasma Chemistry* (Eds. J. R. Hollahan, A. T. Bell) John Wiley and Sons, USA, **1974**, Chapter 7.

29 F. K. McTaggart in *Plasma Chemistry in Electrical Discharges* Elsevier Publishing Company, Netherlands, **1967**, Chapter 11.

30 R. H. Sahasrabudhey, A. Kalyanasundaram, *Proc. Indian Acad. Sci.* **1948**, *27A*, 366.

31 K. F. Bonhoeffer, *Z. Phys. Chem.* **1924**, *113*, 199.

32 T. G. Pearson, P. L. Robinson, E. M. Stoddart, *Proc. Royal Soc. (London) A* **1933**, *142*, 275.

33 H. E. Radford, *J. Chem. Phys.* **1964**, *40*, 2732.

34 J. D. Blackwood, F. K. McTaggart, *Australian J. Chem.* **1959**, *12*, 533.

35 E. Pietsch, *Z. Elektrochem.* **1933**, *39*, 577.

36 F. K. McTaggart in *Plasma Chemistry in Electrical Discharges* Elsevier Publishing Company, Netherlands, **1967**, Chapter 6.

37 F. K. McTaggart in *Chemical Reactions in Electrical Discharges Advances in Chemistry Series 80* (Ed. R. F. Gould) American Chemical Society, USA, **1969**, Chapter 14.

38 K. F. Bonhoeffer, *Z. Phys. Chem.* **1924**, *113*, 199.

39 F. K. McTaggart, *Nature* **1964**, *201*, 1320.

40 F. K. McTaggart, *Nature* **1963**, *199*, 339.

41 H. Turcicová, H. Arend, O. Jarolímek, *Solid State Comm.* **1995**, *93*, 979.

42 V. M. Sharapov, A. I. Kanaev, A. P. Zakharov, *Atomnaya Energiya* **1985**, *59*, 269.

43 M. Kitajima, M. Fukutomi, A. Hasegawa, M. Okada, *J. Nucl. Mater.* **1986**, *141-143*, 234.

44 V. I. Vasil'ev, L. I. Gomozov, M. I. Guseva, V. A. Dergachev, A. N. Mansurova, S. S. Tserevitinov, *Izvestiya Rossiiskoi Akademii Nauk. Metally* **1994**, *5*, 3.

45 T. D. Radzhabov, L. Ya. Alimova, V. G. Dyskin, F. Sh. Melkumyan, B. G. Skorodumov, T. A. Radyuk, V. N. Kadushkin, I. I. Trinkin, *Atomnaya Energiya* **1985**, *59*, 269.

46 A. V. Sharudo, R. E. Mukhamadiev, *Vacuum* **1992**, *43*, 623.

47 D. V. Schur, V. A. Lavrenko, *Vacuum* **1993**, *44*, 897.

48 V. N. Verbetskii, M. V. Lototskii, S. V. Mitrokhin, K. N. *Semenenko, Vestnik Moskovskogo Universiteta. Khimiya* **1983**, *38*, 414.

49 M. P. Seah, W. A. Dench, *Surf. Interface Anal.* **1979**, *1*, 2.

50 *Practical Surface Analysis Volume 1 - Auger and X-ray Photoelectron Spectroscopy* (Eds. D. Briggs, M. P. Seah) John Wiley and Sons, Great Britain, 2nd Edition, **1990**, Chapter 2.

51 *Methods of Surface Analysis Techniques and Applications* (Ed. J. M. Walls) Cambridge University Press, Great Britain, **1990**, Chapter 5.

52 *Surface Analysis Methods in Materials Science* (Eds. D. J. O'Connor, B. A. Sexton, R. St. C. Smart) Springer - Verlag, Germany, **1992**, Chapter 7.

53 *Practical Surface Analysis Volume 1 - Auger and X-ray Photoelectron Spectroscopy* (Eds. D. Briggs, M. P. Seah) John Wiley and Sons, Great Britain, 2nd Edition, **1990**, Chapter 5.

54 *Practical Surface Analysis Volume 1 - Auger and X-ray Photoelectron Spectroscopy* (Eds. D. Briggs, M. P. Seah) John Wiley and Sons, Great Britain, 2nd Edition, **1990**, Chapter 3.

55 J. F. Moulder, W. F. Stickle, P. E. Sobol, K. D. Bomben in *Handbook of X-ray Photoelectron Spectroscopy* (Ed. J. Chastain) Perkin - Elmer Corporation, USA, **1992**, Section E.

56 G. Beamson, D Briggs in High Resolution XPS of Organic Polymers - The Scienta ESCA300 Database John Wiley and Sons, **1992**, Chapter 9.

57 *Solid State Chemistry Techniques* (Eds. A. K. Cheetam, P. Day) Oxford University Press, USA, **1990**, Chapter 3.

58 C. N. Banwell in *Fundamentals of Molecular Spectroscopy* McGraw-Hill, Great Britain, **1983**, 3rd Edition, Chapter 1.

59 C. N. Banwell in *Fundamentals of Molecular Spectroscopy* McGraw-Hill, Great Britain, **1983**, 3rd Edition, Chapter 3.

60 *Solid State Chemistry Techniques* (Eds. A. K. Cheetam, P. Day) Oxford University Press, USA, **1990**, Chapter 2.

61 P. W. Atkins in *Physical Chemistry* Oxford University Press, Great Britain, **1990**, 4th Edition, Chapter 21.

62 T. R. Gilson, P. J. Hendra in *Laser Raman Spectroscopy* John Wiley and Sons, Great Britain, **1970**, Chapter 1.

63 J. G. Grasselli, M. K. Snavely, B. J. Bulkin *in Chemical Applications of Raman Spectroscopy* John Wiley and Sons, USA, **1981**, Chapter 1.

64 P. W. Atkins in *Physical Chemistry* Oxford University Press, Great Britain, **1990**, 4th Edition, Chapter 16.

65 T. R. Gilson, P. J. Hendra in *Laser Raman Spectroscopy* John Wiley and Sons, Great Britain, **1970**, Chapter 7.

66 T. R. Gilson, P. J. Hendra in *Laser Raman Spectroscopy* John Wiley and Sons, Great Britain, **1970**, Chapter 6.

67 P. W. Atkins in *Physical Chemistry* Oxford University Press, Great Britain, **1990**, 4th Edition, Chapter 25.

68 *Handbook of Thin Film Technology* (Eds. L. I. Maissel, R. Glang) McGraw-Hill, USA, **1983**, Chapter 13.

CHAPTER 2

NON-ISOTHERMAL HYDROGEN PLASMA METALLIZATION OF POLYMER SUPPORTED GOLD(III) COMPLEXES

CHAPTER 2

NON-ISOTHERMAL HYDROGEN PLASMA METALLIZATION OF POLYMER SUPPORTED GOLD(III) COMPLEXES

The aim of this chapter is to show that a non-isothermal hydrogen plasma can be used for the reduction of polymer supported gold(III) chloride layers, resulting in the production of thin gold films.

2.1 INTRODUCTION

Gold has occupied a special place throughout history due to its colour, rarity and chemically inert nature.[1] Thin gold films form the basis of many everyday applications, including decorative coatings and jewellery,[2] and electronic circuit components.[3] Methods currently employed for their deposition are evaporation under vacuum conditions, curing of screen printing inks containing gold compounds, electroplating, and chemical vapor deposition based processes.[4] Evaporation techniques have long been used for the production of gold films. It is still a widely utilized technique, and has been reported recently for the production of extremely smooth, large area gold surfaces on clean glass slides.[5] The films were about 150 nm thick and were reported to be free of contaminants. Screen printing inks consisting of a gold based metallo-polymer are applied to a surface and cured to form a gold film, either by thermal treatment of the whole sample, or the use of lasers to cause localized heating and degradation of the metallo-polymer for the generation of gold patterns.[6] However, the screen printing inks must be baked at relatively high temperatures (e.g. around 100 °C for long periods) after coating onto the sample to drive off any remaining solvent. Also the production of gold

by this technique is a thermal process, and as such is not applicable to the coating of heat sensitive substrates. The formation of electroplated gold deposits is usually carried out from a bath consisting of the gold(I) cyanide anion in slightly acidic media.[7] Electrodeposition of gold is used in the manufacture of jewelry, reflectors, and electrical contacts,[7] however disposal of the large amount of cyanide waste produced is a problem. Chemical vapor deposition (CVD) of gold using dimethylgold(III) acetylacetonate, and various fluorinated derivatives has been reported at temperatures of 300 °C.[8] Laser induced CVD of gold films has been reported using dimethylgold(III) acetylacetonate, and various fluorinated derivatives, using different laser types such as xenon chloride and Ar^+.[9, 10] Other methods have been used for the production of thin gold films, including: photolytic curing of ammoniumtetrachloroaurate/nitrocellulose films using a UV lamp,[11] direct deposition from an Au^+ ion beam,[12] or by the deposition of colloidal gold from solution.[13]

All of the methods described above require either UHV conditions, expensive metal precursors, high operating temperatures, or copious solvent use, and as such are not ideal. An alternative approach is described in this chapter which is based on the cold hydrogen plasma reduction of supported gold(III) chloride layers. Metallization via this route offers distinct advantages in terms of being able to coat heat-sensitive, three dimensional substrates, as well as virtually eliminating wastage of the metal precursor during application.

Normally, spin coated gold(III) chloride layers are unstable due to their deliquescent nature.[14] However, careful selection of solvent and substrate has been found to produce a supported film of gold(III) chloride which is stable in air. This precursor layer is made by spin coating gold(III) chloride dissolved in acetonitrile onto a Nylon 66 polymer substrate. Subsequent cold metallization is then carried out via exposure to a non-equilibrium hydrogen glow discharge, to form either continuous layers or colloidal coatings (depending on the experimental conditions), Scheme 2.1. X-ray diffraction (XRD), X-ray photoelectron spectroscopy (XPS), attenuated total reflectance Fourier transform infrared spectroscopy (ATR-FTIR), laser Raman spectroscopy, and electrical resistance measurements have been used to follow the various stages of this low temperature metallization process.

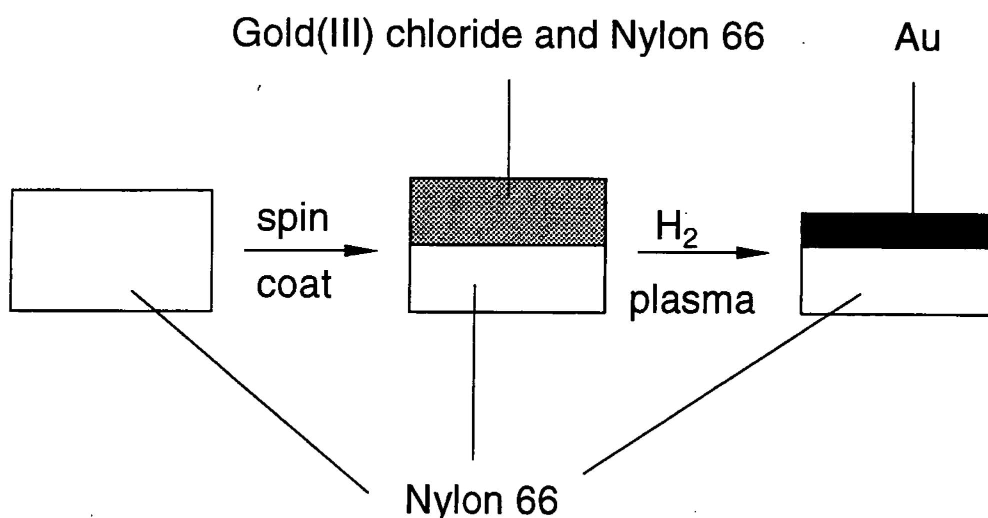

Scheme 2.1. Overview of the plasma metallization technique.

2.2 EXPERIMENTAL

A 20% wt/v solution of gold(III) chloride was prepared by dissolving 0.2 g of gold(III) chloride (Alfa, 99.99% pure) in 1 ml of acetonitrile (Sigma, Analar grade). Nylon 66 (Goodfellow) was cleaned by rinsing in a 50/50 iso-propanol/cyclohexane solvent mixture for 30 s followed by drying in air. Application of gold(III) chloride onto the Nylon substrate was carried out using a Cammax Precima spin coater, operating at a rotation speed of 1700 rpm.

Hydrogen plasma reduction of the supported gold(III) complex was performed in a custom-built plasma reactor attached directly to a VG ESCALAB surface analysis chamber (base pressure of 3×10^{-10} mbar), Figure 2.1. The glass plasma reactor (4cm diameter) was enclosed within a Faraday cage. Power was supplied from a 13.56 MHz source to a copper coil (4mm external diameter, 10 turns) wound around the plasma chamber, via a L-C matching unit and power meter. A Balzers molecular drag pump backed by a KNF diaphragm pump was used to pump the system resulting in an oil-free environment. The base pressure of the plasma chamber was better than 2×10^{-6} mbar. Hydrogen (BOC, >99.99% purity) was admitted via an needle valve (Edwards LV10K) to the required pressure. This apparatus allowed *in-situ* XPS surface analysis of the metallized coatings, without any exposure to air following glow discharge reduction. A 30 W hydrogen glow discharge running at a pressure of 0.15 mbar, was used to reduce

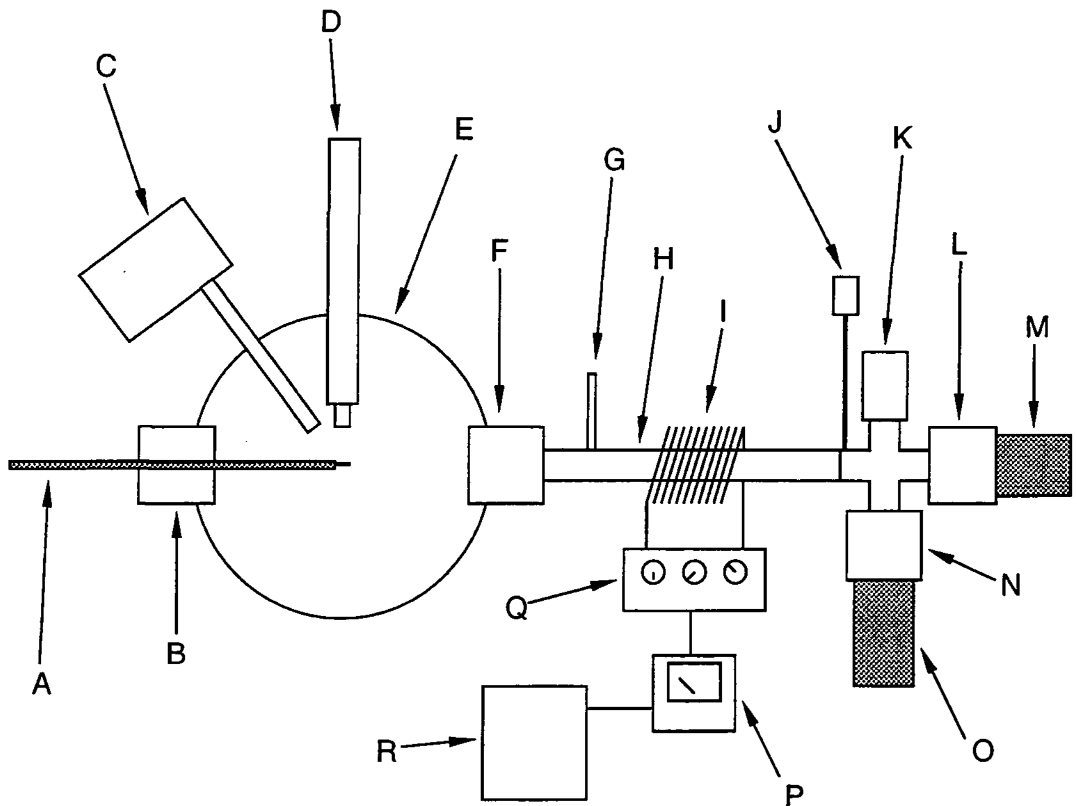

Figure 2.1. Schematic of custom built plasma chamber and XPS chamber; A, probe with sample mounted on end, B, gate valve and insertion lock, C, CHA, D, X-ray source, E, UHV chamber, F, second insertion lock and gate valve, G, gas inlet for plasma chamber, H, plasma chamber, I, copper coils, J, thermocouple pressure gauge, K, Penning pressure gauge, L, shut-off valve, M, ion pump, N, gate valve, O, molecular drag pump backed by diaphragm pump, P, SWR meter, Q, matching unit, R, r.f. generator.

the supported gold(III) chloride overlayer. XPS studies were performed using an unmonochromatised Magnesium K_α photoexcitation source and a hemispherical analyser operating in the constant analyser energy mode (CAE, 50 eV pass energy), with an electron take off angle of 30° from the substrate normal. A PC computer was used for XPS data accumulation and component peak analysis, assuming linear background subtraction and Gaussian fits. Theoretically determined sensitivity factors[15] for unit stoichiometry were taken as C(1s) : O(1s) : N(1s) : Cl(2p) : Au(4f) : Si(2p) equals 1.00 : 0.35 : 0.56 : 0.35 : 0.05 : 0.97. Trace amounts of absorbed hydrocarbon from the chamber background gases served as a reference for the photoelectron binding energy scale by setting the C(1s) peak to 285.0 eV.[16] Ar^+ ion depth profiling was carried out using a Vacuum Generators AG21 cold cathode ion gun, operating at 3 keV energy with a background argon (BOC, 99.9% purity) pressure of 2×10^{-6} mbar, and an ion current of 1.5 μA. A reference gold coated Nylon 66 sample of known thickness was used to calibrate the etch rate of gold under these Ar^+ ion gun operating conditions.

XRD scans were taken of the coated Nylon 66 substrates mounted onto glass slides using a Philips PW1050 powder diffractometer (Cu K_α X-rays generated at 35 kV and 20mA). Diffraction patterns were recorded from 4 to 110 degrees 2θ at 0.05 degree intervals with 4 s residence time at each point.

ATR-FTIR spectra were acquired on a Mattson Polaris spectrometer fitted with a Greasby Specac Golden Gate ATR accessory, over the 600-4000 cm^{-1} wavenumber range at a resolution of 4 cm^{-1}. Spectra were averaged over 32 scans, in conjunction with background subtraction.

Raman spectroscopy was performed on a Dilor LabRam Raman microscope equipped with an 1800 lines mm^{-1} diffraction grating. A helium-neon laser (632.8 nm line operating at 11mW power) was used as the excitation source, and spectra were collected over the 50 - 500 cm^{-1} region as an average of 3 scans each lasting 10 s. A 1% optical filter was used to prevent sample degradation.

Electrical resistance measurements were carried out using a Keithley model 2000 multimeter, attached to a four point resistivity probe. Electrical resistivity was then calculated, using the relationship;

$$\rho = RA / L \qquad \text{Equation 2.1}$$

where ρ (Ωcm) and R (Ω) are the resistivity and resistance of the sample respectively, A (cm^2) and L (cm) its cross sectional area (calculated using the thickness obtained from Ar^+ ion depth profiling) and length.[17]

2.3 RESULTS

XRD characterization of the coated Nylon 66 substrate revealed two scan regions of interest, corresponding to 2θ values between 35 - 110 degrees and 4 - 35 degrees: The Nylon 66 substrate itself displayed no structure in the 35 - 110 degrees 2θ region, whilst gold(III) chloride spin coated onto Nylon 66 gave rise to a tiny peak at 38.2 degrees 2θ, Figure 2.2(a). 10 s hydrogen plasma reduction of gold(III) chloride supported on Nylon 66 resulted in an increase in the size of the peak at 38.2 degrees 2θ. After 30 mins of treatment, very well defined lines at 38.2, 44.4, 64.6, 77.6, 81.7, and 98.2 degrees 2θ were discernible, which are attributable to face centred cubic (f.c.c.) crystallographic planes of metallic gold.[18] A detailed inspection of the 4 - 35 degrees 2θ range showed diffraction peaks attributable to Nylon 66 at 20.4 degrees 2θ (hydrogen bonding between chains of Nylon 66) and 23.3 degrees 2θ (hydrogen bonding between sheets of hydrogen bonded Nylon 66 chains),[19] as well as features associated with the presence of gold(III) chloride at 15.8 and 22.6 degrees 2θ, Figure 2.2(b). Diffraction lines in the 4 - 35 degrees 2θ region due to gold(III) chloride were still discernible after 10 s hydrogen glow discharge reduction of gold(III) chloride supported on Nylon 66; however, only the original diffraction peaks from the underlying Nylon 66 substrate remained in this region following 30 mins glow discharge reduction.

A shift in the XPS N(1s) binding energy from 399.8 eV to 400.6 eV was found upon spin coating Nylon 66 with gold(III) chloride (not shown). XPS analysis (without

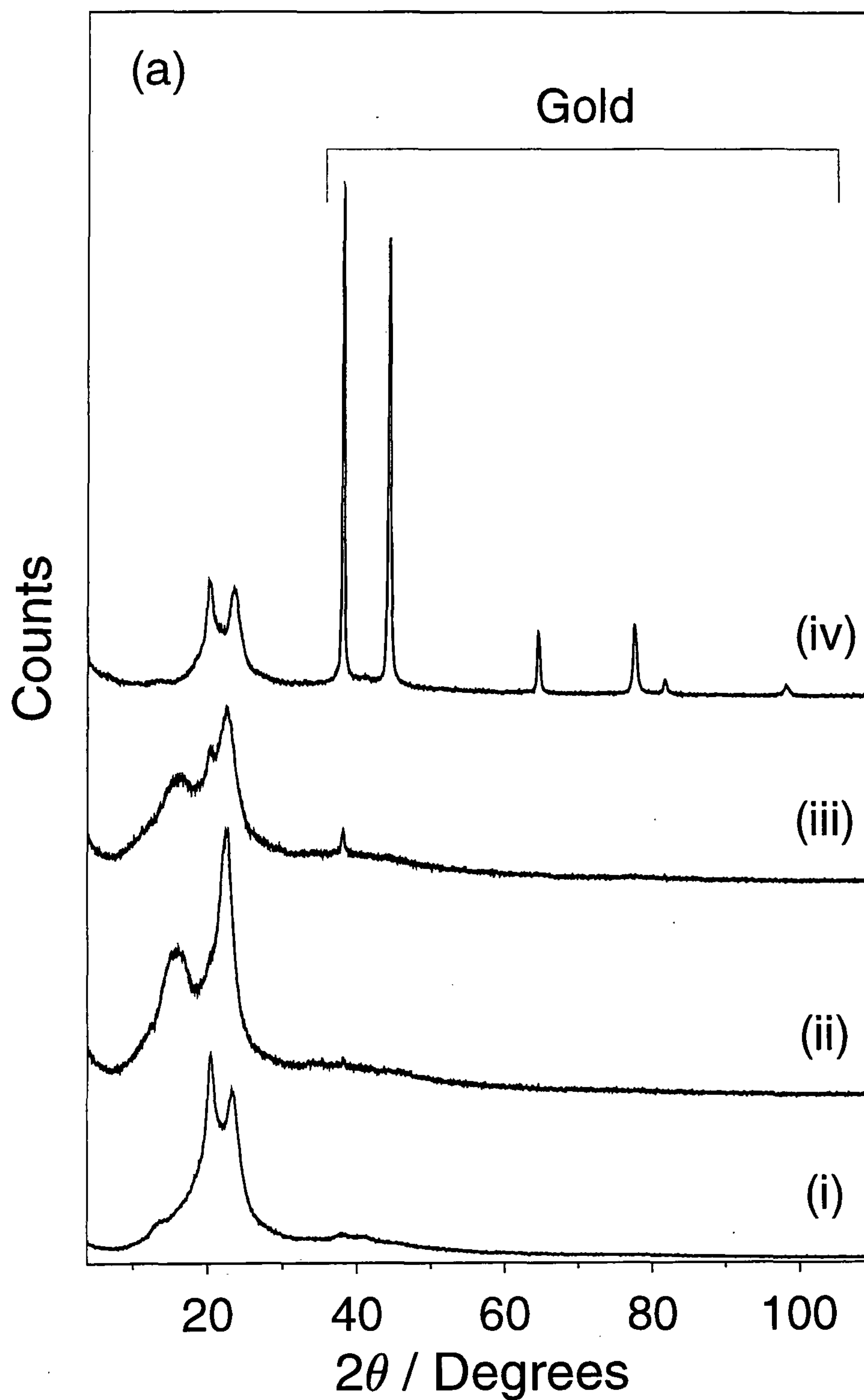

Figure 2.2(a). XRD patterns: (i) Nylon 66; (ii) Nylon 66 spin coated with gold(III) chloride; (iii) gold(III) chloride coated Nylon 66 reduced by hydrogen plasma treatment for 10 s; and (iv) gold(III) chloride coated Nylon 66 reduced by hydrogen plasma treatment for 30 mins. Note - diffraction patterns were obtained from different samples in each case.

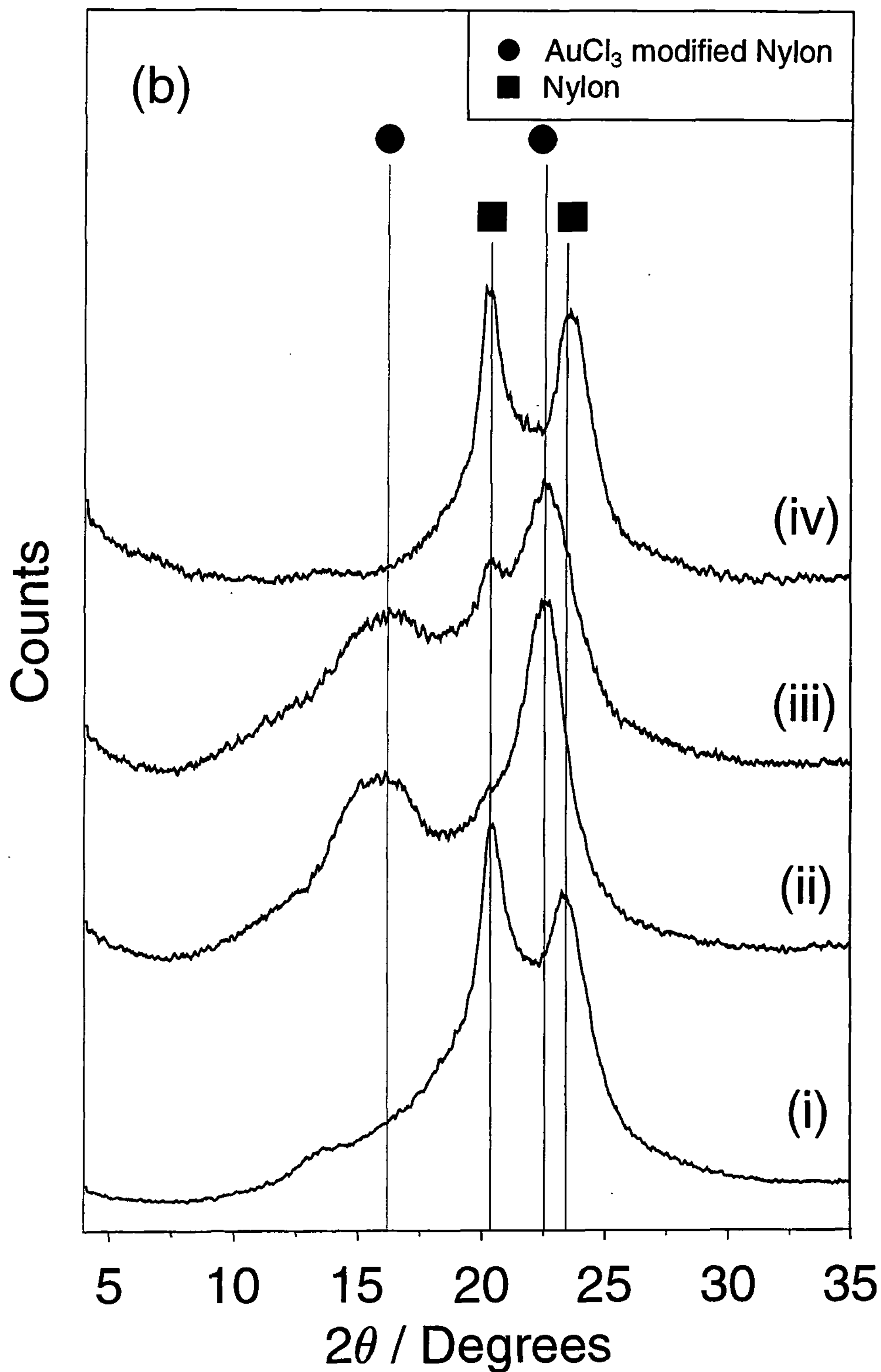

Figure 2.2(b). Expanded XRD region from 4 to 35 degrees 2θ: (i) Nylon 66; (ii) Nylon 66 spin coated with gold(III) chloride; (iii) gold(III) chloride coated Nylon reduced by hydrogen plasma treatment for 10 s; and (iv) gold(III) chloride coated Nylon 66 reduced by hydrogen plasma treatment for 30 mins. Note - diffraction patterns were obtained from different samples in each case.

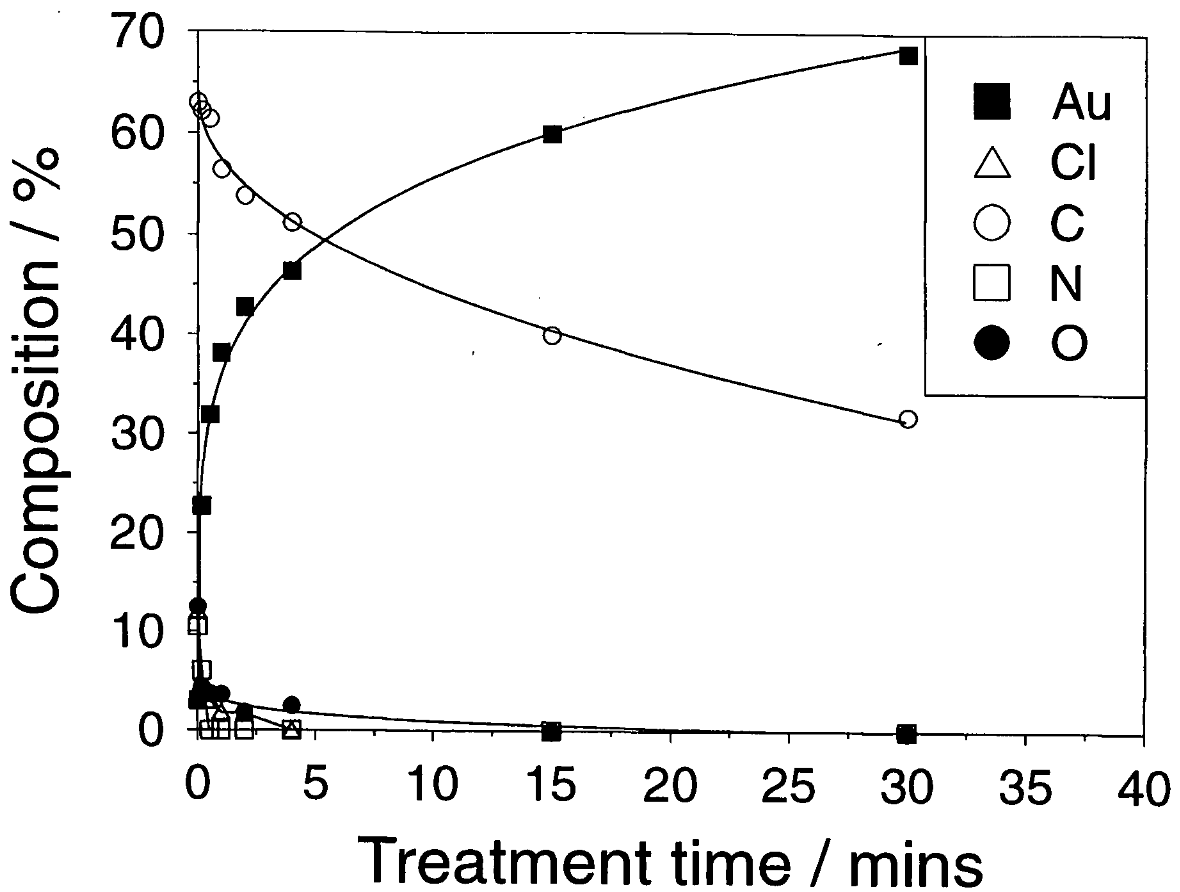

Figure 2.3. Variation in chemical composition at the surface of supported gold(III) chloride on Nylon 66 during hydrogen plasma treatment as measured by XPS.

exposure to air) following hydrogen plasma treatment, clearly showed that nitrogen disappears from the surface after just 1 min of plasma treatment, whereas chlorine takes about 4 mins, and oxygen requires approximately 15 mins. The Au(4f) doublet shifted from 87.4 eV ($4f_{7/2}$) and 91.1 eV ($4f_{5/2}$) for gold(III) chloride,[20, 21] to 84.1 and 87.8 eV respectively after just 10 s treatment time (i.e. conversion to metallic gold[22]). The XPS sampling depths for Au(4f), C(1s), Cl(2p), N(1s) and O(1s) are between 1 - 2 nm.[23] Longer plasma reduction treatments resulted in a gradual rise in gold concentration and the disappearance of carbon, Figure 2.3. The C(1s) signal can be interpreted in terms of carbon being present either at the surface, or continuously throughout the gold layer. Ar^+ ion depth profiling, indicated that most of the carbon was in fact present just at the surface (due to adsorption of background gases present in the UHV surface analysis chamber). The underlying gold layer was found to be greater than 95 ± 2% pure. Typical gold film thickness' were measured by Ar^+ ion depth profiling to be approximately 0.1 μm (although this could be varied by altering the concentration of the gold(III) chloride/acetonitrile solution employed for spin coating). The purity and thickness quoted above are both for a 30 mins hydrogen plasma reduced supported gold(III) chloride layer.

Electrical resistance measurements performed on the metallized layers indicated that the onset of metallic behaviour occurred around approximately 15 mins of hydrogen plasma treatment. The electrical resistivity of the resultant gold film was measured to be 3×10^{-5} Ωcm, which is comparable to that reported for bulk metallic gold (2.24×10^{-6} Ωcm).[24]

ATR-FTIR spectra taken of Nylon 66 displayed absorption features corresponding to hydrogen bonded N-H stretches (3290 cm^{-1}), amide groups (1630 and 1535 cm^{-1}) and CH_2 stretches (2934 and 2859 cm^{-1})[25], Figure 2.4. Spin coating of gold(III) chloride onto Nylon 66 gave rise to a new peak at about 3350 cm^{-1} due to the formation of weakly bound hydrogen bonds (e.g. the interaction between N-H···Cl groups from Nylon 66 and gold(III) chloride respectively[29]) in conjunction with a broadening and attenuation of the N-H stretch at 3290 cm^{-1} associated with hydrogen bonding between adjacent Nylon 66 chains.[26] In addition a new absorption band appeared at 1600 cm^{-1} located in-between the Amide I (1630 cm^{-1}) and Amide II (1535 cm^{-1}) regions, which can be attributed to bonding between gold centres and -NHCO- linkages in Nylon 66 giving rise to a $[L_xAuCl_2]^+$ type structure, where L is Nylon 66.[29] The infra-red absorption features

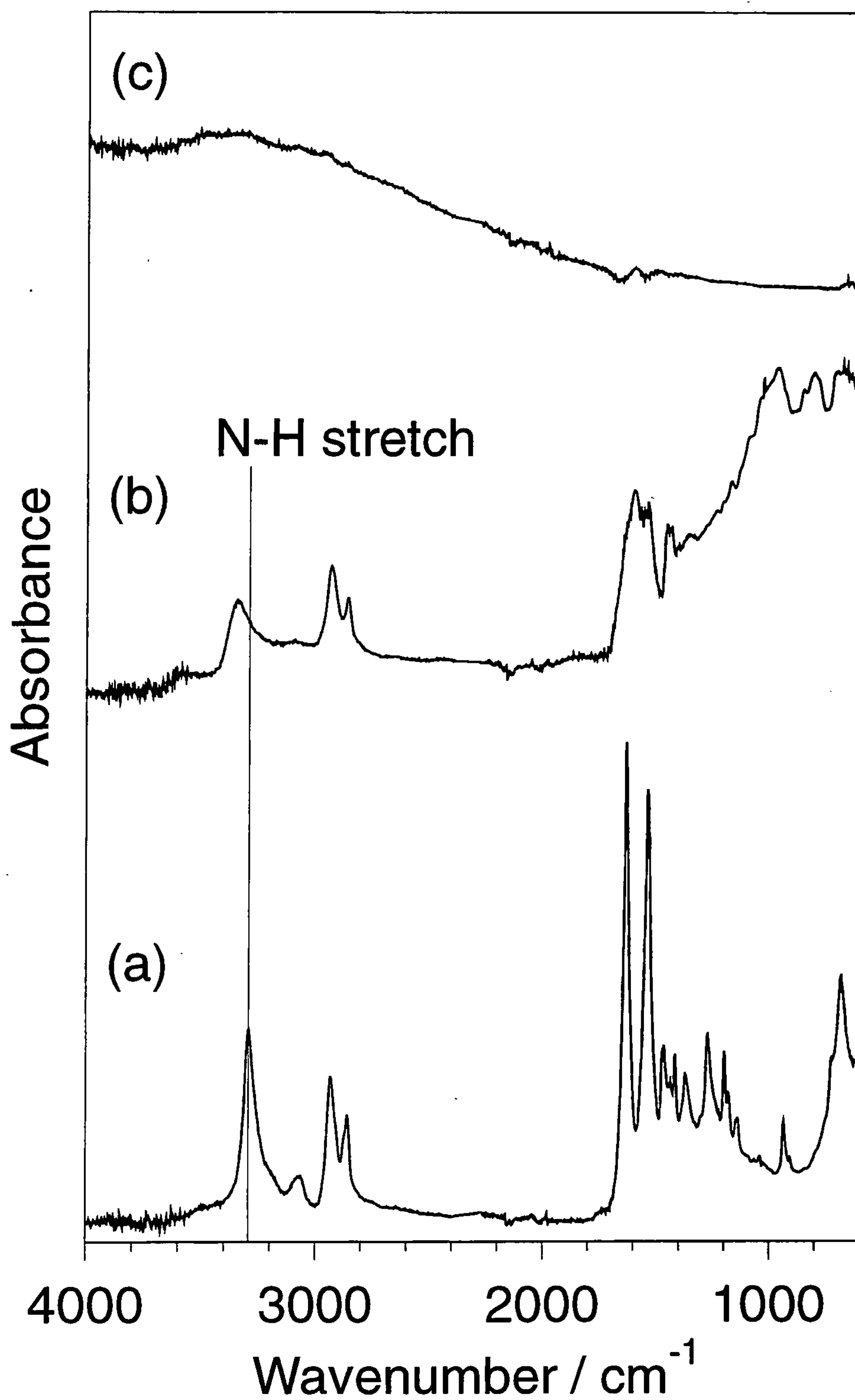

Figure 2.4. ATR-FTIR spectra of: (a) Nylon 66; (b) Nylon 66 spin coated with gold(III) chloride; and (c) 30 mins hydrogen plasma reduced gold(III) chloride coated Nylon 66.

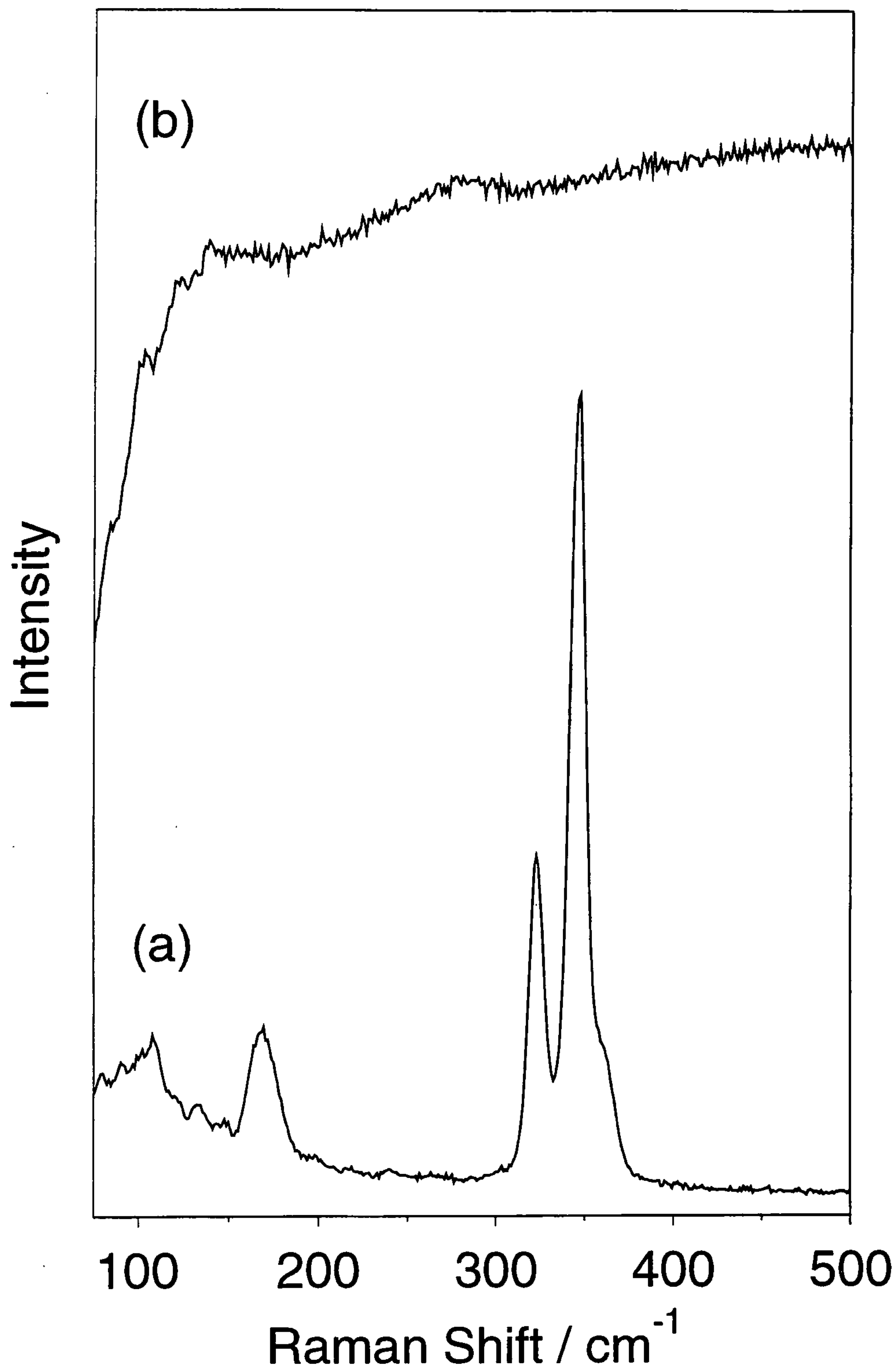

Figure 2.5. Raman spectra of: (a) Nylon 66 coated with gold(III) chloride and; (b) after 30 mins hydrogen reduction of gold(III) chloride coated Nylon 66.

characteristic of Nylon 66 were no longer discernible following 30 mins hydrogen glow discharge reduction. Instead a broad featureless continuum produced by metallic gold was evident (a sample of gold foil was analysed for verification).

Raman spectra taken of gold(III) chloride coated onto Nylon 66 displayed strong features at 167, 322 and 346 cm^{-1}, which were not present in the spectra of just the Nylon 66 substrate, Figure 2.5. These bands appear in the same region as those previously reported for the Raman spectra of the $[AuCl_4]^-$ anion.[27] Following hydrogen plasma reduction, these features were no longer observable, and only a broad fluorescence background signal due to the metallic gold layer remained.

2.4 DISCUSSION

Nylon 66 was selected as a substrate in this particular case since its amide groups are able to participate in bonding with gold(III) chloride, due to the affinity of gold in the +3 oxidation state (which is a hard Lewis acid) towards nitrogen based ligands,[28] thereby promoting co-ordination of the gold(III) chloride onto the Nylon 66 substrate. Such a Lewis acid-base interaction between metal chlorides (e.g. $FeCl_3$ and $NiCl_2$) and polyamides in solution has been noted previously,[29, 30] this generally leads to the formation of ionic species of the type $[L_xMCl_{y-2}]^+$ $[MCl_y]^-$, where L is Nylon and M is the metal. In the present study, ATR-FTIR analysis has shown that there is indeed an interaction between Nylon 66 and gold(III) chloride upon spin coating: The ATR-FTIR absorption feature at 3350 cm^{-1} is attributed to the formation of weakly bound hydrogen bonds between the N-H···Cl groups from Nylon 66 and gold(III) chloride respectively,[29] and the new band at approximately 1600 cm^{-1} can be assigned to an interaction between -NHCO- groups of the Nylon 66 and gold in an $[L_xAuCl_2]^+$ type structure.[29] This is consistent with the observed shift in binding energy of the N(1s) XPS peak from 399.8 eV to 400.4 eV upon spin coating (not shown). Furthermore, Raman spectroscopy has provided supporting evidence for the presence of the $[AuCl_4]^-$ anion. Therefore a possible structure of the co-ordinated gold(III) chloride can therefore be inferred as being $[L_xAuCl_2]^+$ $[AuCl_4]^-$, Scheme 2.2.

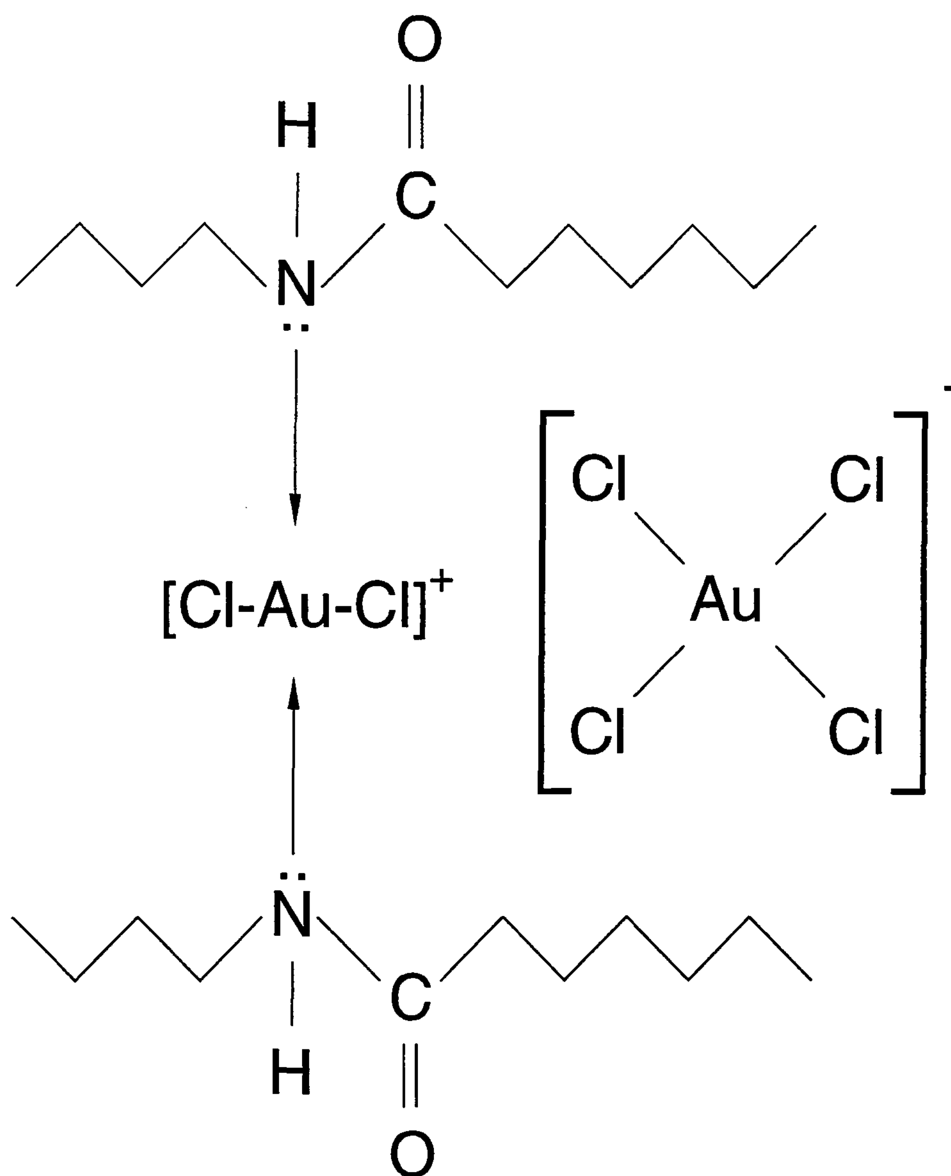

Scheme 2.2. Proposed co-ordination of gold(III) chloride onto the Nylon 66 surface.

Nylon 66 is soluble in the gold(III) chloride/acetonitrile solution and one would expect gold(III) chloride to become co-ordinated to chains of Nylon 66 during spin coating; this is consistent with the XRD results, where an increase in d- spacing between both adjacent chains and sheets of Nylon 66 following spin coating with gold(III) chloride is observed. The high affinity of gold in the +3 oxidation state towards nitrogen ligands could in principle also lead to complex formation between gold(III) chloride and acetonitrile, however no increase in N(1s) XPS signal intensity was seen, and -CN group infra-red stretch (expected at 2253 cm^{-1}) from acetonitrile were absent for spin coated

gold(III) chloride layers on Nylon 66. Other solvents (e.g. methanol, iso-propanol, and water) and substrates (e.g. PE, PET, PVC, PTFE) were found to yield deliquescent layers of gold(III) chloride which absorbed water from the laboratory atmosphere forming droplets at the surface, and thereby producing non-uniform metallic layers upon hydrogen plasma reduction.

The highly efficient hydrogen plasma reduction of gold(III) chloride supported on Nylon 66 can be attributed to the reaction between atomic hydrogen, generated by the electrical discharge, and the supported metal salt complex,[31, 32, 33, 34, 35] leading to the removal of O, N, Cl and C from the surface via the desorption of OH_x, HCl, NH_y and CH_z moieties[31] to leave behind a gold layer (since gold does not form a stable hydride species[36, 37]), Scheme 2.1. It was found that variation of the plasma processing conditions (power and duration of treatment) could be used to change the surface appearance from yellow (due to gold(III) chloride) to green, red or purple gold films (metallic gold as detected by XPS). However, all of these treated films were found to be electrically insulating. These colour variations can be attributed to the formation of colloidal gold.[38] Prolonged hydrogen plasma reduction times (i.e. greater than 15 mins), always gave rise to a strong gold coloration in association with good electrical conductivity, thereby corresponding to the bulk metallic state.

2.5 CONCLUSIONS

This chapter has shown that formation of both continuous gold films and colloidal gold can be achieved using a non-isothermal hydrogen plasma, by varying the reaction conditions. During plasma treatment chlorine, carbon, nitrogen and oxygen were selectively removed from the surface of the Nylon 66 coated gold(III) chloride layer. The gold fraction at the surface increased as the treatment time was increased. For the longest reduction (30 mins) the resultant gold films were 95% pure as shown by XPS. The method of metal layer formation described here offers many potential new uses in areas where conventional metallization techniques are considered to be inappropriate, e.g. for the coating of heat sensitive materials in the micro-electronics industry, and the production of catalytic membranes. Furthermore, careful choice of metal salt/polymer/ solvent combinations will allow this plasma metallization methodology to be adapted to other metal/substrate systems. In the case of gold(III) chloride dissolved in acetonitrile,

virtually any solid surface can be coated by this technique if a priming layer of plasma polymer containing amine functionalities is deposited first (this effectively provides the anchoring amine groups needed for the complexation of gold(III) chloride).

2.6 REFERENCES

1 R. J. Puddephatt in *The Chemistry of Gold*, Elsevier Scientific Publishing Company, Amsterdam, **1978**, Chapter 1.

2 *Handbook of Deposition Technologies for Films and Coatings* (Ed. R. F. Bunshah) Noyes Publications, Park Ridge, New Jersey, 2nd Edition, **1994**, Chapter 1.

3 D. M. Brown, W. E. Engeler, M. Garfinkel, F. K. Heumann, *J. Electrochem. Soc.* **1967**, *114*, 730.

4 *Laser Microfabrication: Thin Film Processes and Lithography* (Eds. D. J. Ehrlich, J. Y. Tsao) Academic Press, USA, **1989**, Chapter 8.

5 N. G. Woodard, G. P. Lafjatis, *J. Vac. Sci. Technol. A* **1996**, *14*, 332.

6 G. J. Fisanick, M. E. Gross, J. B. Hopkins, M. D. Fennell, K. J. Schnoes, A. Katzir, *J. Appl. Phys.* **1985**, *57*, 1139.

7 *Handbook of Deposition Technologies for Films and Coatings* (Ed. R. F. Bunshah) Noyes Publications, USA, **1994**, Chapter 10, p. 483.

8 C. E. larson, T. H. Baum, R. L. Jackson, *J. Electrochemical Soc.* **1987**, *134*, 266.

9 D. Wexler, J. I. Zink, L. W. Tutt, S. R. Lunt, *J. Phys. Chem.* **1993**, *97*, 13563.

10 T. H. Baum, C. R. Jones, *Appl. Phys. Lett.* **1985**, *47*, 538.

11 Y. Ye, R. G. Hunsperger, *Appl. Phys. Lett.* **1987**, *51*, 2136.

12 S. Nagamachi, Y. Yamakage, H. Maruno, M. Ueda, S. Sugimoto, M. Asari, J. Ishikawa, *Appl. Phys. Lett.* **1993**, *62*, 2143.

13 S. Rubin, G. Bar, T. N. Taylor, R. W. Cutts, T. A. Zawodzinski Jr., *J. Vac. Sci. Technol. A* **1996**, *14*, 1870.

14 J. W. Mellor in *A Comprehensive Treatise on Inorganic and Theoretical Chemistry*, Volume 3, Longmans Green, London, **1923**, Chapter 23, Section 16.

15 M. P. Seah, M. T. Anthony *Surf. Inter. Anal.* **1984**, *6*, 230.

16 G. Beamson, D. Briggs in *High Resolution XPS of Organic Polymers The Scienta ESCA300 Database*, John Wiley and Sons, Chicester, England, **1992**, Chapter 6, 26.

17 P. W. Atkins in *Physical Chemistry*, Oxford University Press, Great Britain, 4th Edition, **1990**, Chapter 25.

18 H. E. Swanson, E. Tatge, *Natl. Bur. Stand. (U.S.) Circ.* **1953**, *539*, 33.

19 N. S. Murphy, S. A. Curran, S. M. Aharoni, H. Minor, *Macromolecules* **1991**, *24*, 3215.

20 M. Batista-Leal, J. E. Lester, C. A. Lucchesi, *J. Elect. Spec. Rel. Phenom.* **1977**, *11*, 333.

21 Kosaku Kishi, Shigero Ikeda, *J. Phys. Chem.* **1974**, *78*, 107.

22 J. F. Moulder, W. F. Stickle, P. E. Sobol, K. D. Bomben in *Handbook of X-ray Photoelectron Spectroscopy* (Ed. J. Chastain) Perkin Elmer Corporation, Minnesota, USA, **1992**, Chapter II.

23 M. P. Seah, W.A. Dench, *Surf. Interface Anal.* **1979**, *1*, 2.

24 *Handbook of Physics and Chemistry* (Ed. R. C. Weast) CRC Press, 63rd Edition, Florida, USA, **1982**, Section F-133.

25 K. T. Hecht, D. L. Wood, *Proc. Roy. Soc. Lond. A.* **1956**, *235*, 174.

26 L. R. Schroeder, S. L. Cooper, *J. Appl. Phys.* **1976**, *47*, 4310.

27 I. A. Degen, A. J. Rowlands, *Spectrochmica Acta* **1991**, *47A*, 1263.

28 R. J. Puddephatt in *The Chemistry of Gold*, Elsevier Scientific Publishing Company, Amsterdam, **1978**, Chapter 5.

29 J. C. Lassègues, J. Grondin, M. Hernandez, I. Rey, L. Servant, S. - J. Wen, *New J. Chem.* **1996**, *20*, 317.

30 C.-C. Yen, C.-J. Huang, T.-C. Chang, *J. Appl. Poly. Sci.*, **1991**, *42*, 439.

31 F. K. McTaggart in *Plasma Chemistry in Electrical Discharges*, Elsevier Publishing Company, Amsterdam, **1967**, Chapter 6.

32 H. Turcicova, H. Arend, O. Jarolimek, *Solid State Comm.* **1995**, *93*, 979.

33 F. K. McTaggart, *Austr. J. Chem.* **1965**, *18*, 937.

34 F. K. McTaggart, *Austr. J. Chem.* **1965**, *18*, 949.

35 F. K. McTaggart, A. G. Turnbull, *Austr. J. Chem.* **1964**, *17*, 727.

36 H. Ringstrom, *Nature* **1963**, *198*, 981.

37 H. Ringstrom, *Ark. Fiz.* **1964**, *27*, 227.

38 R. J. Puddephatt in *The Chemistry of Gold*, Elsevier Scientific Publishing Company, Amsterdam, **1978**, Chapter 2.

CHAPTER 3

NON-ISOTHERMAL NOBLE GAS PLASMA METALLIZATION OF POLYMER SUPPORTED GOLD(III) COMPLEXES

CHAPTER 3

NON-ISOTHERMAL NOBLE GAS PLASMA METALLIZATION OF POLYMER SUPPORTED GOLD(III) COMPLEXES

Chapter 2 has illustrated that the reduction of polymer supported gold(III) chloride films using a non-isothermal plasma is possible. It is well known that the gas used for plasma treatment has a strong effect on the nature of the surface modification experienced by the sample. An alternative approach is described in this chapter which is based on the reduction of supported gold(III) chloride using argon and helium cold plasmas. These plasmas will not chemically reduce the supported gold(III) chloride layers like the hydrogen plasma, but do contain excited metastable species and generate vacuum ultra-violet radiation, and have been used widely for surface modification.

3.1 INTRODUCTION

Noble gas plasma treatment result in the creation of free radical centres, and cross-linking of polymer chains. This treatment can result in a number of physical changes to the sample: the topology of polymer substrates can be altered by varying the noble gas used for treatment,[1, 2, 3] and the frictional[4] and electrical[5] properties of the polymer samples can also be altered. Energy transfer from the plasma to the surface of the sample is thought to occur by both direct energy transfer, e.g. by ions and neutrals, and from photons.[6] However, modification of the bulk of the sample takes place mainly through the action of the electromagnetic radiation.[7] Ablation of the substrate by the plasma is more predominant for the heavier gases, e.g. argon > helium. Metastable states in noble gas discharges have greater energy (for example He 19.8 eV, Ar 11.5 eV) than

bonds in the polymer backbone and will be able to cause chain scission.[8] Plasmas are a good source of electromagnetic radiation, ranging in frequency from radio frequency up to vacuum ultraviolet (VUV).[9] The intensity of VUV produced decreases the higher the atomic number of the noble gas used for the plasma. Polymers are excellent absorbers of UV radiation and undergo free radical formation in the process.[10] From the modeling of interactions between low energy ion beams and polymer surfaces it has been shown that there is no chemical interaction during noble gas plasma treatment.[11, 12] Although helium, neon and argon are all used in plasma technology, argon is the most commonly used due to its lower cost.[13] The CASING (cross-linking by activated species in inert gases) process uses inert gas plasmas to induce hydrogen abstraction and free radical formation to produce cross-linking and removal of low molecular weight material, which allows stronger adhesive joints to be made to the polymer.[14, 15]

As has been previously reported, spin coated gold(III) chloride layers are unstable due to their deliquescent nature.[16] However, in this work careful selection of solvent and substrate has been found to produce a supported film of gold(III) chloride which is stable in air. This precursor layer is made by spin coating gold(III) chloride dissolved in acetonitrile onto a Nylon 66 polymer substrate. Subsequent cold metallization is then carried out via exposure to a non-equilibrium glow discharge of either argon or helium, to form continuous gold layers. X-ray diffraction (XRD), X-ray photoelectron spectroscopy (XPS), attenuated total reflectance Fourier transform infrared spectroscopy (ATR-FTIR), and electrical resistance measurements have been used to follow the various stages of this low temperature metallization process.

3.2 EXPERIMENTAL

Spin coated gold(III) chloride layers on Nylon 66 were produced as described in Chapter 2. Plasma reduction of the supported gold(III) complex was performed in a custom-built plasma reactor attached directly to a VG ESCALAB surface analysis chamber (base pressure of 3×10^{-10} mbar). The glass plasma reactor (4cm diameter) was enclosed within a Faraday cage (see Chapter 2 for diagram). Power was supplied from a 13.56 MHz source to a copper coil (4mm external diameter, 10 turns) wound around the plasma chamber, via a L-C matching unit and power meter. A Balzers molecular drag pump backed by a KNF diaphragm pump was used to pump the system resulting in an oil-free

environment. The base pressure of the plasma chamber was better than 2 x 10^{-6} mbar. Argon (BOC, > 99.99% purity) or helium (BOC, >99.99% purity) was admitted via an needle valve (Edwards LV10K) to the required pressure. This apparatus allowed *in-situ* XPS surface analysis of the metallized coatings, without any exposure to air following glow discharge reduction. A 30 W helium or 20 W argon glow discharge running at a pressure of 0.15 mbar for a duration of 30 mins, was used to reduce the supported gold(III) chloride overlayer. XPS studies were performed using an unmonochromatised Magnesium K_α photoexcitation source and a hemispherical analyzer operating in the constant analyser energy mode (CAE, 50 eV pass energy), with an electron take off angle of 30° from the substrate normal. A PC computer was used for XPS data accumulation and component peak analysis, assuming linear background subtraction and Gaussian fits. Theoretically determined sensitivity factors[17] for unit stoichiometry were taken as C(1s) : O(1s) : N(1s) : Cl(2p) : Au(4f) : Si(2p) equals 1.00 : 0.35 : 0.56 : 0.35 : 0.05 : 0.97. Trace amounts of absorbed hydrocarbon from the chamber background gases served as a reference for the photoelectron binding energy scale by setting the C(1s) peak to 285.0 eV.[18] Ar^+ ion depth profiling was carried out using a Vacuum Generators AG21 cold cathode ion gun, operating at 3 keV energy with a background argon (BOC, 99.9% purity) pressure of 2×10^{-6} mbar, and an ion current of 1.5 μA. A reference gold coated Nylon 66 sample of known thickness was used to calibrate the etch rate of gold under these Ar^+ ion gun operating conditions.

XRD, ATR-FTIR, and electrical resistance measurements were performed on the spin coated and reduced samples according to Chapter 2.

3.3 RESULTS

As in Chapter 2 XRD characterization of the coated Nylon 66 substrate revealed two scan regions of interest, corresponding to 2θ values between 35 - 110 degrees and 4 - 35 degrees: The Nylon 66 substrate itself displayed no structure in the 35 - 110 degrees 2θ region, whilst gold(III) chloride spin coated onto Nylon 66 gave rise to a tiny peak at 38.2 degrees 2θ, Figure 3.1. After 30 mins of plasma treatment with both argon and helium, very well defined lines at 38.2, 44.4, 64.6, 77.6, 81.7, and 98.2 degrees 2θ were discernible, which are attributable to face centred cubic (f.c.c.) crystallographic planes of

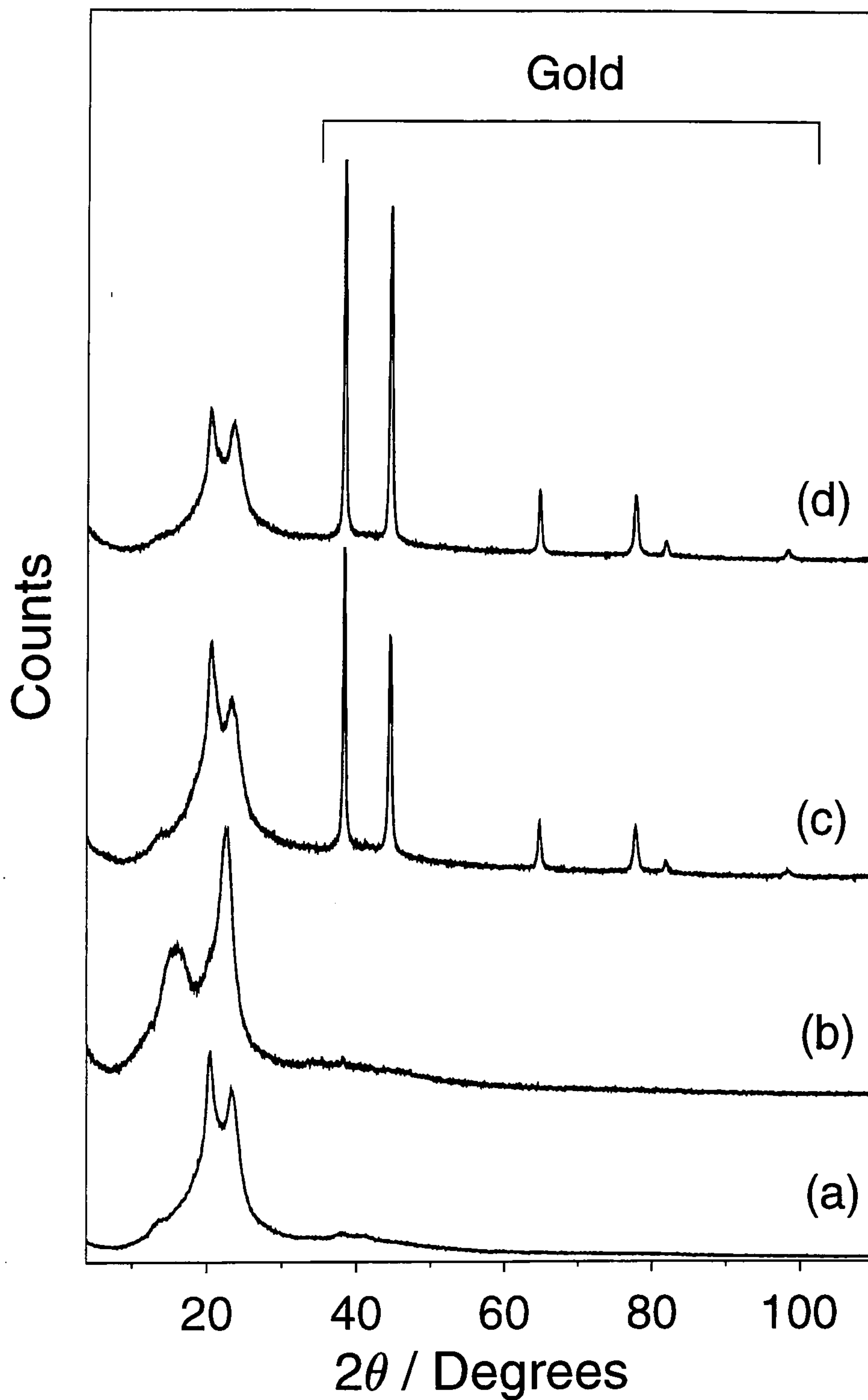

Figure 3.1. XRD patterns: (a) Nylon 66; (b) Nylon 66 spin coated with gold(III) chloride; (c) gold(III) chloride coated Nylon 66 reduced by argon plasma treatment for 30 mins; and (d) gold(III) chloride coated Nylon 66 reduced by helium plasma treatment for 30 mins. Note - diffraction patterns were obtained from different samples in each case.

metallic gold.[19] A detailed inspection of the 4 - 35 degrees 2θ range showed diffraction peaks attributable to Nylon 66 at 20.4 degrees 2θ (hydrogen bonding between chains of Nylon 66) and 23.3 degrees 2θ (hydrogen bonding between sheets of hydrogen bonded Nylon 66 chains),[20] as well as features associated with the presence of gold(III) chloride at 15.8 and 22.6 degrees 2θ. However, only the original diffraction peaks from the underlying Nylon 66 substrate remained in this region following 30 mins glow discharge decomposition with both argon and helium.

XPS analysis (without exposure to air) following plasma treatment, clearly showed that nitrogen and chlorine disappear from the surface of the supported gold(III) chloride layers, and that the amount of carbon is drastically reduced with a concomitant increase in the gold signal, Figure 3.2. Helium plasma reduction results in a large amount a silicon and oxygen appearing on the sample, in the ratio Si : O ≈ 1 : 2, whilst after argon plasma reduction only a small amount of oxygen contamination is seen and no silicon is observed. For treatment in both gases the Au(4f) doublet shifted from 87.4 eV ($4f_{7/2}$) and 91.1 eV ($4f_{5/2}$) for gold(III) chloride,[21, 22] to 84.1 and 87.8 eV respectively after plasma reduction (i.e. conversion to metallic gold[23]). The XPS sampling depths for Au(4f), C(1s), Cl(2p), N(1s) and O(1s) are between 1 - 2 nm.[24]

Ar^+ ion depth profiling, indicated that all of the carbon, oxygen and silicon seen on the plasma treated samples was in fact present just at the surface (due to deposition during the plasma reduction stage). The underlying gold layer was found to be 100% pure, as shown by the absence of lines others than those attributable to gold in the XPS widescans, Figure 3.3. Typical gold film thickness' were measured by Ar^+ ion depth profiling to be approximately 180 nm for both helium and argon plasma reduced gold(III) layers (the sputter rate was calibrated using a standard gold sample of known thickness as outlined in Chapter 2). Helium plasma reduction lead to a relatively sharp interface between the gold film and underlying layer, whilst argon plasma reduction produced a diffuse interfacial layer, Figure 3.4.

The electrical resistivity of the resultant gold films was measured to be 9×10^{-6} Ωcm and 2×10^{-5} Ωcm for the argon and helium plasma reduced films respectively, both of which are comparable to that reported for bulk metallic gold (2.24×10^{-6} Ωcm).[25]

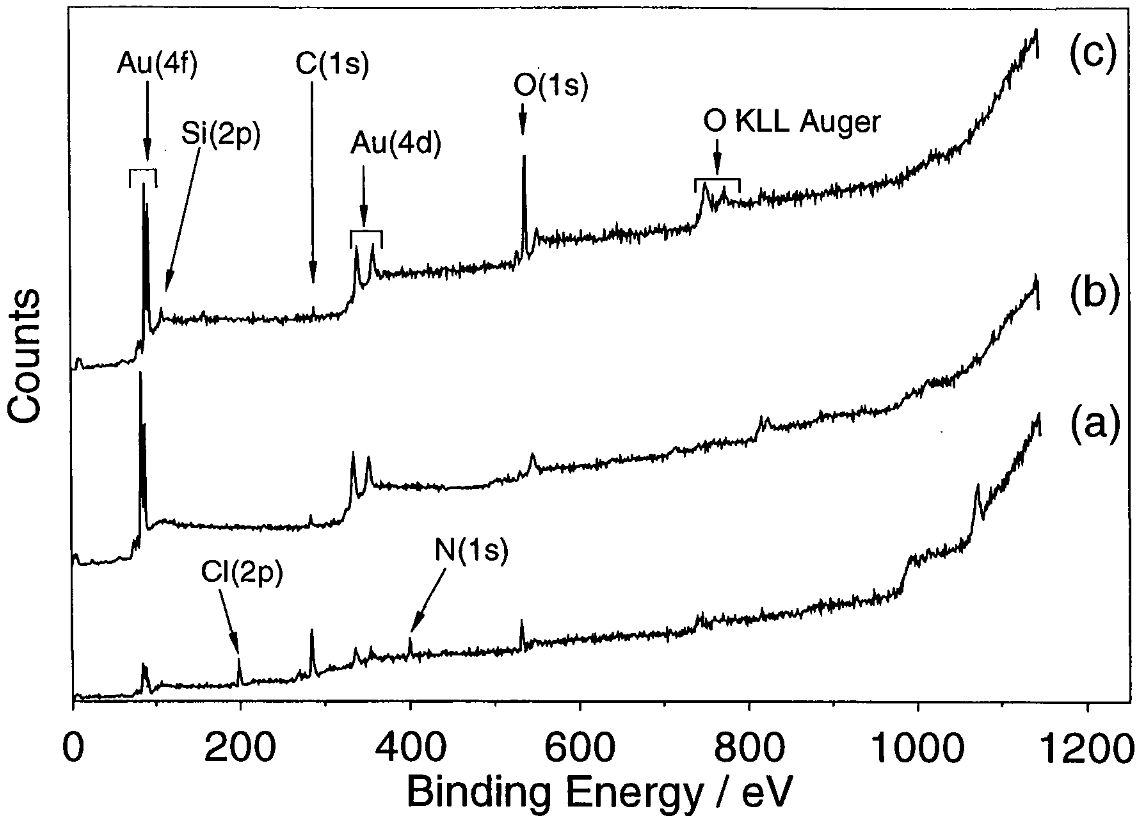

Figure 3.2. XPS widescans of a) Nylon 66 spin coated with gold(III) chloride; b) gold(III) chloride coated Nylon 66 reduced by 30 mins argon plasma; and c) gold(III) chloride coated Nylon 66 reduced by 30 mins helium plasma.

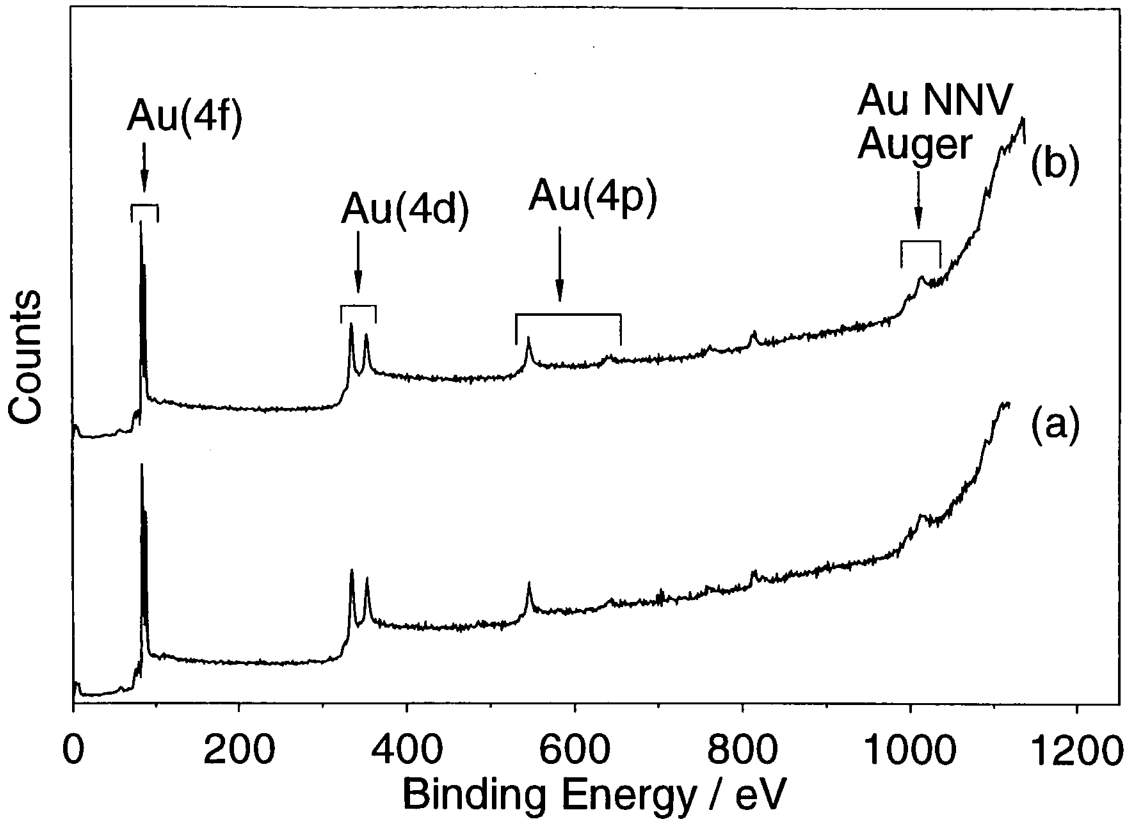

Figure 3.3. XPS widescans of argon ion cleaned layers of a) gold(III) chloride coated Nylon 66 reduced by 30 mins argon plasma; and b) gold(III) chloride coated Nylon 66 reduced by 30 mins helium plasma.

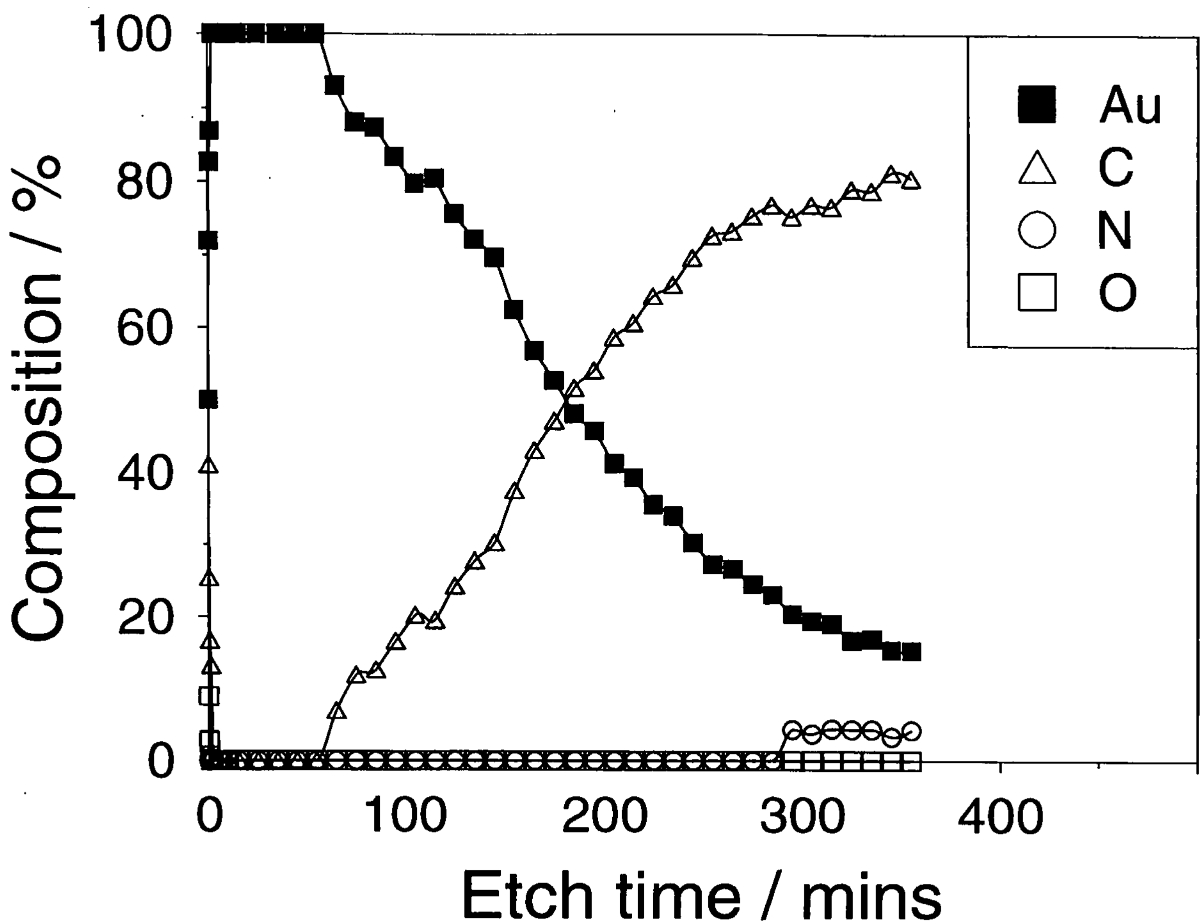

Figure 3.4(a). Depth profile of 30 mins argon plasma reduced Nylon 66 coated gold(III) chloride layer.

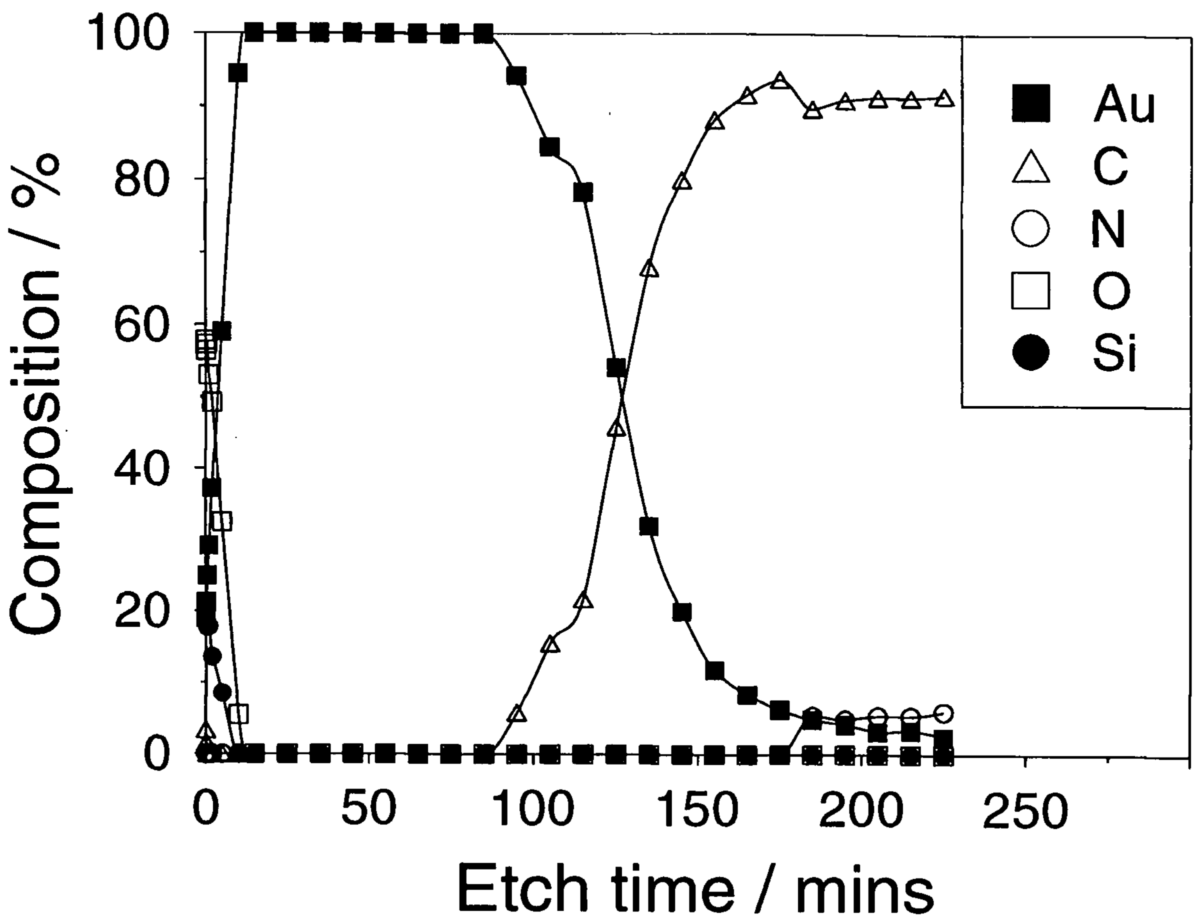

Figure 3.4(b). Depth profile of 30 mins helium plasma reduced Nylon 66 coated gold(III) chloride layer.

ATR-FTIR spectra taken of Nylon 66 displayed absorption features corresponding to hydrogen bonded N-H stretches (3290 cm^{-1}), amide groups (1630 and 1535 cm^{-1}) and CH_2 stretches (2934 and 2859 cm^{-1})[26], Figure 3.5. Spin coating of gold(III) chloride onto Nylon 66 gave rise to a new peak at about 3350 cm^{-1} due to the formation of weakly bound hydrogen bonds (e.g. the interaction between N-H···Cl groups from Nylon 66 and gold(III) chloride respectively[27]) in conjunction with a broadening and attenuation of the N-H stretch at 3290 cm^{-1} associated with hydrogen bonding between adjacent Nylon 66 chains.[28] In addition a new absorption band appeared at 1600 cm^{-1} located in-between the Amide I (1630 cm^{-1}) and Amide II (1535 cm^{-1}) regions, which can be attributed to bonding between gold centres and -NHCO- linkages in Nylon 66 giving rise to a $[L_xAuCl_2]^+$ type structure, where L is Nylon 66.[27] The infra-red absorption features characteristic of Nylon 66 were no longer discernible following 30 mins glow discharge reduction in both argon and helium. Instead a broad featureless continuum produced by metallic gold was evident (a sample of gold foil was analyzed for verification). Also helium plasma reduction gave rise to a small feature around 1200 cm^{-1}, which was not seen on the argon plasma treated sample.

3.4 DISCUSSION

The nature of the interaction between gold(III) chloride and Nylon 66 has been outlined already in Chapter 2. In the present study, ATR-FTIR analysis has shown that as in hydrogen plasma reduction, noble gas plasma treatment leads to removal of all trace of bands attributed to Nylon 66. This is consistent with the removal of the polymeric species during treatment; only the broad metallic continuum is observed. For helium plasma reduction there is a small feature at around 1200 cm^{-1}, which if the large amount of silicon and oxygen detected by XPS is considered, can be attributed to the presence SiO_x type species.[29] This band is not present on argon plasma treated supported gold(III) chloride layers, and is probably due to deposition of glass from the walls of the reactor during the plasma treatment. Electrical resistance methods have also indicated the high purity of the resultant films. It should be noted here that argon plasma reduction was performed at a lower power than the helium to reduce the degree of thermal degradation experienced by the sample during treatment.

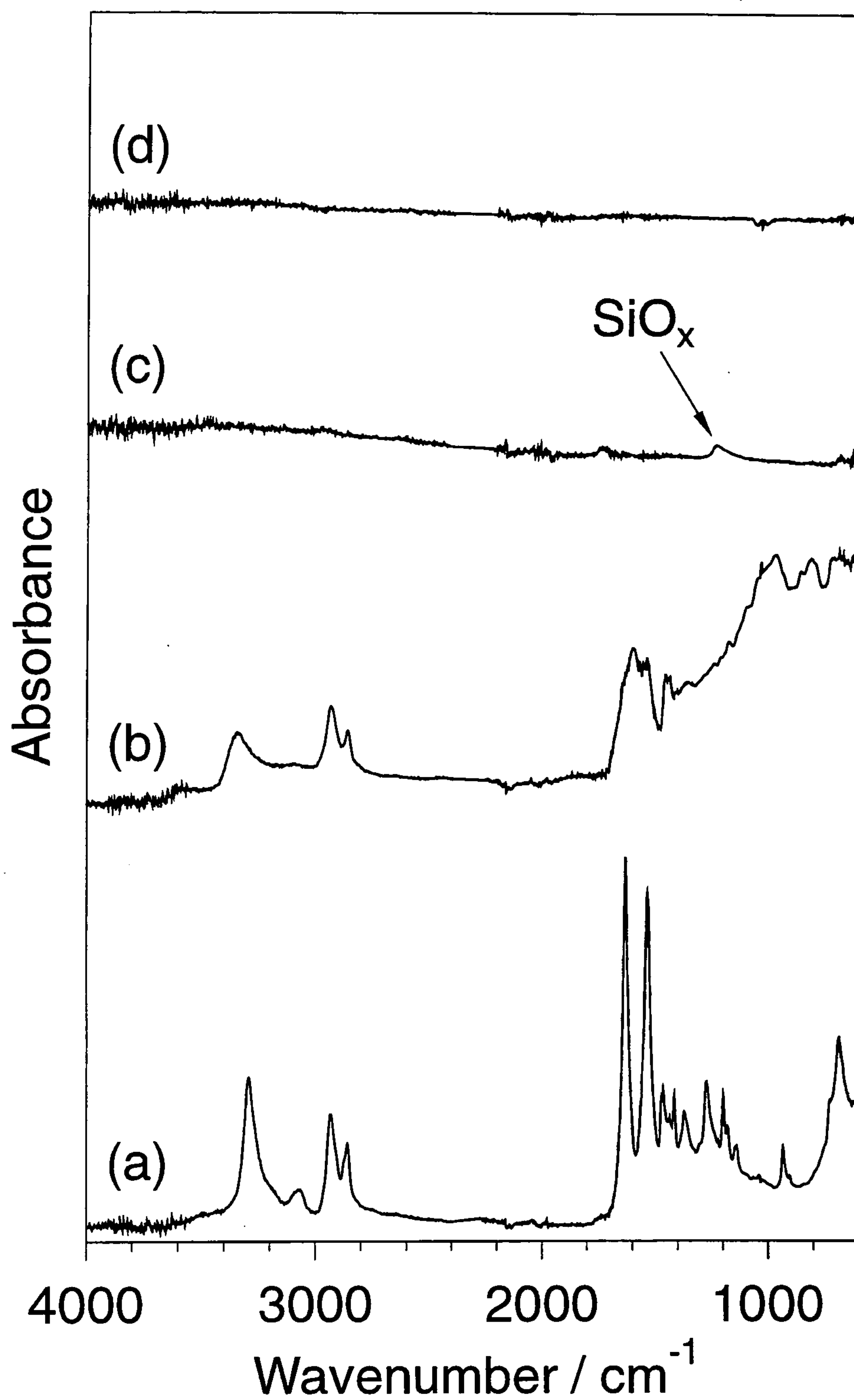

Figure 3.5. ATR-FTIR spectra of: (a) Nylon 66; (b) Nylon 66 spin coated with gold(III) chloride; (c) 30 mins helium plasma reduced gold(III) chloride coated Nylon 66; and (d) 30 mins argon plasma reduced gold(III) chloride coated Nylon 66.

The highly efficient plasma reduction of gold(III) chloride supported on Nylon 66 can be attributed to two main factors: physical sputtering of the sample by the noble gas plasma, and the interaction of VUV from the plasma with the sample. Noble gas plasma treatment results in chain scission, and ablation of low molecular weight species as well as cross-linking of the polymer.[13] This will tend to leave behind the heavier gold atoms to form the layer. VUV is capable of penetrating deeper into the surface than the physically corporeal species[7] and will also assist in breaking down the polymer backbone to lower molecular weight species, thereby aiding in removal of the polymeric species during the reduction process. The ability of argon and helium glow discharges to reduce metal salts has been reported before.[30] Also, the susceptibility of gold(III) chloride to decomposition by UV laser resulting in the production of gold features has been reported before.[31]

3.5 CONCLUSION

This chapter has shown that argon and helium plasma reduction of supported gold(III) chloride layers results in the production of ultra-pure gold films. Helium plasma reduction of supported gold(III) chloride films leads to appreciable deposition of SiO_x on the sample from the glass reactor walls. This behaviour is not observed for argon plasmas treatment. The use of noble gases for the treatment results in a higher purity gold film than was observed for the equivalent hydrogen plasma reduction. This reduction process can be ascribed to the action of metastable species, and VUV in the plasma, on the Nylon 66 support and the gold(III) chloride, resulting in decomposition of the metal salt, and ablation of low molecular weight species from the surface to leave behind a pure gold film.

3.6 REFERENCES

1 Y. L. Hseih, D. A. Timm, M .Wu, *J. Appl. Poly. Sci.* **1989**, *38*, 1719.

2 J. Hopkins, J. P. S. Badyal, *Macromolecules* **1994**, *27*, 5498.

3 J. Hopkins, J. P. S. Badyal, *J. Poly. Sci. A: Poly. Chem.* **1996**, *34*, 1385.

4 P. Triolo, J. D. Andrade, *J. Biomed. Mater. Res.* **1983**, *17*, 129.

5 M. Collaud, P. Groenig, S. Nowak, L. Schalpbach, *J. Adhesion Sci.* **1994**, *8*, 1115.

6 L. J. Gerenser, *J. Adhesion Sci.* **1987**, *1*, 303.

7 D. T. Clark, A. Dilks, *J. Poly. Sci. Poly. Chem.* **1978**, *16*, 911.

8 *Techniques and Applications of Plasma Chemistry* (Eds. J. R. Hollahan, A. T. Bell) John Wiley and Sons, USA, **1974**, p. 126.

9 D. T. Clark, A. Dilks, *J. Poly. Sci. Poly. Chem.* **1977**, *15*, 2321.

10 *Techniques and Applications of Plasma Chemistry* (Eds. J. R. Hollahan, A. T. Bell) John Wiley and Sons, USA, **1974**, Chapter 3.

11 R. K. Wells, M. E. Ryan, J. P. S. Badyal, *J. Phys. Chem.* **1993**, *97*, 12879.

12 M. Collaud, S. Nowak, O. M. Kuttel, P. Groning, L. Schalpbach, *Appl. Surf. Sci.* **1993**, *72*, 19.

13 C. M. Chan, T. M. Ko, H. Hiraoka, *Surf. Sci. Rep.* **1996**, *24*, 1.

14 R. H. Hansen, H. Schonborn, *J. Poly. Sci. B: Poly. Phys.* **1966**, *4*, 203.

15 H. Schonborn, R. H. Hansen, *J. Appl. Poly. Sci.* **1967**, *11*, 1461.

16 J. W. Mellor in *A Comprehensive Treatise on Inorganic and Theoretical Chemistry*, Volume 3, Longmans Green, London, **1923**, Chapter 23, Section 16.

17 M. P. Seah, M. T. Anthony *Surf. Inter. Anal.* **1984**, *6*, 230.

18 G. Beamson, D. Briggs in *High Resolution XPS of Organic Polymers The Scienta ESCA300 Database*, John Wiley and Sons, Chicester, England, **1992**, Chapter 6.

19 H. E. Swanson, E. Tatge, *Natl. Bur. Stand. (U.S.) Circ.* **1953**, *539*, 33.

20 N. S. Murphy, S. A. Curran, S. M. Aharoni, H. Minor, *Macromolecules* **1991**, *24*, 3215.

21 M. Batista-Leal, J. E. Lester, C. A. Lucchesi, *J. Elect. Spec. Rel. Phenom.* **1977**, *11*, 333.

22 Kosaku Kishi, Shigero Ikeda, *J. Phys. Chem.* **1974**, *78*, 107.

23 J. F. Moulder, W. F. Stickle, P. E. Sobol, K. D. Bomben in *Handbook of X-ray Photoelectron Spectroscopy* (Ed. J. Chastain) Perkin Elmer Corporation, Minnesota, USA, **1992**, Chapter II.

24 M. P. Seah, W.A. Dench, *Surf. Interface Anal.* **1979**, *1*, 2.

25 *Handbook of Physics and Chemistry* (Ed. R. C. Weast) CRC Press, 63rd Edition, Florida, USA, **1982**, Section F-133.

26 K. T. Hecht, D. L. Wood, *Proc. Roy. Soc. Lond. A* **1956**, *235*, 174.

27 J. C. Lassègues, J. Grondin, M. Hernandez, I. Rey, L. Servant, S. - J. Wen, *New J. Chem.* **1996**, *20*, 317.

28 L. R. Schroeder, S. L. Cooper, *J. Appl. Phys.* **1976**, *47*, 4310.

29 G. H. Sigel in *Treatise on Materials Science and Technology Volume 12* (Eds. M. Tomozawa, R. H. Doremus) Academic Press, London, Great Britain, **1977**.

30 F. K. McTaggart, *Austr. J. Chem.* **1965**, *18*, 949.

31 Y. Ye, R. G. Hunsperger, *Appl. Phys. Lett.* **1987**, *51*, 2136.

CHAPTER 4

X-RAY ASSISTED METALLIZATION OF SUPPORTED GOLD COMPLEXES

CHAPTER 4

X-RAY ASSISTED METALLIZATION OF SUPPORTED GOLD COMPLEXES

The ability of soft X-rays to reduce gold(III) chloride to metallic gold has been reported in the literature. This chapter describes the effect that X-rays used during XPS have on Nylon 66 supported gold(III) chloride, and the subsequent formation of a gold rich film when these X-ray irradiated samples are exposed to the laboratory atmosphere.

4.1 INTRODUCTION

Lithographic techniques find many uses, these include the fabrication of integrated circuits and gas sensors. A typical process involves the transfer of a pattern onto the substrate surface either by the use of a mask or rastering a finely focused beam.

Current methods employ optical, ultraviolet, electron, or ion beams, and more recently X-ray radiation.[1] Optical and ultraviolet lithographies are mainly used to recreate the image of a mask onto a photosensitive resist layer. Their resolution limit is typically 0.25 - 0.5 μm, due to wavelength limitations. Patterning below 0.2 μm requires the use of shorter wavelength radiation, i.e. electron, ion beam or X-ray techniques. Electron beam lithography operates by projecting a beam of high energy electrons onto a polymer resist, to cause either excitation or ionization of the resist. This leads to a change in solubility of the polymer resist in regions corresponding to where there has been electron beam irradiation. Electron beam lithography is widely used to make masks required for the fabrication of Very Large Scale Integration (VLSI) IC's. Ion beam lithography is a relatively recent technique, however it has already become well established due to ion

beam techniques being utilized by the electronics industry for ion implantation. Compared to electrons, the much heavier ions are capable of generating Frenkel defects in inorganic targets which can affect their solubilities, thereby eliminating the need for polymer resist layers.[2] Over the last few years various technologies have been developed to allow the use of X-rays for lithography, these include: X-ray masks,[3, 4] X-ray steppers,[5, 6, 7, 8] and X-ray lenses.[9] Pattern resolution is primarily governed by incident radiation wavelength and the distance between the mask and the substrate.[10] This limitation arises due to diffraction of the incident radiation occurring around the edges of the mask, leading to pattern blurring. Currently 5 μm is used as a typical working distance, which enables features down to 70 nm to be produced.

Direct deposition of metal tracks is a key variation of such lithographic techniques. Successful approaches have included: low energy Au^+ ion beam irradiation onto GaAs and Si to deposit gold features;[11, 12] the direct deposition of sodium onto a silicon substrate using a neutral sodium atom beam;[13] the passage of an electron beam through a gas containing suitable volatile metal precursors to deposit copper,[14] tungsten[15] and platinum[16] films.

A new approach for localized metallization is described in this article. This is based on the soft X-ray irradiation of supported metal precursor layers (e.g. gold(III) chloride), followed by exposure to air. Normally gold(III) chloride is unstable in air due to its deliquescent nature;[17] however, stable layers of supported gold(III) chloride can be fabricated by spin coating from acetonitrile solution onto Nylon 66 substrate. The various stages of metallization have been characterized by X-ray diffraction (XRD), X-ray photoelectron spectroscopy (XPS), and electrical resistance measurements.

4.2 EXPERIMENTAL

Preparation of supported metal complex was achieved as described in Chapter 2. X-ray treatment was performed in a VG ESCALAB surface analysis chamber (base pressure of 3×10^{-10} mbar), using an unmonochromatised Magnesium K_α soft X-ray source (photon energy 1253.6 eV) operating at 10 kV and 20 mA with a flux 6×10^{13} photons s^{-1}.[18] The samples were treated for a duration of 3 hours (clearly shorter X-ray exposures at higher

fluxes would be just as effective). In-situ, real time XPS characterization of the metallization process was achieved using a hemispherical analyser operating in the constant analyser energy mode (CAE, 50 eV pass energy), with an electron take off angle of 30° from the substrate normal. XPS data was acquired on a PC computer. Peak analysis assumed linear background subtraction and Gaussian fits. Theoretically determined sensitivity factors[19] for unit stoichiometry were taken as C(1s) : O(1s) : N(1s) : Cl (2p) : Au(4f) : Si(2p) equals 1.00 : 0.35 : 0.58 : 0.35 : 0.05 : 0.97. Trace amounts of adsorbed hydrocarbon served as a reference for the XPS binding energy scale by setting the C(1s) peak to 285.0 eV.[20] A VG AG21 cold cathode ion gun, operating at 3 keV energy and 1.5 μA ion current was used for Ar^+ ion depth profiling studies. The gold etch rate for these ion gun operating conditions was calibrated using a gold coated reference sample.

XRD and electrical resistance measurements were performed as described in Chapter 2.

4.3 RESULTS

Carbon, nitrogen, oxygen (due to Nylon) and gold and chlorine were the major elements present at the surface of gold(III) chloride spin coated onto Nylon 66. The surface composition of the supported gold(III) chloride layer changed upon X-ray irradiation: a drop in chlorine signal coincided with a rise in gold concentration, Figure 4.1. A slight rise in the carbon intensity was also observed. Furthermore, the Au($4f_{7/2}$) and ($4f_{5/2}$) XPS peaks shifted from 87.6 and 90.3 eV to 85.1 and 88.7 eV respectively, reflecting a reduction in the oxidation state of gold from +3 to zero. i.e. the formation of metallic gold, Figure 4.2. The slightly higher XPS binding energy found here compared to reported values for bulk gold (Au($4f_{7/2}$) at 84.0 eV)[21] can be attributed to the formation of finely dispersed gold particles.[22] An accompanying increase in the background pressure of the UHV chamber during X-ray irradiation indicated the concurrent loss of volatile species (this increase in pressure was not due outgassing of the X-ray source).

Storage of these X-ray irradiated gold(III) chloride layers under vacuum over long periods resulted in no further change in surface chemistry. Whereas exposure to the laboratory atmosphere for just 20 mins led to a dramatic enrichment of gold (from 8% to 25%) at the surface, Figure 4.3. Longer times in air resulted in a slight rise in carbon

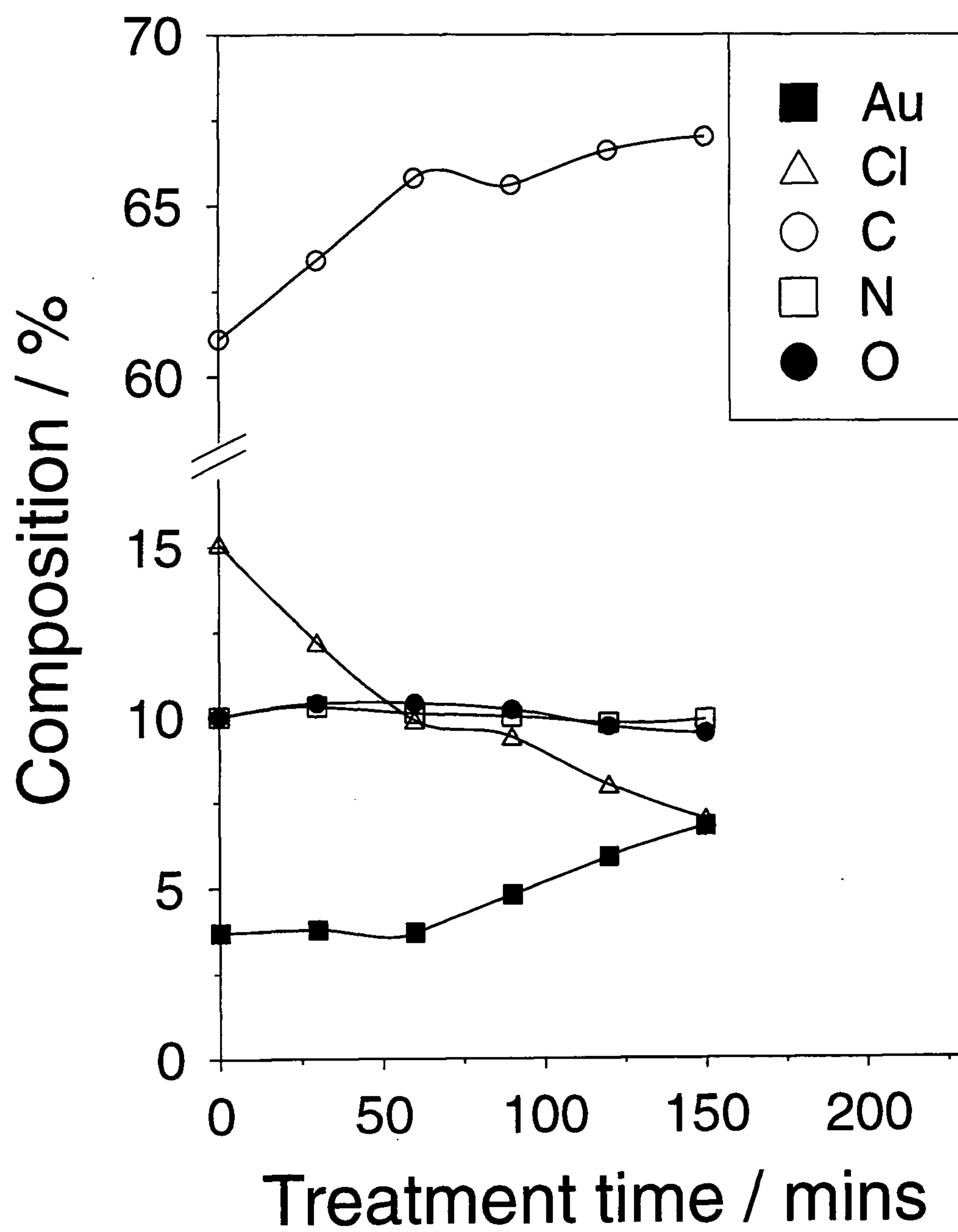

Figure 4.1. Surface composition during X-ray treatment.

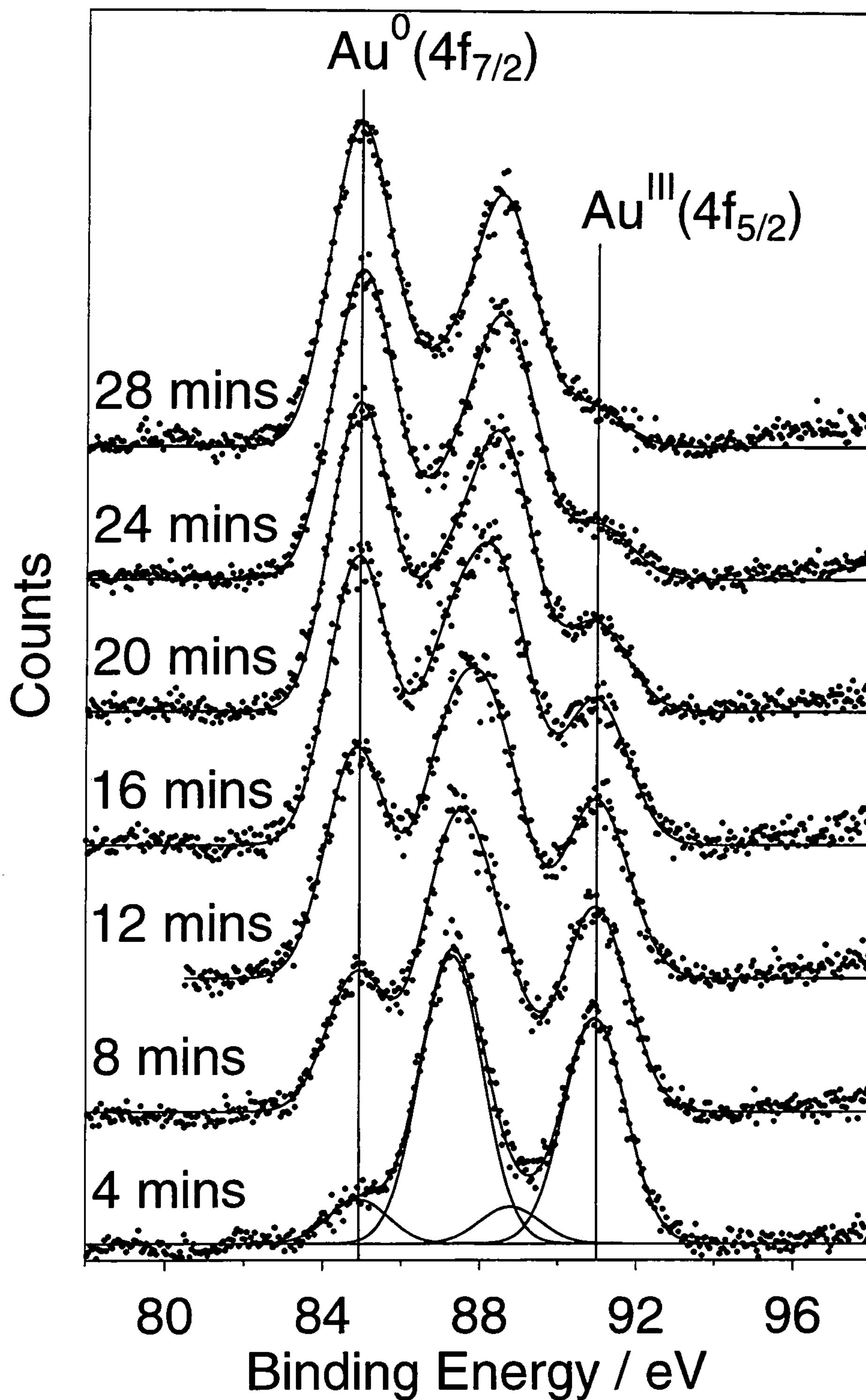

Figure 4.2. Au(4f) region during X-ray treatment. Each spectra took 4 minutes to collect.

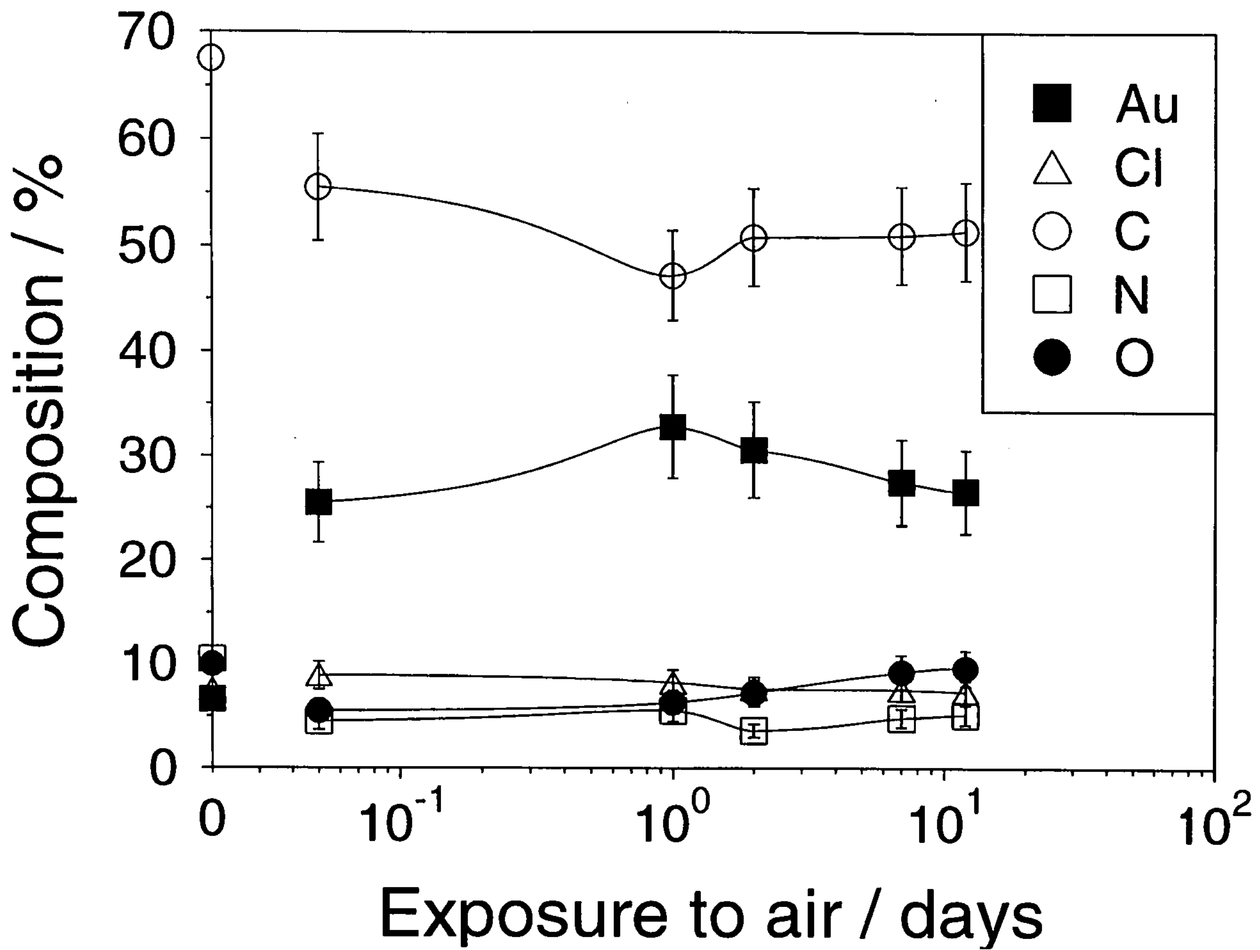

Figure 4.3. Surface composition of X-ray treated sample after exposure to air.

concentration at the expense of gold; which was probably due to aerial contamination. A further shift in the Au($4f_{7/2}$) and ($4f_{5/2}$) XPS peaks occurred from 85.1 and 88.7 eV to 84.3 and 87.9 eV respectively, thereby indicating an increase in the size of gold particles present,[23] Figure 4.4. An accompanying colour change was also prevalent: supported gold(III) chloride layers are yellow, these turn slightly brown during X-ray treatment, whilst air exposure causes this brown colour to change to green and eventually to metallic gold. Storage of the X-ray irradiated supported gold(III) chloride layers under vacuum, pure nitrogen, oxygen, or dry air for corresponding periods of time did not produce such behavior.

Argon ion sputter depth profiling of gold(III) chloride spin coated onto Nylon 66 showed a slight surface enrichment of gold, with chlorine, nitrogen, and carbon being present throughout the supported gold(III) chloride layer, Figure 4.5(a). The concentration of gold never exceeded 18% ± 3%. In contrast, Ar^+ ion depth profiling of gold(III) chloride films which had been X-ray treated and exposed to air for two weeks display a significant enrichment in gold at the surface in conjunction with complete loss of chlorine, nitrogen, and oxygen from this region, Figure 4.5(b). Carbon was the only other element present (75% ± 3% Au and 25% ± 3% C). Typical thickness' of the resultant gold films were measured to be 150 nm.

XRD patterns taken of the gold(III) chloride spin coated onto Nylon 66 revealed two regions of interest, corresponding to 2θ values between 35 - 110 degrees and 4 - 35 degrees: The Nylon 66 substrate itself displayed no structure in the 35 - 110 degrees 2θ range, whilst gold(III) chloride spin coated onto Nylon 66 gave rise to a tiny peak at 38.2 degrees 2θ, Figure 4.6(a). A detailed inspection of the 4 - 35 degrees 2θ region showed diffraction peaks attributable to Nylon 66 at 20.4 degrees 2θ (hydrogen bonding between chains of Nylon 66) and 23.3 degrees 2θ (hydrogen bonding between sheets of hydrogen bonded Nylon 66 chains),[23] as well as features associated with the presence of gold(III) chloride at 15.8 and 22.6 degrees 2θ, Figure 4.6(b). Diffraction lines in the 4 - 35 degrees 2θ region due to gold(III) chloride disappeared upon soft X-ray (Mg K_α line at 1253.6 eV) treatment of gold(III) chloride supported on Nylon 66, and remained absent during air exposure. Soft X-ray treatment of gold (III) chloride supported on Nylon 66 resulted in only a very slight increase in the size of the peak at 38.2 degrees 2θ.

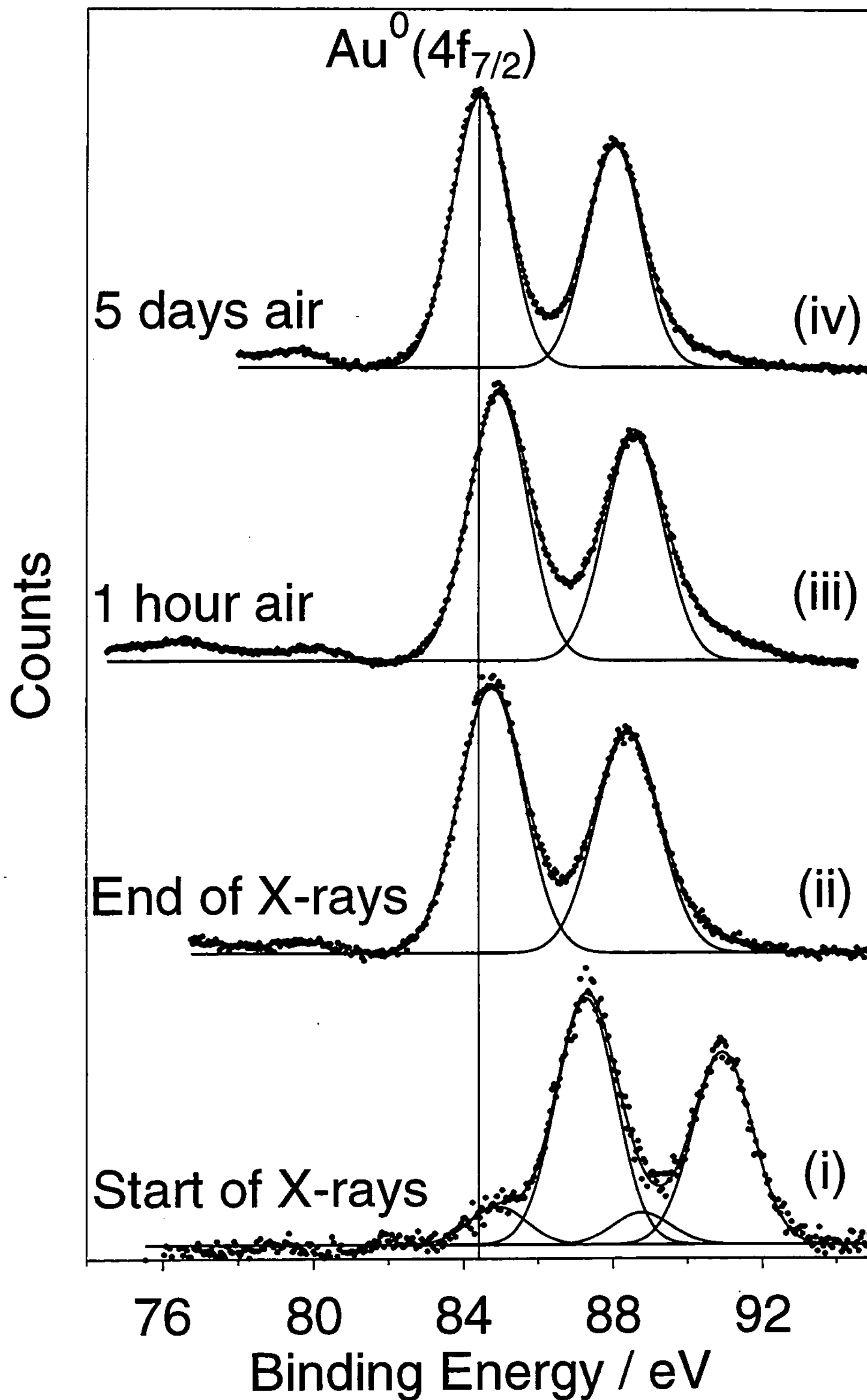

Figure 4.4. X-ray Photoelectron spectra of the Au(4f) region for gold(III) chloride spin coated onto Nylon 66: i) start of X-ray treatment, ii) end of X-ray treatment, iii) 1 hour exposed to air after X-ray treatment, and iv) 5 days exposed to air after X-ray treatment.

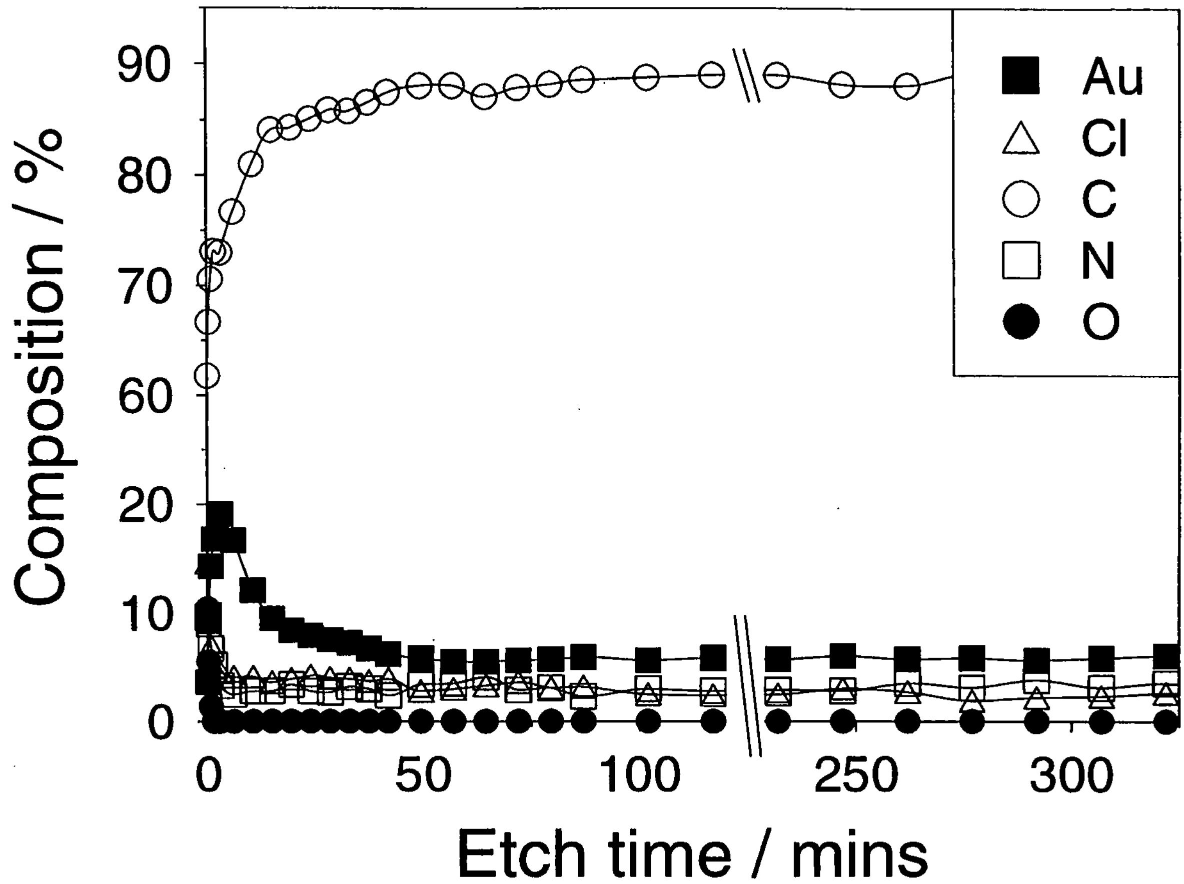

Figure 4.5(a). Depth profile of spin coated gold(III) chloride/Nylon 66 layer.

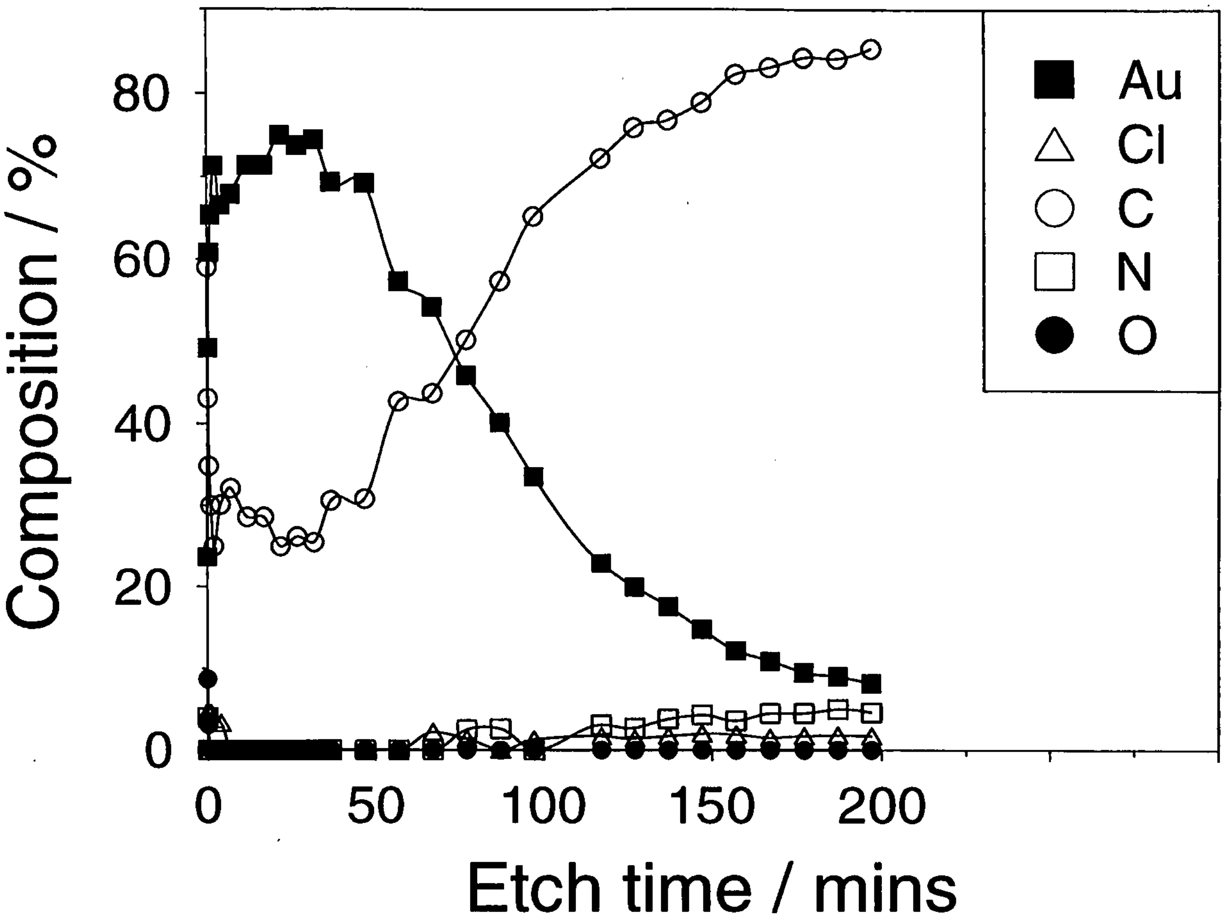

Figure 4.5(b). Depth profile of X-ray treated and air exposed sample.

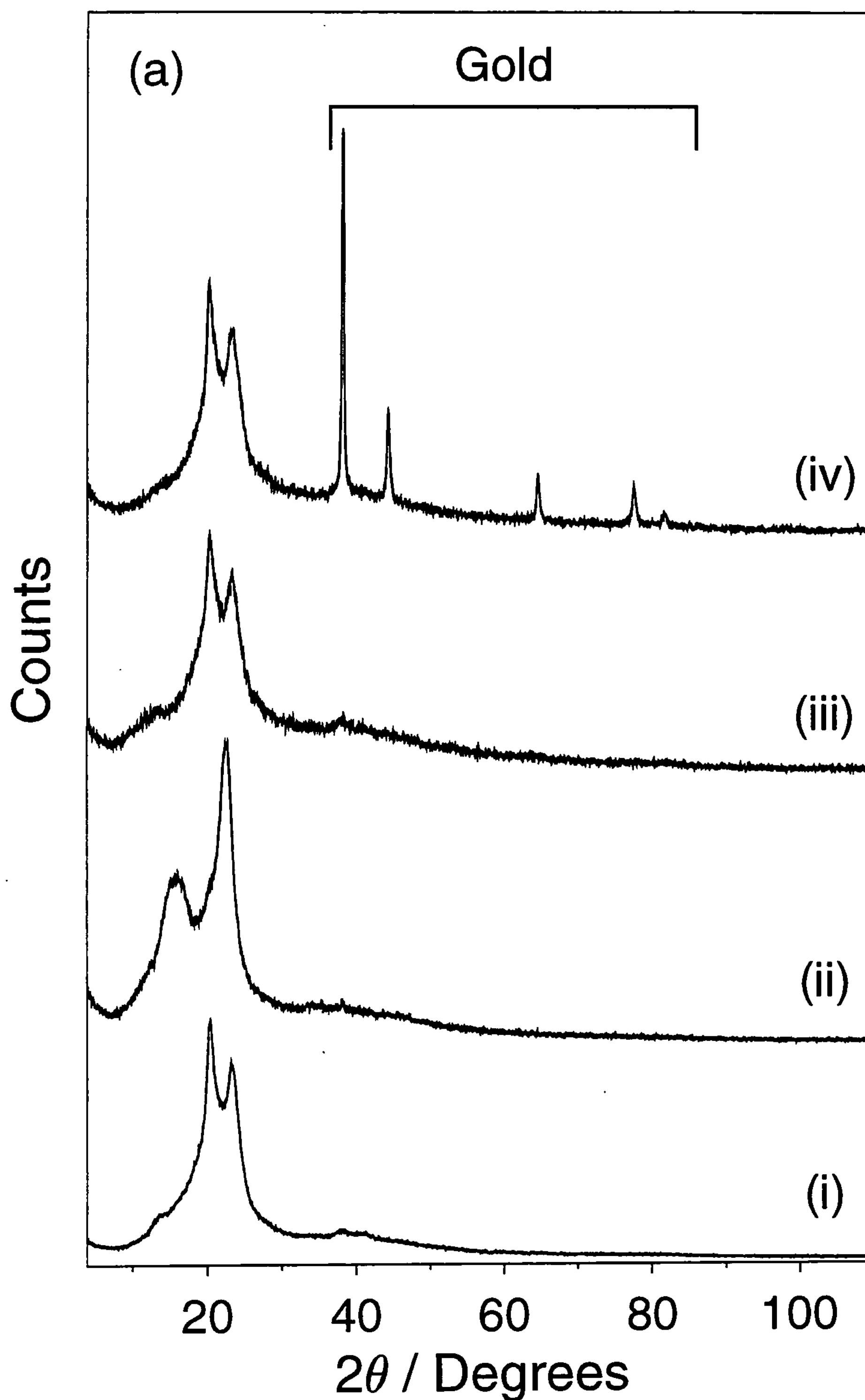

Figure 4.6(a). XRD patterns of: (i) Nylon 66; (ii) gold(III) chloride spin coated onto Nylon 66; (iii) 3 hours X-ray treatment of gold(III) chloride spin coated onto Nylon 66, and (iv) X-ray treated sample after curing in air for 2 weeks. Note - diffraction patterns were obtained from different samples in each case.

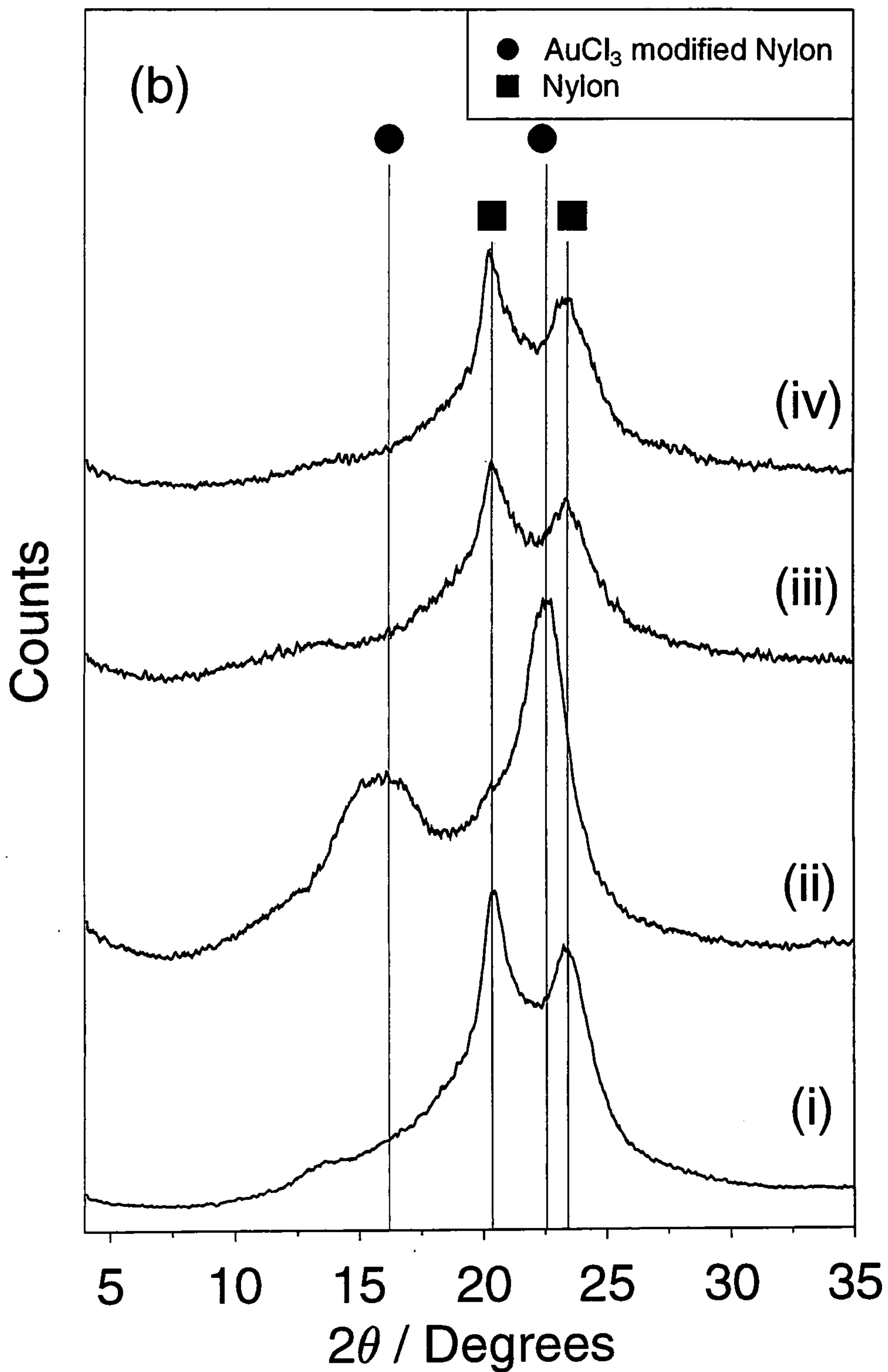

Figure 4.6(b). Magnified view of XRD spectra of: (i) Nylon 66; (ii) gold(III) chloride spin coated onto Nylon 66; (iii) 3 hours X-ray treatment of gold(III) chloride spin coated onto Nylon 66, and (iv) X-ray treated sample after curing in air for 2 weeks. Note - diffraction patterns were obtained from different samples in each case.

Exposure to air gave rise to the emergence of very well defined lines at 38.2, 44.4, 64.6, 77.6, 81.7, and 98.2 degrees 2θ which are attributable to face centred cubic (f.c.c.) crystallographic planes of metallic gold, [24] Figure 4.7. Analysis of peak widths in the gold scans showed no evidence of line narrowing as the air exposure time increased.

XPS was also performed on a sample of spin coated gold(III) chloride which had been used for XRD characterization. No change in gold oxidation state was found to have occurred during the course of the XRD experiment.

Electrical measurements taken at regular intervals during air exposure of the X-ray irradiated gold(III) chloride films showed a steady drop in resistance with time, Figure 4.8. A value of 2×10^{-4} Ωcm was calculated for the electrical resitivity of the resultant gold film (i.e. a drop of approximately 7 orders of magnitude in electrical resistivity) approaching that of bulk metallic gold (2.24×10^{-6} Ωcm).[25] In comparison, the electrical resistance of a spin coated gold(III) chloride/Nylon 66 film which had not been X-ray treated was greater than 100 MΩ.

4.4 DISCUSSION

It has been previously reported that solutions of gold(III) chloride can easily be reduced down to the metal state through various chemical and physical treatments,[26] e.g. addition of hydrogen gas, carbon monoxide, hydrogen peroxide, metal sulphides, hydrazine, or sulphur dioxide. Also gold salts contained within polymers can be reduced by thermal treatment to give reflective, metallized surfaces,[27, 28, 29] and electroactive polymers can cause spontaneous reduction of gold salts, to form metallic gold (this has applications in the recovery of metals from waste solutions).[30, 31, 32] X-ray induced metallization of supported gold(III) complexes is a two stage process; first, gold(III) chloride is reduced to finely dispersed metallic gold during X-ray reduction (as seen be XPS). The effect of soft aluminium K_α X-rays on gold(III) chloride has been reported before, in the reduction of gold(III) down to gold(I) and gold(O) states observed during XPS analysis of alumina supported gold(III) chloride catalyst (which was the precursor to the alumina supported gold catalyst).[33] In the present case the Au(4f) XPS binding energy of the metallic gold produced during X-ray irradiation is about 1 eV higher than that associated with bulk

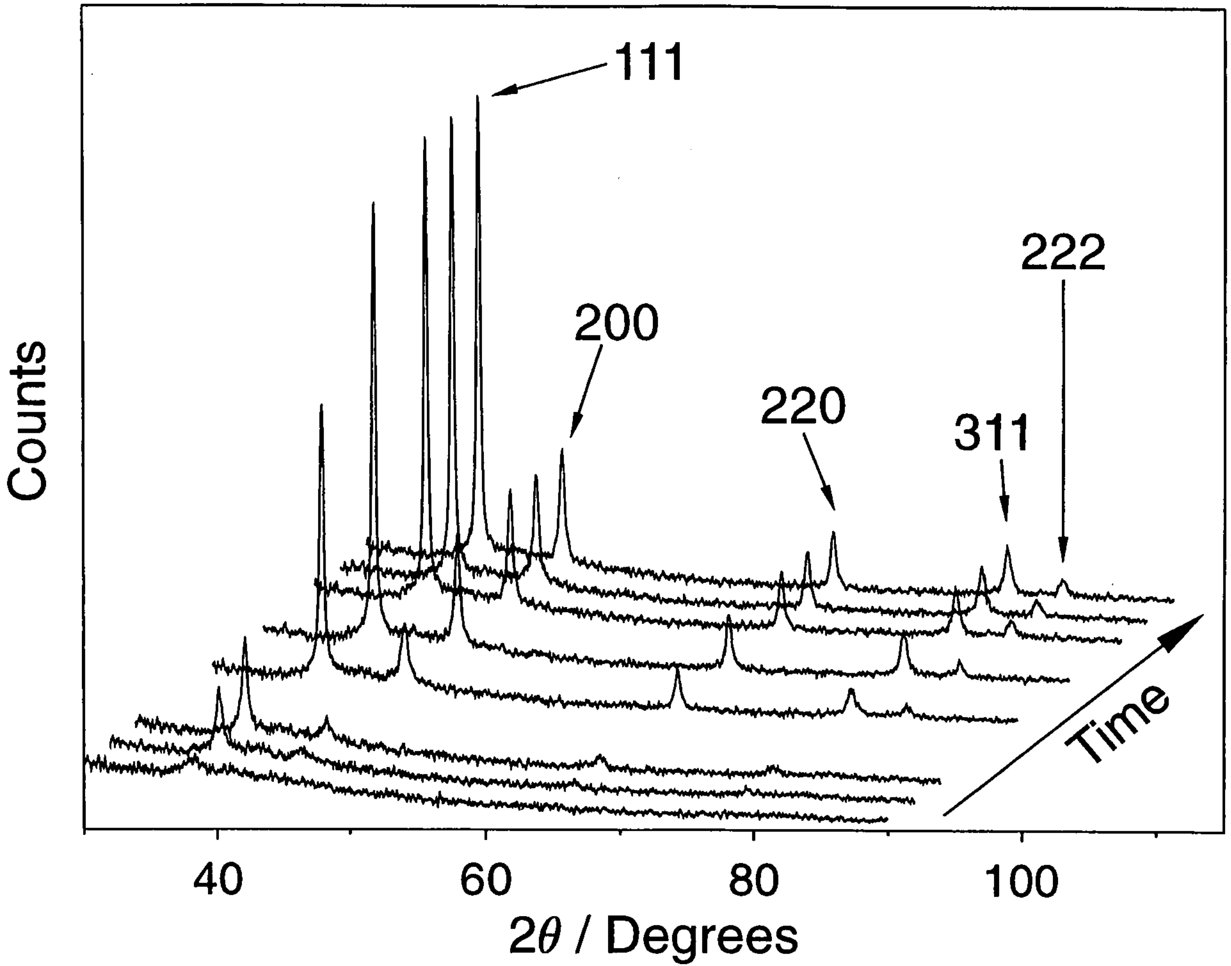

Figure 4.7. XRD stack plot showing the evolution of gold peaks with time on exposure to air, and peak assignments.

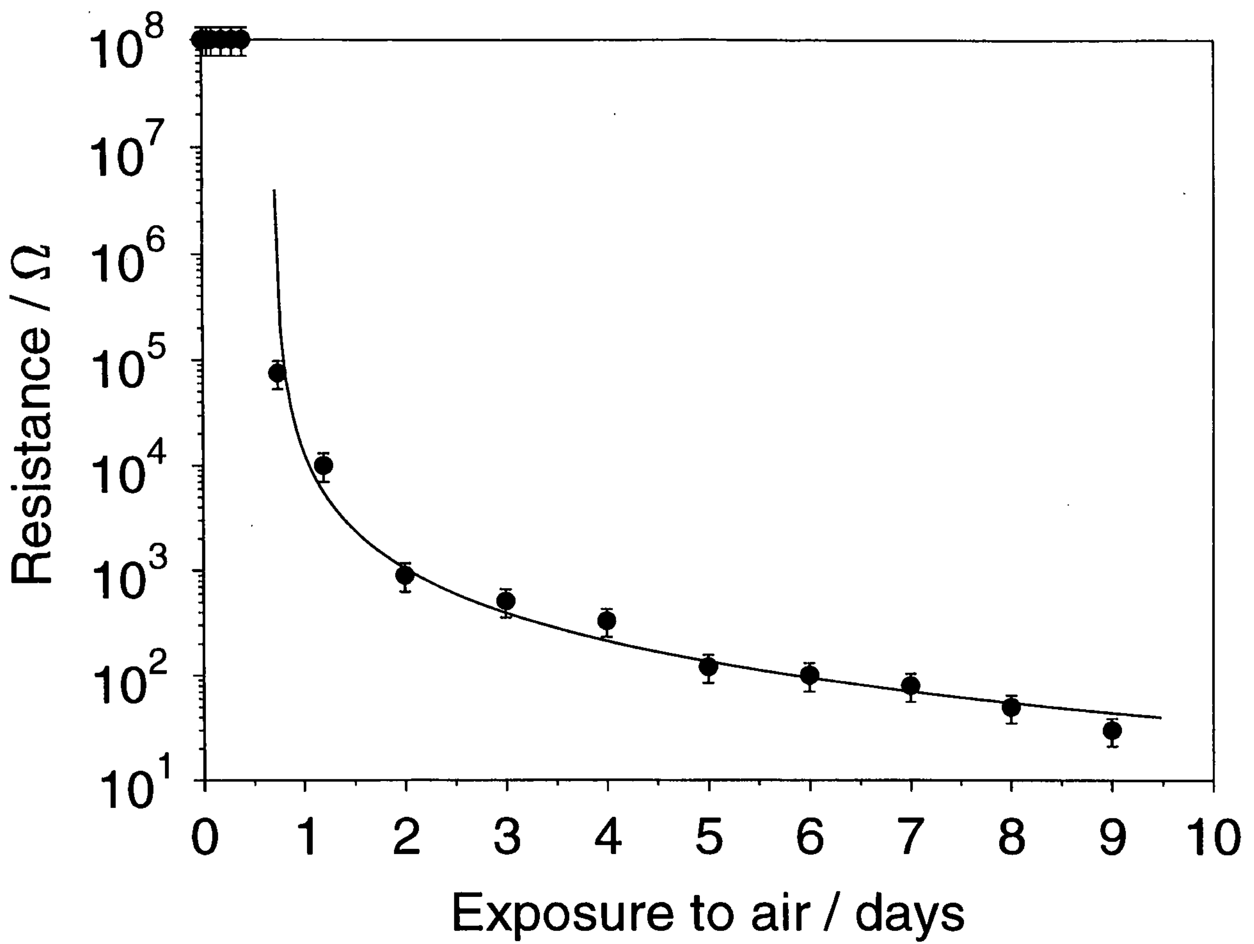

Figure 4.8. Electrical resistance of X-ray treated sample after exposure to air, and the theoretical fit calculated using percolation theory.

gold, and can be attributed to gold being present as small, isolated particles within the polymeric matrix.[22] Since it is well known that ionizing radiation can cause cross-linking of Nylon chains and the evolution of hydrogen,[34, 35] such hydrogen species could, in this case, lead to the reduction of gold(III) chloride. Also large quantities of photoelectrons are emitted by gold during XPS, and the absorption of these within the sample could lead to reduction of the gold. The resultant gold particles were highly dispersed, and subsequent air exposure was necessary for the formation of a continuous gold layer. XRD and electrical resistance measurements have shown that this process requires a number of days to reach completion.

The drop in electrical resistance of gold layer with time, seen in Figure 4.8, is consistent with percolation behavior. Percolation effects have been widely used to model the changes in electrical conductivity of gold filled polymers as the volume fraction of metal is altered.[36, 37, 38] Percolation theory states that as the volume fraction of a conductive species in a non-conducting matrix increases then at certain point, the critical volume fraction, the conductive particles come into contact with one another and a drastic increase in conductivity is observed.[39] The percolation equation is given below;

$$\sigma \propto (\rho - \rho_c)^t \qquad \text{Equation 4.1}$$

where σ is conductivity (i.e. the reciprocal of the resitivity), ρ the volume fraction of metal in the polymer, ρ_c the critical volume fraction, and t the critical exponent (typically 1.7 ± 0.1 for a three dimensional lattice). By assuming that the volume fraction of metal within the sample is related to the number of days that the sample has been exposed to the atmosphere, and by fitting of the electrical resitivity data to this equation produced to the line shown in Figure 4.8. The value of t used was 1.7 and the critical volume fraction was found to occur after 0.72 ± 0.06 days.

Ar^+ ion depth profiling of the irradiated sample showed that the gold layer probably contains entrapped polymer chains between the growing gold crystallites. Metallization only occurred in regions where the substrate had been exposed to X-rays; the sample remained yellow (characteristic of gold(III) chloride) where it had not been exposed. A slight green coloration appeared in the X-ray treated areas after only a few minutes in air,

which can be attributed to the formation of colloidal gold (colloidal gold goes from red to blue to green as the particle size increases).[40] Longer periods of air exposure led to the colour of the sample changing from green to gold. This transformation did not occur if the sample was stored in vacuum, in pure oxygen, nitrogen or dry air at atmospheric pressure. This implies that it is water in the atmosphere that drives the reduction process. This is similar to the typical mechanism of colloid formation which requires two processes; nucleation and growth.[41] In the present case, nucleation of the colloidal particles proceeds via X-ray reduction of the gold(III) chloride, and growth takes place upon sample exposure to moisture.

As for the precise mechanism by which the gold layer is produced when the X-ray irradiated sample is left in the laboratory atmosphere, there are various possibilities including:

i) When an n-type semi-conductor is in contact with a metal, negative charge flows from the metal to the semiconductor in order to equalize the Fermi levels.[42] This is known as the Schottky effect. There have been numerous reports of this Schottky effect occurring at organic/metal interfaces.[43, 44, 45, 46] X-ray treatment of the spin coated gold(III) chloride/Nylon 66 layers results in the formation of metallic gold as shown by XPS. Any damage induced in the spin coated layer could lead to the formation of a weakly semi-conducting state when the sample is exposed to moisture in the atmosphere. This would lead to the formation of a metal/semiconductor interface, and flow of electrons from the metal to its surroundings. This in turn would allow further reduction of any remaining gold(III) chloride by electron transfer. A similar effect has been reported for the reduction of gold(III) chloride on the surface of FeS_2 crystals,[47] and for the photo-reduction of gold(III) chloride supported on titanium dioxide.[48]

ii) If the X-ray degradation of the Nylon 66 resulted in the formation of an organic species capable of being oxidized, then this process could lead to the reduction of gold(III) chloride (the oxidation potential for the $[AuCl_4]^- + 3e^- \leftrightarrow Au + 4Cl^-$ is only about 1 V in acidic media[49]). There are many reports of gold(III) chloride oxidizing polymers, and thereby being reduced down to the metal.[30, 31, 32] However, no increase in the amount of oxygen present at the surface was seen after the gold layer had started to form, which indicates that oxidation of the polymer is unlikely.

It is difficult at present to prove either of these theories, however it is hoped that further work will clarify the reduction mechanism.

4.5 CONCLUSIONS

This chapter has shown that it is possible to produce gold rich films by the soft X-ray irradiation of Nylon 66 supported gold(III) chloride. However, the exact nature by which the gold rich films are formed has not been determined.

The ability of gold(III) chloride to undergo reduction after soft X-ray treatment opens up the area of X-ray lithography on spin coated layers of gold(III) chloride on Nylon 66. Placement of a mask between the X-ray source and the gold(III) chloride / Nylon 66 layer would allow the transference of a pattern to the gold(III) chloride layer and the formation of gold nuclei where the sample has been exposed. After X-ray treatment the sample is left in air to allow the gold pattern to develop. Any excess gold(III) chloride form the unexposed areas can then be removed by washing in water or iso-propanol, thereby leaving behind gold structures supported on a Nylon 66 layer.

This metallization process could find use in the micro-electronics industry, the formation of new X-ray detectors, and for intelligent packaging. Also the use of X-rays in the lithographic process will allow high resolution IC's, and self assembled monolayers (SAM's) to be created.

4.6 REFERENCES

1 K. A. Valiev in *The Physics of Submicron Lithography*, Plenum Press, New York, USA, **1992**, Chapter 1.

2 K. A. Valiev in *The Physics of Submicron Lithography*, Plenum Press, New York, USA, **1992**, Chapter 3.

3 R. Viswanathan, R. E. Acosta, D. Seeger, H. Voelker, A. Wilson, I. Babich, J. Maldonado, J. Warlaumont, O. Vladimirsky, F. Hohn, D. Crockatt, R. Fari, *J. Vac. Sci. Technol. B* **1988**, *6*, 2196.

4 S. Okhi, M. Kakuchi, T. Matsuda, A. Ozawa, T. Ohkubo, M. Oda, H. Yoshihara, *Jap. J. Appl. Phys.* **1989**, *28*, 2074.

5 E. Cullmann, K. A. Cooper *J. Vac. Sci. Technol. B* **1988**, *6*, 2123.

6 S. Ishihara, M. Kanai, A. Une, M. Suzuki, *J. Vac. Sci. Technol. B* **1989**, *7*, 1652.

7 K. Koga, N. Nomura, J. Yasui, Y. Terui, H. Nagano, K. Fujita, S. Kusumoto, K. Nakano, S. Nakatani, S. Mizuguchi, S. Aoki, M. Yamamoto, K. Yamaguchi, T. Sato, K. Matsuo, K. Yanagida, *J. Vac. Sci. Technol. B* **1990**, *8*, 1633.

8 N. Uchida, O. Kuwabara, Y. Ishibashi, N. Kikuiri, R. Hirano, J. Nishida, T. Nishizaka, Y. Kikuchi, H. Yoshino, *J. Vac. Sci. Technol. B* **1993**, *11*, 2997.

9 A. G. Peele, K. A. Nugent, A. V. Rode, K. Gabel, M. C. Richardson, R. Strack, W. Siegmund, *Applied Optics*, **1996**, *35*, 4420.

10 H. I. Smith, *J. Vac. Sci. Technol. B* **1995**, *13*, 2323.

11 J. Yanagisawa, K. Kito, K. Monden, K. Gamo, *J. Vac. Sci. Technol. B* **1995**, *13*, 2621.

12 S. Nagamachi, Y. Yamakage, H. Maruno, M. Ueda, S. Sugimoto, M. Asari, J. Ishiwara, *Appl. Phys. Lett.* **1993**, *62*, 2143.

13 V. Natarajan, R. E. Behringer, D. M. Tennant, G. Timp, *J. Vac. Sci. Technol. B* **1995**, *13*, 2823.

14 Y. Ochiai, J. Fujita, S. Matsui, *J. Vac. Sci. Technol. B* **1996**, *14*, 3887.

15 K. T. Kohlmann-von Platen, L. - M. Buchmann, H. - C. Petzold, W. H. Brünger, *J. Vac. Sci. Technol. B* **1992**, *10*, 2690.

16 H. W. P. Koops, A. Kaya, M. Weber, *J. Vac. Sci. Technol. B* **1995**, *13*, 2400.

17 J. W. Mellor in *A Comprehensive Treatise on Inorganic and Theoretical Chemistry*, Volume 3, Longmans Green, London, **1923**, Chapter 23, Section 16.

18 Private communication with Vacuum Generators Ltd., 25th November 1996.

19 M. P. Seah, M. T. Anthony, *Surf. Inter. Anal.* **1984**, *6*, 230.

20 G. Beamson, D. Briggs in *High Resolution XPS of Organic Polymers The Scienta ESCA300 Database*, John Wiley and Sons, Chicester, England, **1992**, Chapter 6.

21 J. F. Moulder, W. F. Stickle, P. E. Sobol, K. D. Bomben in *Handbook of X-ray Photoelectron Spectroscopy* (Ed. J. Chastain) Perkin Elmer Corporation, Minnesota, USA, **1992**, Chapter II.

22 *Pratical Surface Analysis Volume 1 - Auger and X-ray Photoelectron Spectroscopy* (Eds. D. Briggs, M. P. Seah) John Wiley and Sons, Great Britain, 2nd Edition, **1990**, Chapter 8.

23 N. S. Murphy, S. A. Curran, S. M. Aharoni, H. Minor, *Macromolecules* **1991**, *24*, 3215.

24 H. E. Swanson, E. Tatge, *Natl. Bur. Stand. (U.S.) Circ.* **1953**, *539*, 33.

25 *Handbook of Physics and Chemistry* (Ed. R. C. Weast) CRC Press, 63rd Edition, Florida, USA, **1982**, Section F-133.

26 J. W. Mellor in *A Comprehensive Treatise on Inorganic and Theoretical Chemistry*, Volume 3, Longmans Green, London, **1923**, Chapter 23, Section 16.

27 D. G. Madeleine, T. C. Ward, L. T. Taylor, *J. Poly. Sci. B Poly. Phys.* **1988**, *26*, 1641.

28 M. L. Caplan, D. M. Stoakley, A. K. St. Clair, *J. Appl. Poly. Sci.* **1995**, *56*, 995.

29 Y. Yonezawa, T. Sato, I. Kawabata, *Chem. Letts.* **1994**, 355.

30 E. T. Kang, Y. P. Ting, K. L.Tan, *J. Appl. Poly. Sci.* **1994**, *53*, 1539.

31 W. Lin, Y. Lu, H. Zeng, *J. Appl. Poly. Sci.* **1993**, *49*, 1635.

32 E. T. Kang, Y. P. Ting, K. G. Neoh, K. L. Tan, *Synthetic Metals* **1995**, *69*, 477.

33 M. Batista-Leal, J. E. Lester, C. A. Lucchesi, *J. Elect. Spec. Rel. Phenom.* **1977**, *11*, 333.

34 E. J. Lawton, A. M. Bueche, J. S. Balwit, *Nature* **1953**, *172*, 356.

35 K. Little, *Nature* **1954**, *173*, 680.

36 J. Perrin, B. Despax, V. Hanchett, E. Kay, *J. Vac. Sci. Technol. A* **1986**, *4*, 46.

37 C. Laurent, E. Kay, N. Souag, *J. Appl. Phys.* **1988**, *64*, 336.

38 B. Bridge, M. J. folkes, B. R. Wood, *J. Phys. D: Appl. Phys.* **1990**, *23*, 890.

39 F. Lux, *J. Mater. Sci.* **1993**, *28*, 285.

40 E. C. H. Davies, *J. Am. Chem. Soc.* **1923**, *45*, 2261.

41 J. Turkevich, P. C. Stephenson, J. Hillier, *Disc. Farad. Soc.* **1951**, *11*, 55.

42 P. A. Cox in *The Electronic Structure and Chemistry of Solids* Oxford University Press, Great Britain, **1991**, Chapter7.

43 R. Gupta, S. C. K. Misra, B. D. Malhotra, N. N. Beladakere, S. Chandra, *Appl. Phys. Letts.* **1991**, *58*, 51.

44 J. T. Lei, W. B. Liang, C. J. Brumlik, C. R. Martin, *Synthetic Metals* **1992**, *47*, 351-359.

45 M. Willander, A. Assadi, C. Svensson, *Synthetic Metals* **1993**, *57*, 4099.

46 I. H. Campbell, S. Rubin, T. A. Zawodzinski, J. D. Kress, R. L. Martin, D. L. Smith, N. N. Barashkov, J. P. Ferraris, *Phys. Rev. B Cond. Matt.* **1996**, *54*, 14321.

47 G. E. Jean, G. M. Bancroft, *Geochimica et Cosmochimica Acta* **1985**, *49*, 979.

48 A. Fernández, A. Caballero, A.R. González-Elipe, J.-M. Herrmann, H. Dexpert, F. Villain, *J. Phys. Chem.* **1995**, *99*, 3303.

49 W. M. Latimer in *Oxidation Potentials* Prentice-Hall, USA, 2nd Edition, **1952**, Chapter 11.

CHAPTER 5

COLD HYDROGEN PLASMA METALLIZATION OF SUPPORTED SILVER & PALLADIUM SALT LAYERS

CHAPTER 5

COLD HYDROGEN PLASMA METALLIZATION OF SUPPORTED SILVER & PALLADIUM SALT LAYERS

The formation of thin gold films using a hydrogen glow discharge has been demonstrated in Chapter 2. Thin films of others metals are also important for electrical and catalytically active purposes. This chapter describes the production of thin silver and palladium films from layers of their salts spin coated on to glass substrates.

3.1 INTRODUCTION

The deposition of silver and palladium metal coatings on to polymeric and inorganic substrates forms the basis of many everyday applications; these include, decorative finishings,[1] electronic circuit components,[2] gas barrier layers,[3] gas sensors,[4] and gas separation membranes.[5] Methods currently employed for their fabrication include; chemical vapour deposition (CVD),[6, 7, 8] electroplating,[9] laser reduction of supported salts,[10] electron or ion beams,[11, 12] sputter deposition,[13] electroless plating,[14] physical vapour deposition,[15, 16] retroplating,[17] thermal treatment of polymer supported metal salts,[18, 19] and metal hydride reduction.[20] All of these methods suffer from at least one of the following drawbacks: copious solvent use, high temperatures, ultra-high vacuum conditions, or exotic metal precursors.

An alternative approach is described in this chapter which is based on the non-isothermal hydrogen plasma reduction of supported metal precursors (e.g. silver nitrate or palladium acetate). This metallization technique benefits from being capable of coating heat-

sensitive substrates, as well as complex shaped objects without the need for large quantities of solvent or complicated chemical syntheses. X-ray diffraction (XRD), X-ray photoelectron spectroscopy (XPS), attenuated total reflectance Fourier transform infrared spectroscopy (ATR-FTIR), optical microscopy, and electrical resistance measurements have been used to follow the various stages of this low temperature metallization technique.

5.2 EXPERIMENTAL

20% wt/v solutions of silver nitrate (Alfa, 99.99% purity) in acetonitrile (Sigma, HPLC grade) and palladium acetate (Fluorochem, 99.9% purity) in chloroform (Sigma, Analar grade) were prepared by dissolving 0.2 g of each metal salt in 1 ml of the corresponding solvent. Glass substrates were cleaned by rinsing in a 50/50 iso-propanol/cyclohexane solvent mixture for 30 s followed by drying in air. Subsequently, metal salt layers were deposited from solution using a Cammax Precima spin coater operating at a rotation speed of 1700 rpm.

Hydrogen plasma reduction of the metal salt layers was performed in a custom-built plasma reactor (described in Chapter 2) attached directly to a VG ESCALAB surface analysis chamber (base pressure of 3×10^{-10} mbar). Typically, 10 W hydrogen plasma operating at a pressure of 0.15 mbar, was used to reduce the supported metal precursor species. XPS studies employed an unmonochromatised Magnesium K_α photo-excitation source and a hemispherical analyser operating in the constant analyzer energy mode (CAE, 50 eV pass energy), with an electron take off angle of 30° from the substrate normal. A PC computer was used for XPS data accumulation and component peak analysis, assuming linear background subtraction and Gaussian fits. Theoretically determined sensitivity factors[21] for unit stoichiometry were taken as C(1s) : O(1s) : N(1s) : Pd(3d) : Ag(3d) : Si(2p) equals 1.00 : 0.35 : 0.56 : 0.05 : 0.05 : 0.97. Trace amounts of absorbed hydrocarbon served as a reference for the photoelectron binding energy scale by setting the C(1s) peak to 285.0 eV.[22] Ar^+ ion depth profiling studies were carried out using a Vacuum Generators AG21 cold cathode ion gun, operating at a background argon (BOC, Research Grade) pressure of 2×10^{-6} mbar, and 3 keV energy with an ion current of 1.5 μA. A reference gold coated sample of known thickness was used to

calibrate the etch rate of gold under these Ar^+ ion gun operating conditions. This allowed calculation of relative sputter rates for silver and palladium by comparison with literature values.[23]

XRD scans were taken of the coated samples mounted onto glass substrate holders using a Philips PW1050 powder diffractometer (Cu K_α X-rays generated at 35 kV and 20mA). Diffraction patterns were recorded from 4 to 110 degrees 2θ at 0.05 degree intervals with 4 s and 10 s residence time at each point for the silver and palladium samples respectively. All peak assignments are accurate to $\pm$ 0.02 degrees 2θ.

Optical images of the spin coated and reduced layers were recorded using an Olympus BX-40 microscope with x10 objective lenses. The samples were illuminated from above, using a white light source. Images were recorded with a CCD camera attached to a PC computer.

ATR-FTIR and electrical resistance measurements were carried out using the parameters given in Chapter 2.

5.3 RESULTS

XRD analysis of metal salt coated glass slides revealed three regions of interest: the broad amorphous background from the glass substrate, metal salt diffraction features and lines arising from the formation of metal, Figure 5.1. Characteristic diffraction lines corresponding to d-spacings for silver nitrate (main lines at 19.62, 21.72, 29.70, 31.92 and 35.52 degrees 2θ)[24] disappeared upon hydrogen plasma reduction, to be replaced by diffraction lines at 38.14, 44.32, 64.54 and 77.46 degrees 2θ, which are attributable to face centered cubic (f.c.c.) crystallographic planes of metallic silver.[25] In contrast, spin coated palladium acetate films were found not to be crystalline in nature, but rather a quasi-amorphous peak in the 10 - 14 degrees 2θ region was discernible, Figure 5.1(b); this behaviour has been observed previously for palladium acetate layers spin coated from chloroform solution.[26] Again, hydrogen glow discharge reduction resulted in the loss of any palladium acetate features, to be replaced by the emergence of f.c.c. metallic palladium diffraction peaks at 39.88, 46.42, 67.66 and 81.76 degrees 2θ;[27] however, these peaks appeared to be shifted to slightly lower values of 2θ as compared to reported

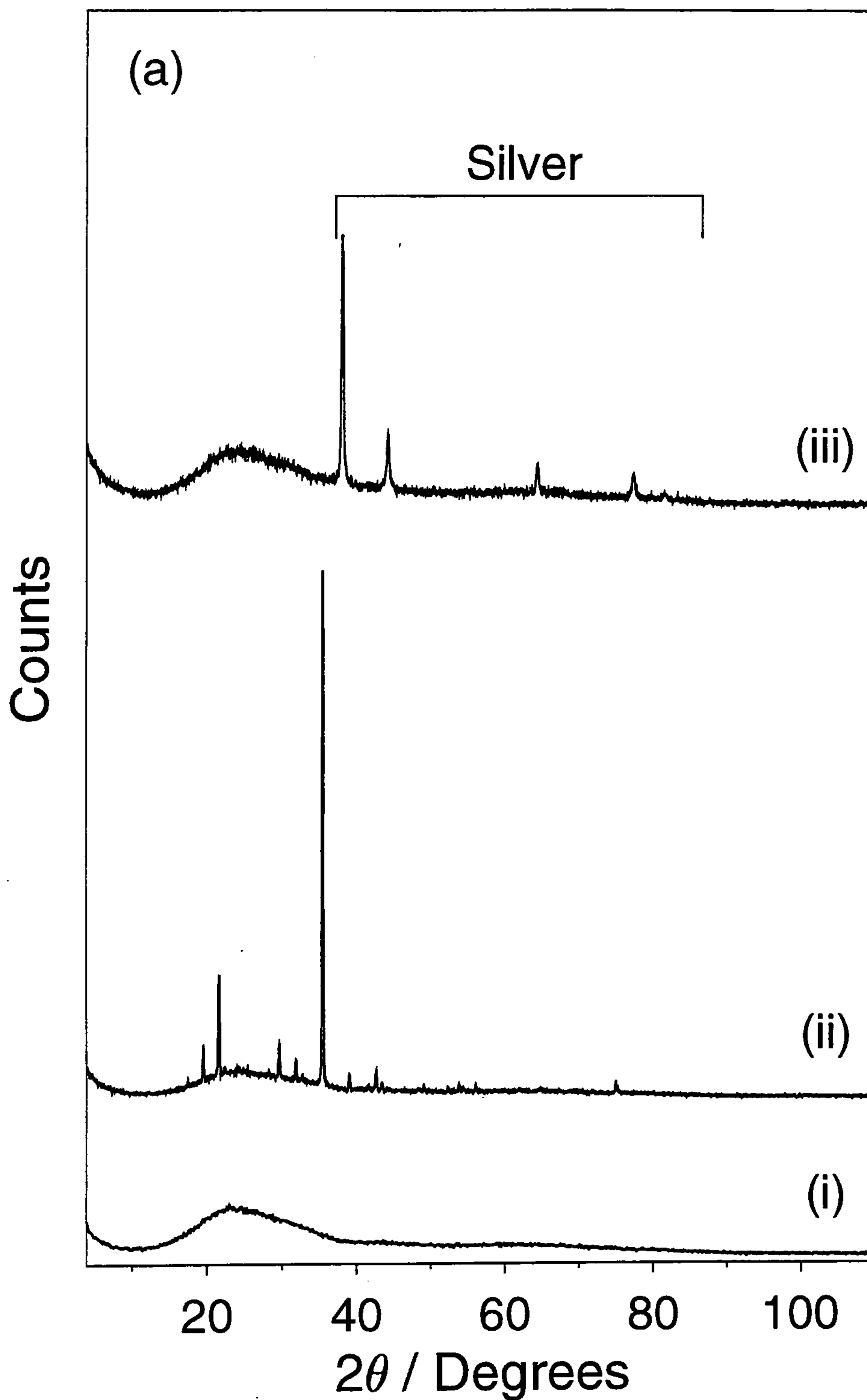

Figure 5.1(a). XRD patterns: (i) glass; (ii) silver nitrate coated onto glass; and (iii) 30 mins hydrogen plasma treatment of silver nitrate spin coated onto glass. Note - diffraction patterns were obtained from different samples in each case.

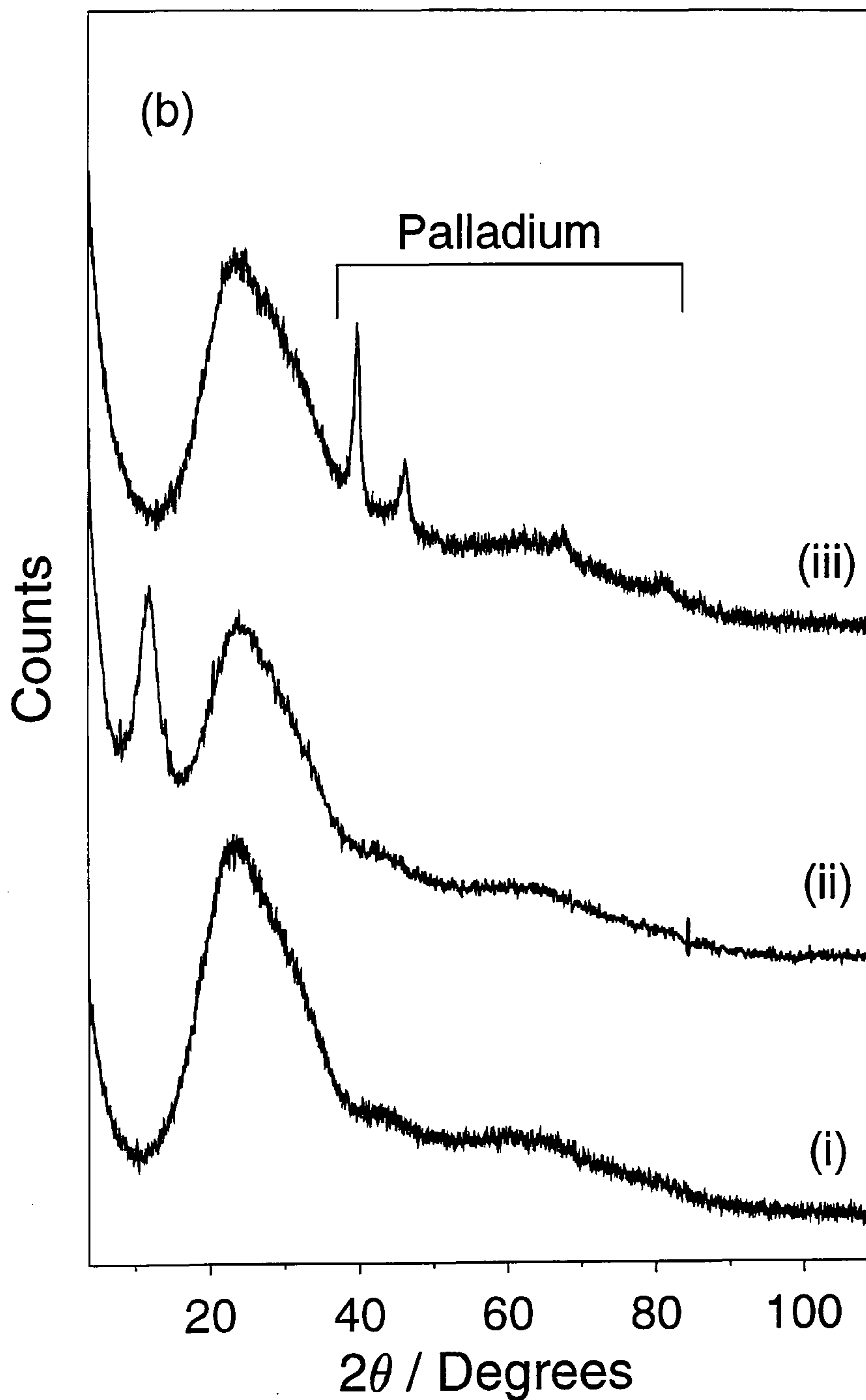

Figure 5.1(b). XRD spectra: (i) glass; (ii) palladium acetate coated onto glass; and (iii) 30 mins hydrogen plasma treatment of palladium acetate spin coated onto glass. Note - diffraction patterns were obtained from different samples in each case.

literature values for the pure metal, thus indicating an increase in the d-spacing of the palladium lattice (i.e. a lattice parameter of 0.391 nm as compared to 0.389 nm for palladium[27]). This lattice expansion is most likely due to the retention of some hydrogen or carbon within the palladium lattice during glow discharge reduction (see XPS depth profiling studies).[28, 29] The observed diffraction lines for metallic silver were found to be much greater in intensity than noted for the reduced palladium layer; this may also be attributed to the distortion of the palladium lattice by entrapped hydrogen/carbon.[28, 29]

XPS analysis showed that spin coating of both salts gave rise to complete coverage of the glass substrate (as indicated by the absence of any Si(2p) signal at 103.4 eV binding energy[30]), Figure 5.2. Furthermore no chlorine, associated with the casting solvent, was detected in the spin coated palladium acetate samples. Hydrogen glow discharge reduction resulted in the loss of carbon, nitrogen and oxygen in the case of silver nitrate, and carbon and oxygen from palladium acetate layers. The accompanying shift in Pd($3d_{5/2,3/2}$) binding energies towards lower values is consistent with a decrease in metal oxidation state,[30] Table 5.1. This shift was not as conclusive for the Ag($3d_{5/2,3/2}$) peaks, since silver(I) nitrate possesses a similar XPS binding energy to that of silver metal,[31] however the small amount of other elements detected by XPS (i.e carbon, nitrogen and oxygen) confirms the formation of the metallic state.

Core level	**Binding Energy / eV ± 0.2 eV**	
	Before reduction	**After reduction**
Ag($3d_{5/2}$)	368.6	369.0
Ag($3d_{3/2}$)	374.6	374.9
Pd($3d_{5/2}$)	339.0	335.9
Pd($3d_{3/2}$)	344.4	341.2

Table 5.1. Metal core level XPS binding energies before and after hydrogen plasma reduction.

Argon ion depth profiling proved that carbon is present just at the surface of the metallized silver layer (i.e. not within the bulk), whereas oxygen is spread throughout the silver film (average layer composition 95% ± 1% Ag and 5% ± 1% O). In contrast, Ar^+

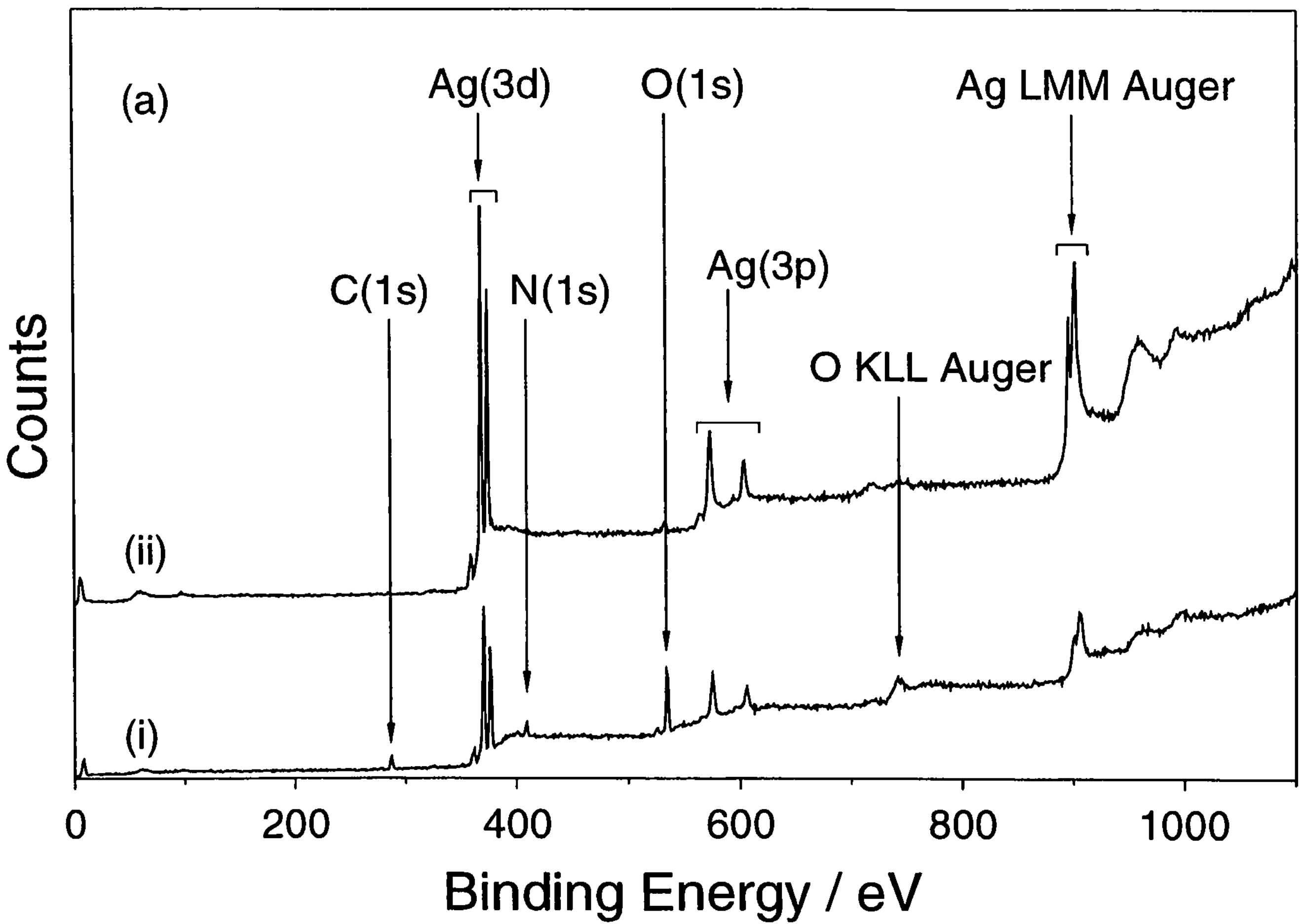

Figure 5.2(a). XPS widescans: (i) silver nitrate on glass; and (ii) 30 mins hydrogen plasma reduced silver nitrate coated glass.

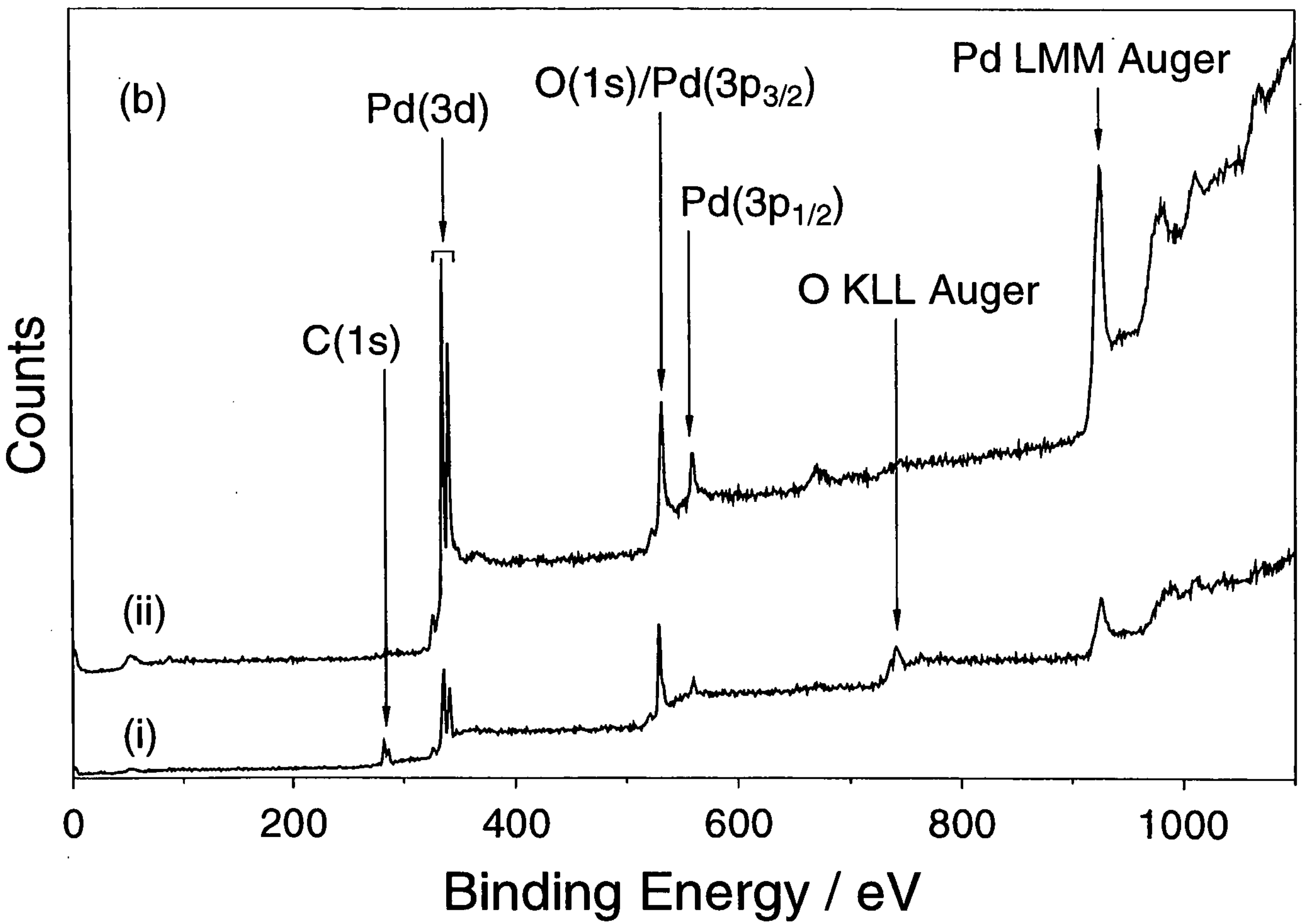

Figure 5.2(b). XPS widescans: (i) palladium acetate on glass; and (ii) 30 mins hydrogen plasma reduced palladium acetate coated glass.

ion depth profiling of the plasma reduced palladium layers showed that oxygen was only a surface contaminant, whilst carbon was also detected in the subsurface (80% ± 3% Pd and 20% ± 3% C). Typical thicknesses of the resultant metal films were measured by argon ion depth profiling and were shown to be 30 nm for silver and 120 nm for palladium (although the precise thickness could be altered by varying the concentration of the metal salt solution employed initially for spin coating the precursor layer).

ATR-FTIR spectra taken of the glass substrate displayed absorption features corresponding to Si-O-Si stretches (around 1150 cm^{-1}), $Si\text{-}O^-$ groups (900 cm^{-1}) and Si-O stretches (760 cm^{-1}),[32] Figure 5.3. Spin coating of a silver nitrate layer onto glass gave rise to new peaks at 1300, 800 and 735 cm^{-1} associated with the nitrate group.[33] Likewise the spin coated palladium acetate layer showed features characteristic of the acetate ligands at 1593, 1562, 1418, 1350, 694 and 624 cm^{-1},[34] and weak peaks at 753 and 667 cm^{-1} from chloroform trapped during spin coating, Figure 5.3(b). The nitrate and acetate ligand components were no longer discernible after 30 mins hydrogen glow discharge reduction (the glass features had also disappeared). Instead, a broad featureless metallic continuum was evident (to verify this a piece of silver foil was run, and infra-red spectra for palladium have been reported previously[26]).

Electrical resistivity of the resultant silver and palladium metal films was calculated to be 7.5×10^{-6} Ωcm and 4.7×10^{-4} Ωcm respectively; these values are slightly higher than those typically reported for the bulk metals (1.6×10^{-6} Ωcm and 1.1×10^{-5} Ωcm for silver and palladium).[35] The higher resistivity value for palladium may be attributed to the presence of impurities, causing lattice distortion and defect sites.

Comparison of the optical images for the spin coated and reduced samples showed that hydrogen glow discharge treatment did not result in any perturbation in the physical appearance of the surface, Figure 5.4. The spin coated silver(I) nitrate layers exhibited a complex crystalline 'fern-like' structure, which remained intact upon reduction, whereas the palladium acetate spin coated layers were featureless prior to and following hydrogen plasma treatment. These observations confirm that the electrical discharge process does not cause any significant heating (sintering) during treatment.

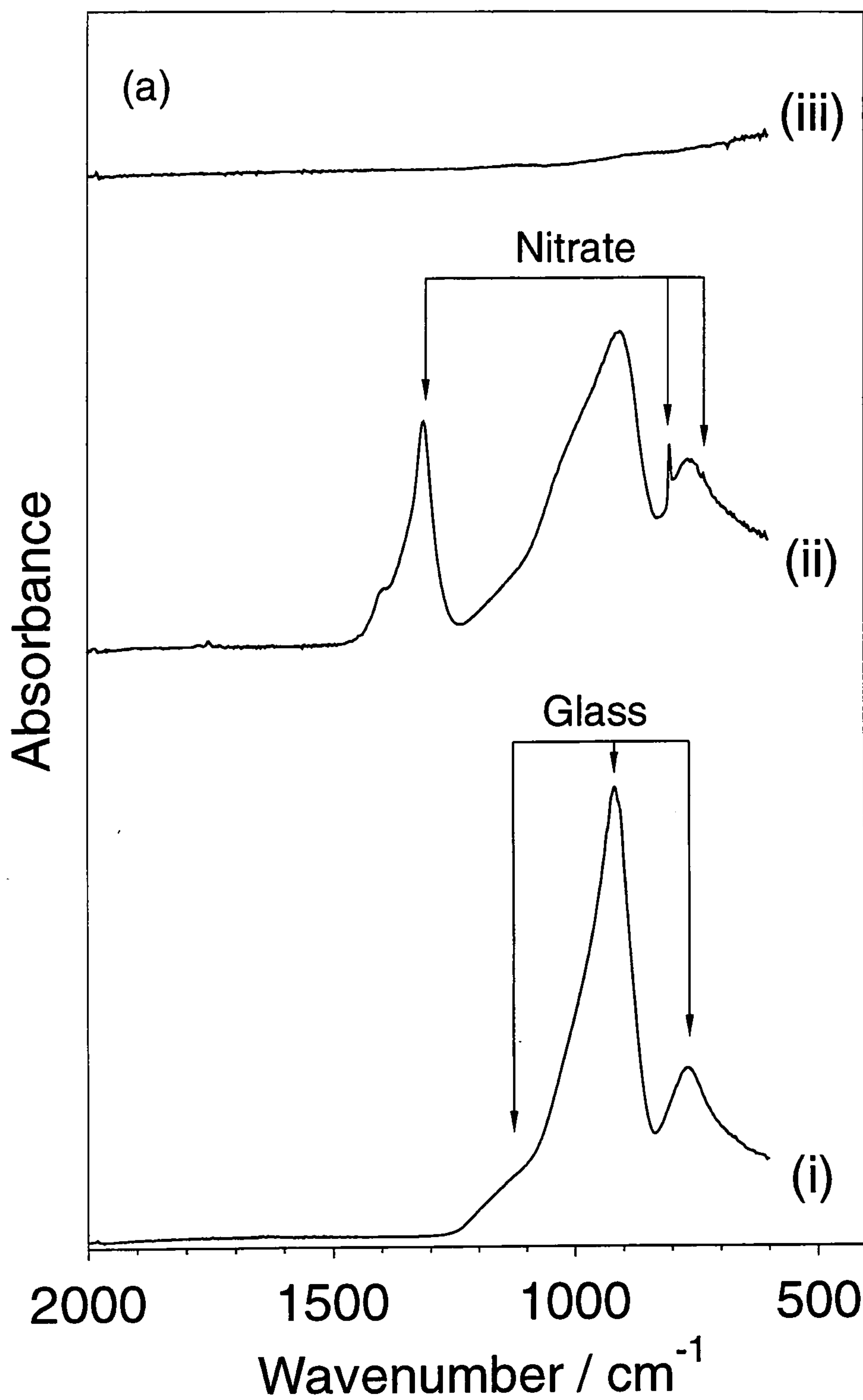

Figure 5.3(a). ATR-FTIR spectra of: (i) glass; (ii) glass spin coated with silver nitrate; and (iii) 30 mins hydrogen plasma treatment of silver nitrate spin coated onto glass.

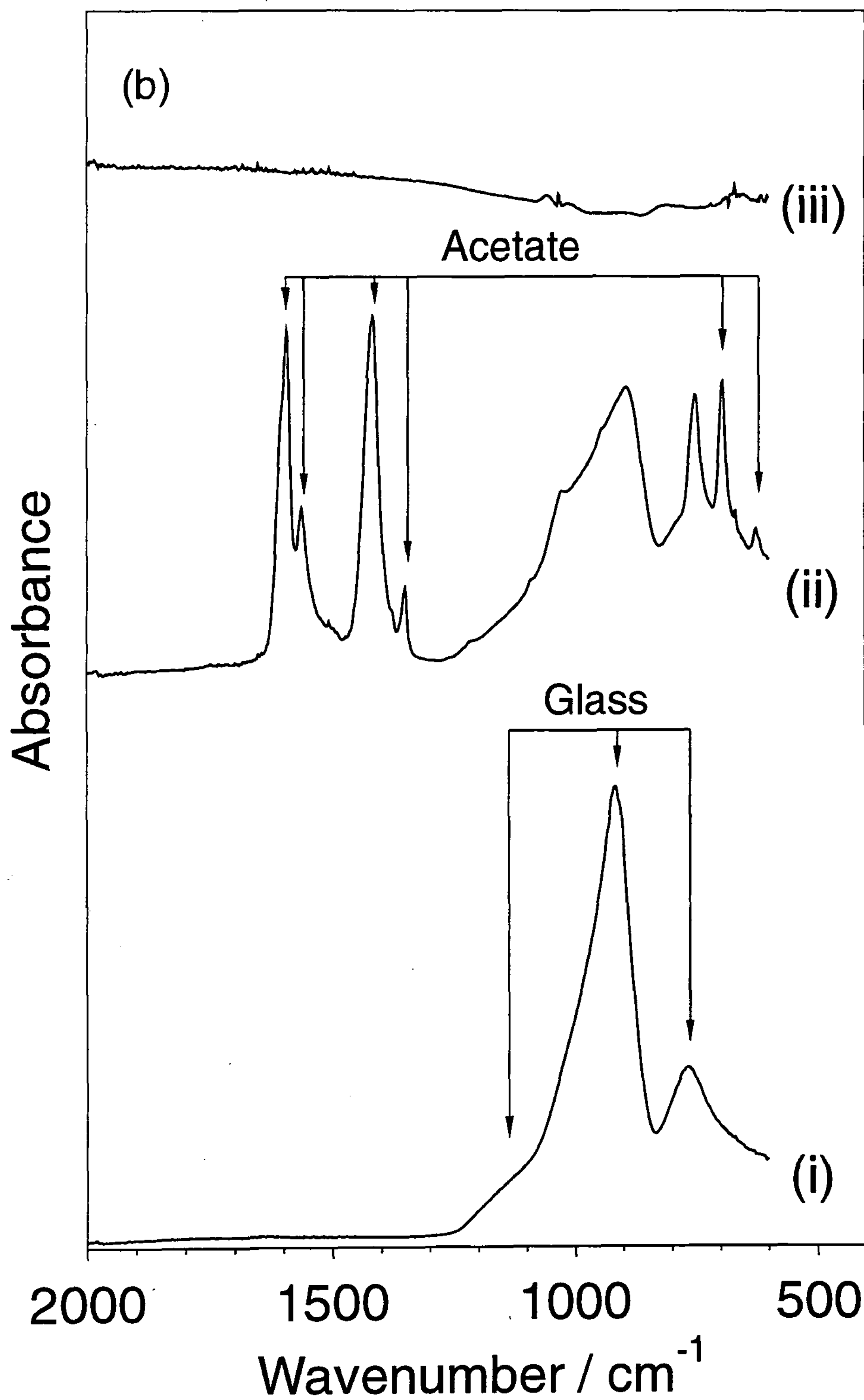

Figure 5.3(b). ATR-FTIR spectra of: (i) glass; (ii) glass spin coated with palladium acetate; and (iii) 30 mins hydrogen plasma treatment of palladium acetate spin coated onto glass.

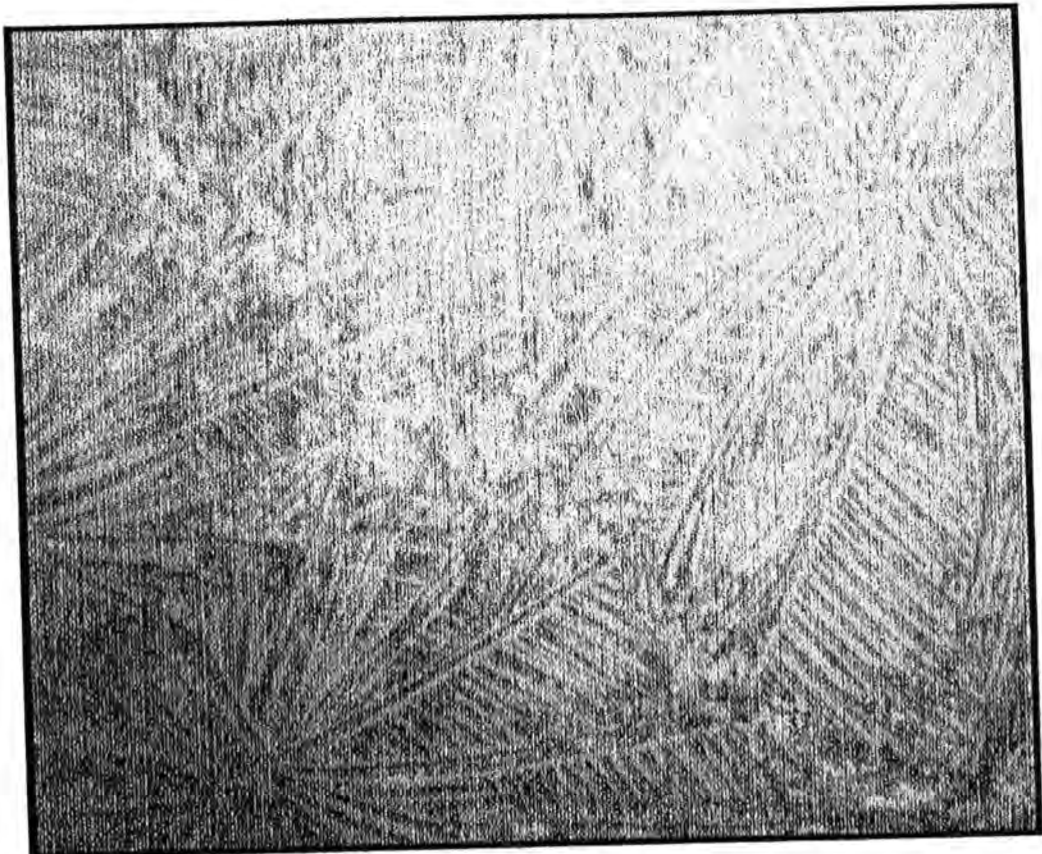

0.2 mm

Figure 5.4(a). x10 optical image of a spin coated layer of silver nitrate on glass.

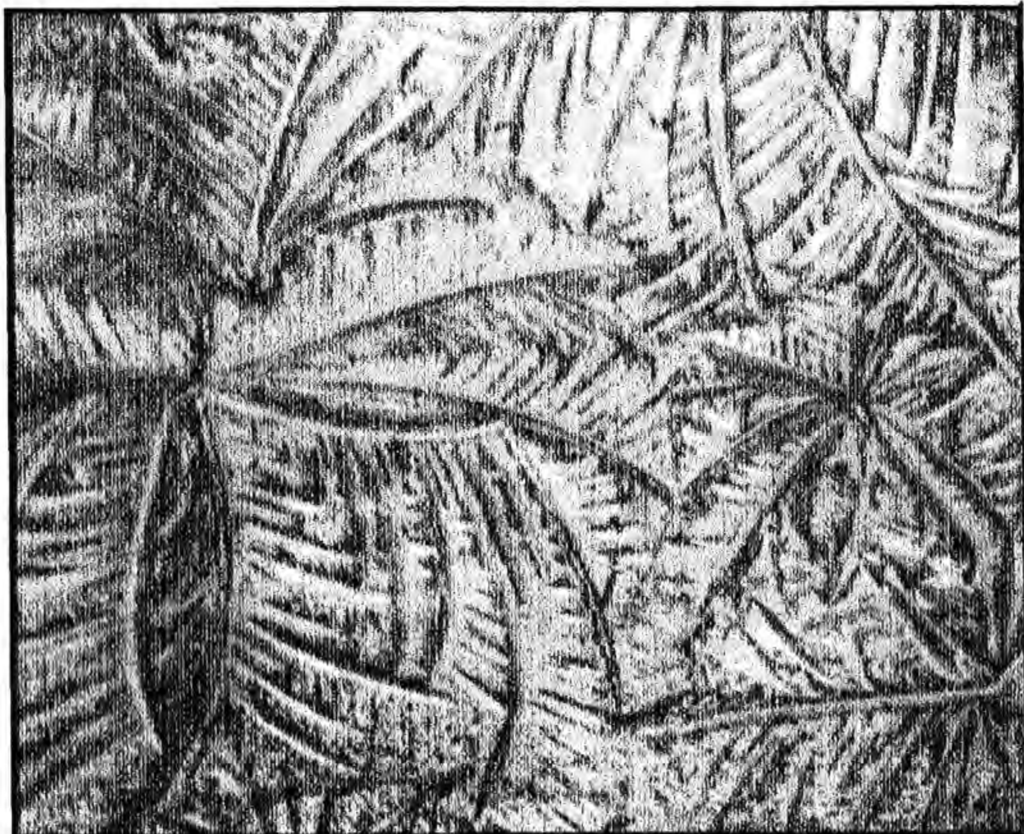

0.2 mm

Figure 5.4(b). x10 optical image of a spin coated layer of 30 mins hydrogen plasma treatment of silver nitrate on glass.

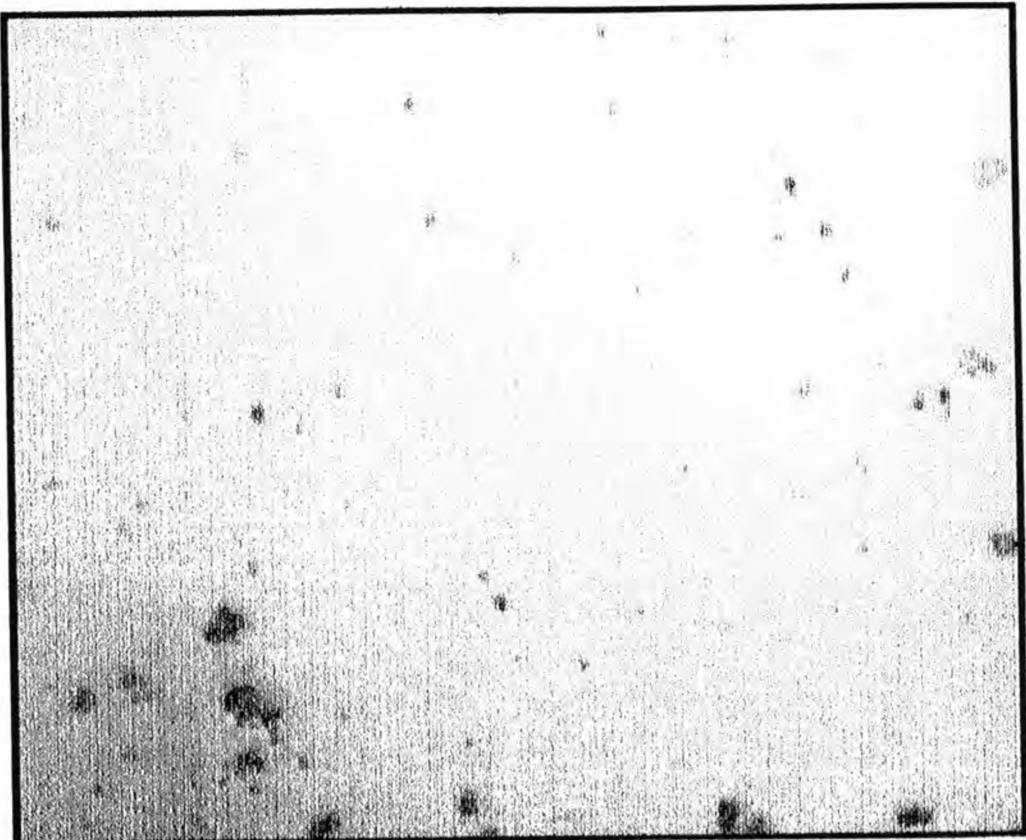

Figure 5.4(c). x10 optical image of a spin coated layer of palladium acetate on glass.

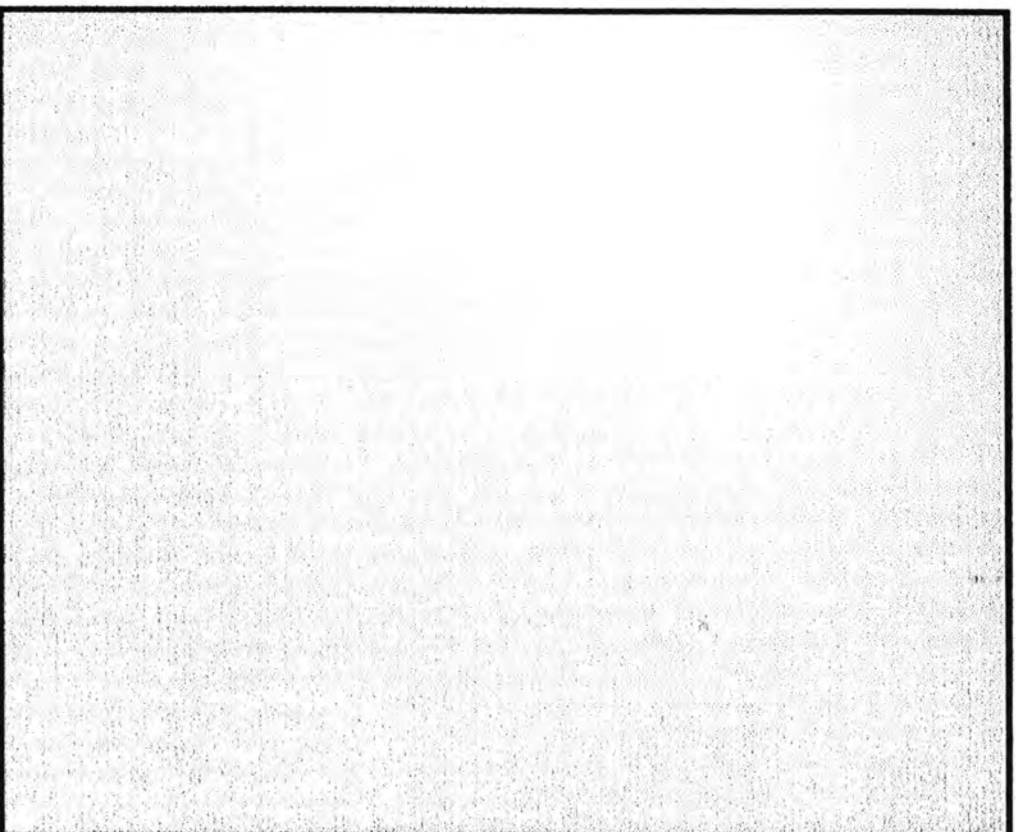

0.2 mm

Figure 5.4(d). x10 optical image of a spin coated layer of 30 mins hydrogen plasma treatment of palladium acetate on glass.

5.4 DISCUSSION

The highly efficient hydrogen plasma reduction of metal salts supported on glass can be attributed to the reaction between atomic hydrogen generated by the electrical discharge and the supported metal salt complexes[36, 37, 38, 39, 40] leading to the removal of O, N and C from the surface via the desorption of OH_x, NH_y and CH_z moieties,[36] to leave behind a metal layer (since neither silver or palladium form volatile hydride species). The incomplete removal of oxygen in the case of silver and carbon for palladium can be attributed to their respective solubilities in these metals.[41, 28]

5.5 CONCLUSIONS

This chapter has shown that glass supported silver and palladium salts can be reduced to the metallic state using a cold hydrogen plasma. The resultant metal films were not completely pure; the impurities they contain have been reported before to be soluble in those metals (i.e. oxygen in silver and carbon in palladium). The films are continuous as shown by XPS, and very thin. In the case of spin coated silver(I) nitrate on glass a complicated fern-like structure is produced, whereas spin coated palladium(II) acetate layers are featureless. The reduction process has little affect on the morphology of the metal salt as the complex structures seen for spin coated silver(I) nitrate remain after treatment. The ability of plasma reduction to retain complex strucures, as seen for the case of spin coated silver nitrate, has potential uses in the fabrication of catalytic systems where high surface areas are used to increase reaction rates.

5.6 REFERENCES

1 *Handbook of Deposition Technologies for Films and Coatings* (Ed. R. F. Bunshah) Noyes Publications, Park Ridge, New Jersey, 2nd Edition, **1994**, Chapter 1.

2 D. M. Brown, W. E. Engeler, M. Garfinkel, F. K. Heumann, *J. Electrochem. Soc.* **1967**, *114*, 730.

3 P. Mercea, L Muresan, V. Mecea, D. Silipas, I. Ursu, *J. Membrane. Sci.* **1988**, *35*, 291.

4 J. Mizsei, J. Harsanyi, *Sensors and Actuators* **1983**, *4*, 397.

5 J. Shu, B. P. A. Grandjean, A. Van Neste, S. Kaliaguine, *Can. J. Chem. Eng.* **1991**, *69*, 1036.

6 E. Feurer, H. Suhr, *Thin Solid Films* **1988**, *157*, 81.

7 J. E. Gozum, D. M. Pollina, J. A. Jensen, G. S. Girolami, *J. Am. Chem. Soc.* **1988**, *110*, 2688.

8 Z. Yuan, N. H. Dryden, J. J. Vittal, R. J. Puddephatt, *Chem. Mater.* **1995**, *7*, 1696.

9 Ch. J. Raub, *Platinum Metals Review* **1982**, *26*, 158.

10 H. Esrom, U. Kogelschatz, *Appl. Surf. Sci.* **1990**, *46*, 158.

11 M. E. Gross, W. L. Brown, L. R. Harriott, K. D. Cummings, J. Linros, H. Funsten, *J. Appl. Phys.* **1989**, *66*, 1403.

12 T. J. Stark, T. M. Mayer, D. P. Griffis, P. E. Russell, *J. Vac. Sci. Technol. B* **1991**, *9*, 3475.

13 V. Jayaraman, Y. S. Lin, M. Pakala, R. Y. Lin, *J. Membrane Sci.* **1995**, *99*, 89.

14 M. L. Chou, N. Manning, H. Chen, *Thin Solid Films* **1992**, *213*, 64.

15 S. E. Roark, K. L. Rowlen, *Anal. Chem.* **1994**, *66*, 261.

16 J. - D. Grunwaldt, F. Atamny, U. Göbel, A. Baiker, *Appl. Surf. Sci.* **1996**, *99*, 353.

17 C. - J. Huang, C. - C. Yen, T. - C. Chang, *J. Appl. Poly. Sci.* **1991**, *42*, 2237.

18 R. E. Southward, D. S. Thompson, D. W. Thompson, M. L. Caplan, A. K. St. Clair, *Chem. Mater.* **1995**, *7*, 2171.

19 R. E. Southward, D. W. Thompson, A. K. St. Clair, *Chem. Mater.* **1997**, *9*, 501.

20 C. - C. Yen, T. - C. Chang, H. Kakinoki, *J. Appl. Poly. Sci.* **1990**, *40*, 53.

21 M. P. Seah, M. T. Anthony *Surf. Inter. Anal.* **1984**, *6*, 230.

22 G. Beamson, D. Briggs in *High Resolution XPS of Organic Polymers The Scienta ESCA300 Database*, John Wiley and Sons, Chicester, England, **1992**, Chapter 6.

23 *Pratical Surface Analysis Volume 2 - Ion and Neutral Spectroscopy* (Eds. D. Briggs, M. P. Seah) John Wiley and Sons, Great Britain, 2nd Edition, **1992**, Appendix 4.

24 H. E. Swanson, N. T. Gilfrich, G. M. Ugrinic, *Natl. Bur. Stand. (U.S.) Circ.* **1955**, *539*, 59.

25 H. E. Swanson, E. Tatge, *Natl. Bur. Stand. (U.S.) Circ.* **1953**, *539*, 25.

26 M. E. Gross, W. L. Brown, L. R. Harriott, K. D. Cummings, J. Linnros, H .Funsten, *J. Appl. Phys.* **1989**, *66*, 1403.

27 H. E. Swanson, E. Tatge, *Natl. Bur. Stand. (U.S.) Circ.* **1953**, *539*, 21.

28 G. L. Selman, P. J. Ellison, A. S. Darling, *Platinum Metals Review* **1970**, *14*, 14.

29 J. E. Worsham, M. K. Wilkinson, C. G. Shull, *J. Phys. Chem. Solids* **1957**, *3*, 303.

30 J. F. Moulder, W. F. Stickle, P. E. Sobol, K. D. Bomben in *Handbook of X-ray Photoelectron Spectroscopy* (Ed. J. Chastain) Perkin Elmer Corporation, Minnesota, USA, **1992**, Chapter II.

31 M. J. Scaini, G. M. Bancroft, J. W. Lorimer, L. M. Maddox, *Geochimica et Cosmochimica Acta*, **1995**, *59*, 2733.

32 G. H. Sigel in *Treatise on Materials Science and Technology Volume 12* (Eds. M. Tomozawa, R. H. Doremus) Academic Press, London, Great Britain, **1977**, 67.

33 F. A. Miller, C. H. Wilkins, *Anal. Chem.* **1952**, *24*, 1253.

34 K Nakamoto in *Infrared and Raman Spectra of Inorganic and Coordination Compounds* John Wiley and Sons, USA, 3rd Edition, **1978**, Chapter III.

35 *Handbook of Physics and Chemistry* (Ed. R. C. Weast) CRC Press, 63rd Edition, Florida, USA, **1982**, Section F-133.

36 F. K. McTaggart in *Plasma Chemistry in Electrical Discharges*, Elsevier Publishing Company, Amsterdam, **1967**, Chapter 6.

37 H. Turcicova, H. Arend, O. Jarolimek, *Solid State Comm.* **1995**, *93*, 979.

38 F. K. McTaggart, *Austr. J. Chem.* **1965**, *18*, 937.

39 F. K. McTaggart, *Austr. J. Chem.* **1965**, *18*, 949.

40 F. K. McTaggart, A. G. Turnbull, *Austr. J. Chem.* **1964**, *17*, 727.

41 D. Wu, R. A. Outlaw, R. L. Ash, *J. Vac. Sci. Technol. A* **1996**, *14*, 408.

CHAPTER 6

COLD HYDROGEN PLASMA METALLIZATION OF SUPPORTED METAL BI-SALT LAYERS

CHAPTER 6

COLD HYDROGEN PLASMA METALLIZATION OF SUPPORTED METAL BI-SALT LAYERS

It has been shown in Chapter 5 that the reduction of silver and palladium salts to give metallic layers can be achieved using a non-isothermal hydrogen plasma. However, it is not only the production of films of single elements that is currently employed. There is also a need for thin films of alloys, for electrical contacts and catalytic membranes. The aim of this chapter is to show that reduction of a mixed metal salt film can be performed using a low temperature hydrogen glow discharge.

6.1 INTRODUCTION

The deposition of silver and palladium alloy coatings on to polymeric and inorganic substrates is of great interest in the production of gas separation membranes, due to their permselectivity towards hydrogen.[1] Palladium/silver alloys offer distinct advantages over pure palladium membranes in the areas of strength, gas permeability and resistance to deformation during operation. Ideally as thin an alloy layer as possible should be created to allow the greatest flux of gas through the membrane, however the layer must also be able to retain mechanical integrity, hence the use of membranes supported on a substrate. Methods currently employed for their fabrication include; chemical vapour deposition (CVD),[2, 3, 4] electroplating,[5] sputter deposition,[6] electroless plating,[7] physical vapour deposition,[8, 9] and spray pyrolysis.[10] All of these methods suffer from at least one of the following drawbacks: copious solvent use, high temperatures, or the need for ultra-high vacuum conditions.

An alternative approach is described in this chapter which is based on the non-isothermal hydrogen plasma reduction of supported metal precursors (e.g. co-deposited silver nitrate and palladium acetate). This metallization technique benefits from being capable of coating heat-sensitive substrates, without the need for large quantities of solvent or complicated chemical syntheses, and is capable of producing films down to 1 nm thickness. X-ray photoelectron spectroscopy (XPS), electrical resistance measurements, and optical microscopy have been used to follow the various stages of this low temperature metallization technique.

6.2 EXPERIMENTAL

3% wt/v solutions of silver nitrate (Alfa, 99.99% purity) and palladium acetate (Fluorochem, 99.9% purity) in acetonitrile (Sigma, HPLC grade) were prepared by dissolving 0.03 g of each metal salt in 1 ml of solvent. The solutions were then mixed in the correct proportions to produce a 1:1 number ratio of silver to palladium. Glass substrates were cleaned by rinsing in a 50/50 iso-propanol/cyclohexane solvent mixture for 30 s followed by drying in air. Subsequently, metal salt layers were deposited from solution using a Cammax Precima spin coater operating at a rotation speed of 1700 rpm. Note - the solutions used here are much more dilute than those used in the previous chapters resulting in a thinner metal layer on plasma reduction.

Hydrogen plasma reduction, XPS analysis, optical microscopy and electrical resistance measurements were carried out on the spin coated and plasma reduced glass supported bi-salt layers according to the specifications outlined in Chapter 5.

6.3 RESULTS

XPS analysis showed that spin coating of both salts gave rise to complete coverage of the glass substrate (as indicated by the absence of any Si(2p) signal at 103.4 eV binding energy in the XPS widescans[11]), Figure 6.1. Hydrogen glow discharge reduction resulted in a loss of carbon, nitrogen and oxygen from the spin coated films. The accompanying shift in Pd($3d_{5/2,3/2}$) binding energies towards lower values is consistent with a decrease in metal oxidation state,[11] Table 6.1. This shift was not as conclusive for

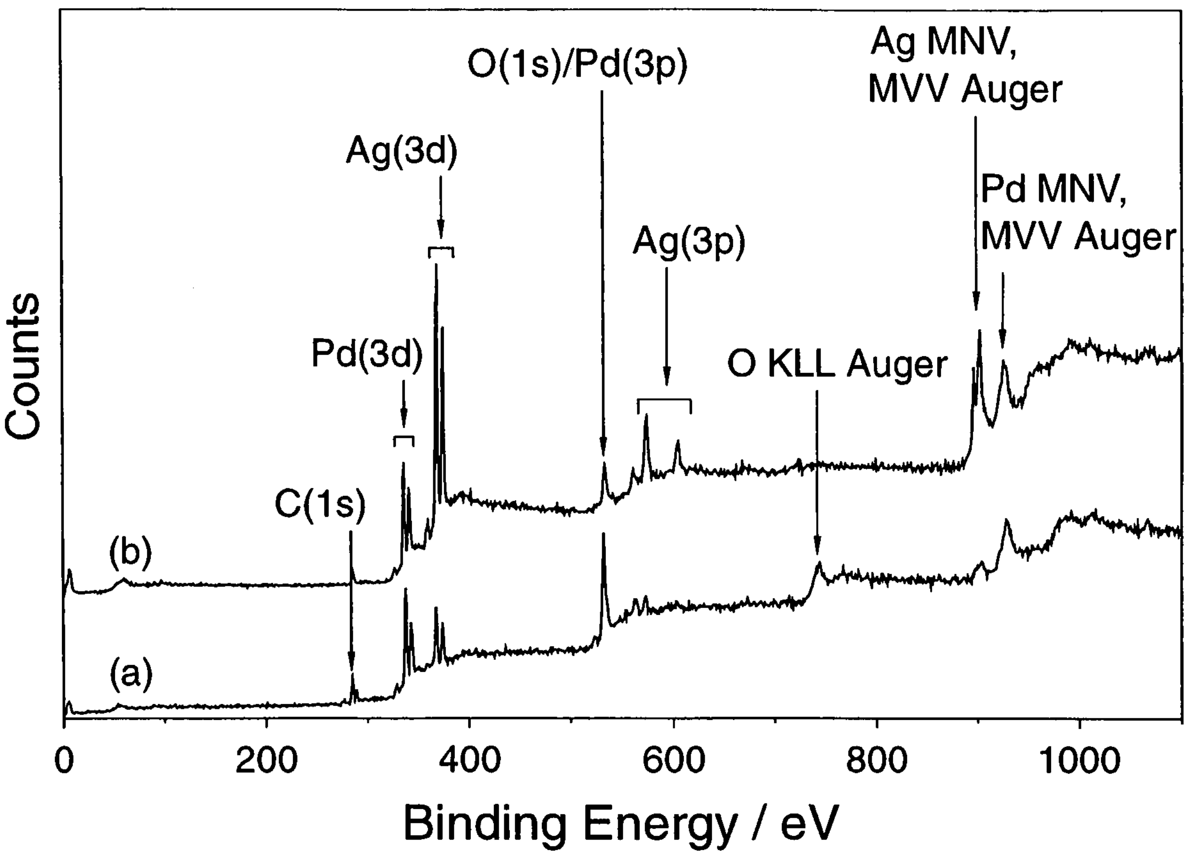

Figure 6.1. XPS widescans: (a) spin coated silver nitrate/palladium acetate on glass; and (b) 2 mins hydrogen plasma reduced silver nitrate/palladium acetate on glass.

the Ag($3d_{5/2,3/2}$) peaks, since silver(I) nitrate possesses a similar XPS binding energy to that of silver metal.[11] However, the small amount of other elements detected by XPS (i.e carbon, nitrogen and oxygen) confirms the formation of the metallic state.

Core level	**Binding Energy eV ± 0.2 eV**	
	Before reduction	**After reduction**
Ag($3d_{5/2}$)	368.7	368.3
Ag($3d_{3/2}$)	374.7	374.3
Pd($3d_{5/2}$)	338.6	335.7
Pd($3d_{3/2}$)	343.9	341.0

Table 6.1. Metal core level XPS binding energies before and after hydrogen plasma reduction.

Analysis of the surface composition after different plasma reduction times shows a distinct time dependency, Figure 6.2. For reductions of 30 s to 2 mins the surface only consists of silver, palladium, and carbon. For longer plasma treatments silicon and oxygen are also detected on the surface. This indicates the glass substrate showing through the metal layer.

Argon ion depth profiling of a 2 mins plasma reduced sample proved that carbon is present throughout the metallized silver/palladium layer (average layer composition 80% ± 1% Ag + Pd and 20% ± 1% C), Figure 6.3. The depth profile also indicates a localization of silver at the surface of the metallized film, with palladium lower down. However, the greater sputter rate for silver as compared to palladium would also tend to produce this type of behavior.[12] After only a few seconds of etching oxygen and silicon were visible on the surface. The carbon observed is associated with the silver/palladium part of the film. By assuming the relative sputter rate of the silver/palladium layer under the Ar^+ etch conditions used to be approximately 1 (c.f. sputter rates of silver and palladium 0.66 and 1.28 respectively)[12] typical thicknesses of the resultant metal films were measured by argon ion depth profiling to be 1 nm.

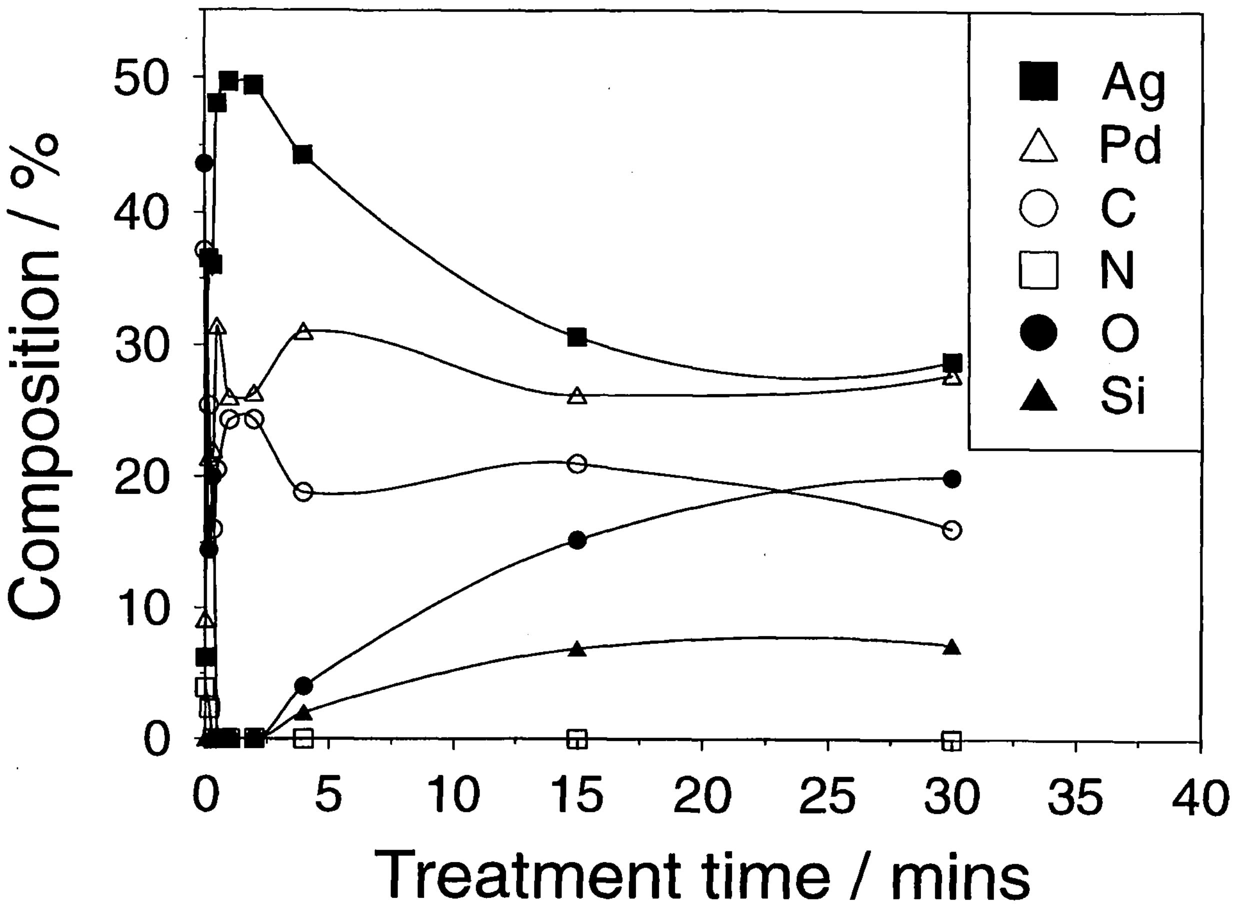

Figure 6.2. Variation in surface composition during hydrogen plasma treatment.

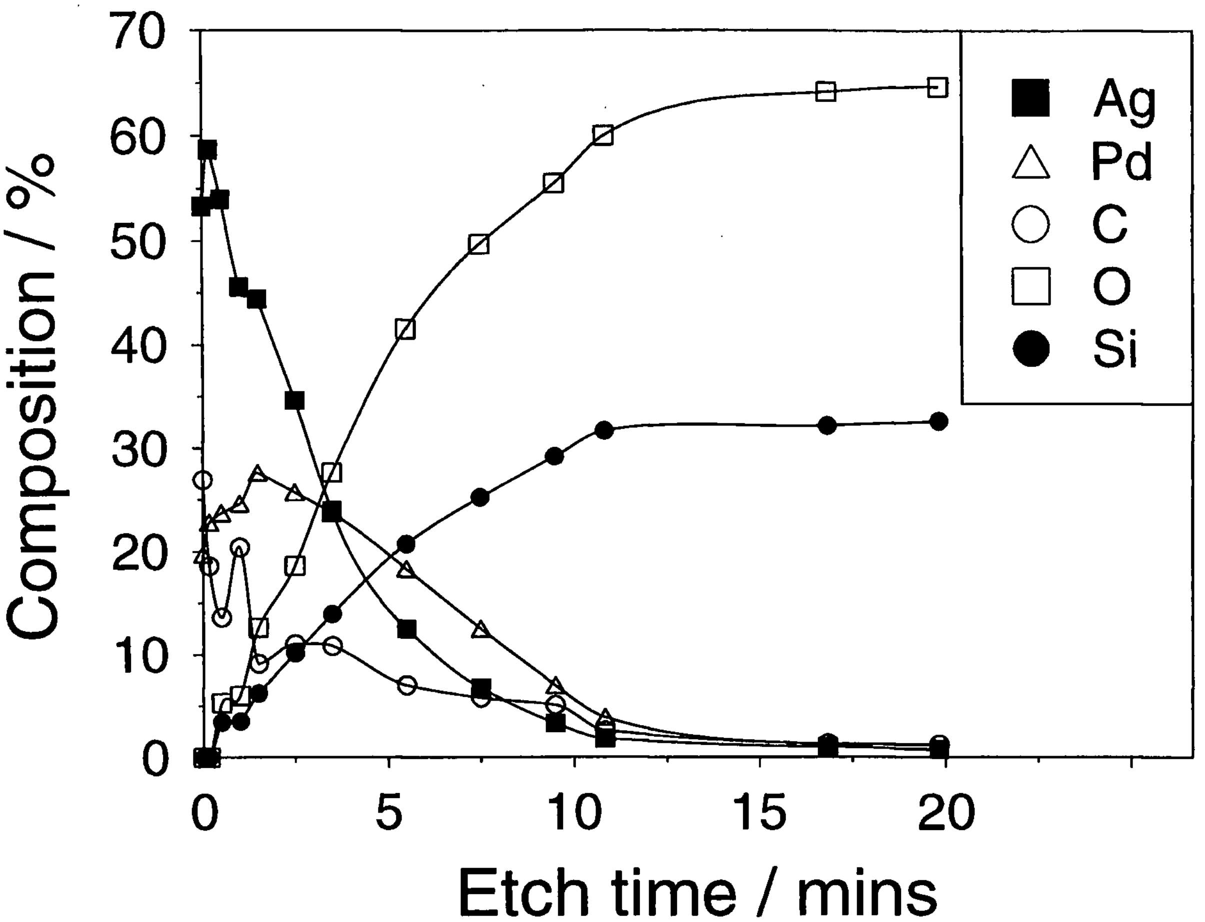

Figure 6.3. Argon ion depth profile of hydrogen plasma reduced silver/palladium layer.

Electrical resistance measurements of reduced silver/palladium films showed a marked dependence on treatment times, Figure 6.4. Electrical resistivity of the resultant silver/palladium film reduced for 2 mins was calculated to be 1.5×10^{-5} Ωcm. This value is of the correct order of magnitude, but slightly higher than those typically reported for the bulk metals (1.6×10^{-6} Ωcm and 1.1×10^{-5} Ωcm for silver and palladium).[13] The higher resistivity value may be attributed to the presence of impurities, causing lattice distortion and defect sites, and also the extreme thinness of the metal films.

Comparison of the optical images for the spin coated and reduced samples showed that hydrogen glow discharge treatment does not result in a perturbation in the physical appearance of the surface for short reduction times, Figure 6.5. The spin coated silver(I) nitrate/palladium(II) acetate layers were featureless prior to and following short, i.e. less than 4 mins hydrogen plasma treatments. After plasma reduction for 4 mins or longer the evolution of cracks can be seen on the surface. These observations confirm that the electrical discharge process can cause significant heating (sintering) for long treatment times of such thin films.

6.4 DISCUSSION

The highly efficient hydrogen plasma reduction of metal salts supported on glass can be attributed to the reaction between atomic hydrogen generated by the electrical discharge and the supported metal salt complexes[14, 15, 16, 17, 18] leading to the removal of O, N and C from the surface via the desorption of OH_x, NH_y and CH_z moieties,[14] to leave behind a metal layer (since neither silver or palladium form volatile hydride species). The surface segregation in palladium/silver alloys has been reported before;[19, 20] the lower surface energy component, in this case silver, migrates to the surface at elevated temperatures. Consequently the enrichment of silver seen here by XPS may only be due to the extremely thin nature of these films. It seems therefore that this method of production does not result in the formation of alloys, at least not in this case. Complete surface coverage is also dependent on the length of plasma reduction; XPS showed that long treatment times results in an increase in the amount of silicon and oxygen at the surface, and the presence of cracks in the metal film is confirmed by the optical microscopy images.

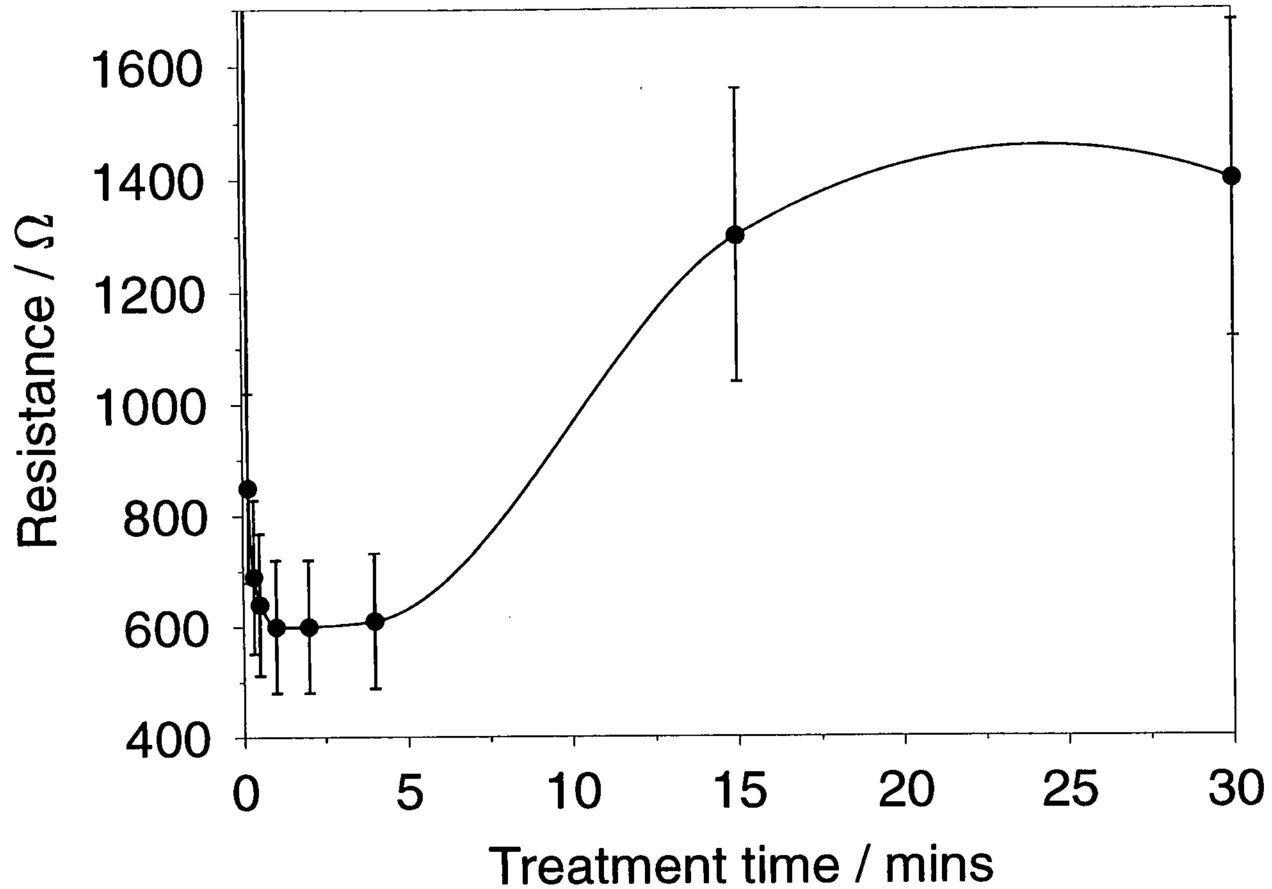

Figure 6.4. Electrical resistance of silver/palladium films after hydrogen plasma reduction.

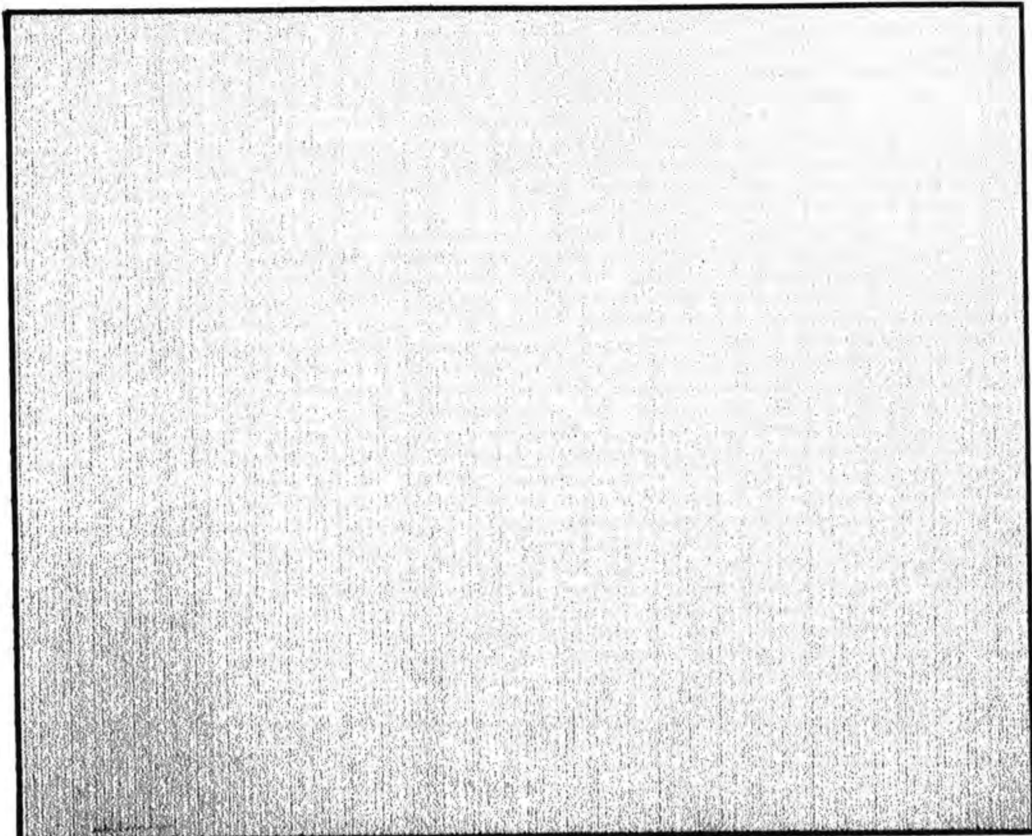

Figure 6.5(a). 10x optical image of a spin coated layer of silver nitrate/palladium acetate on glass

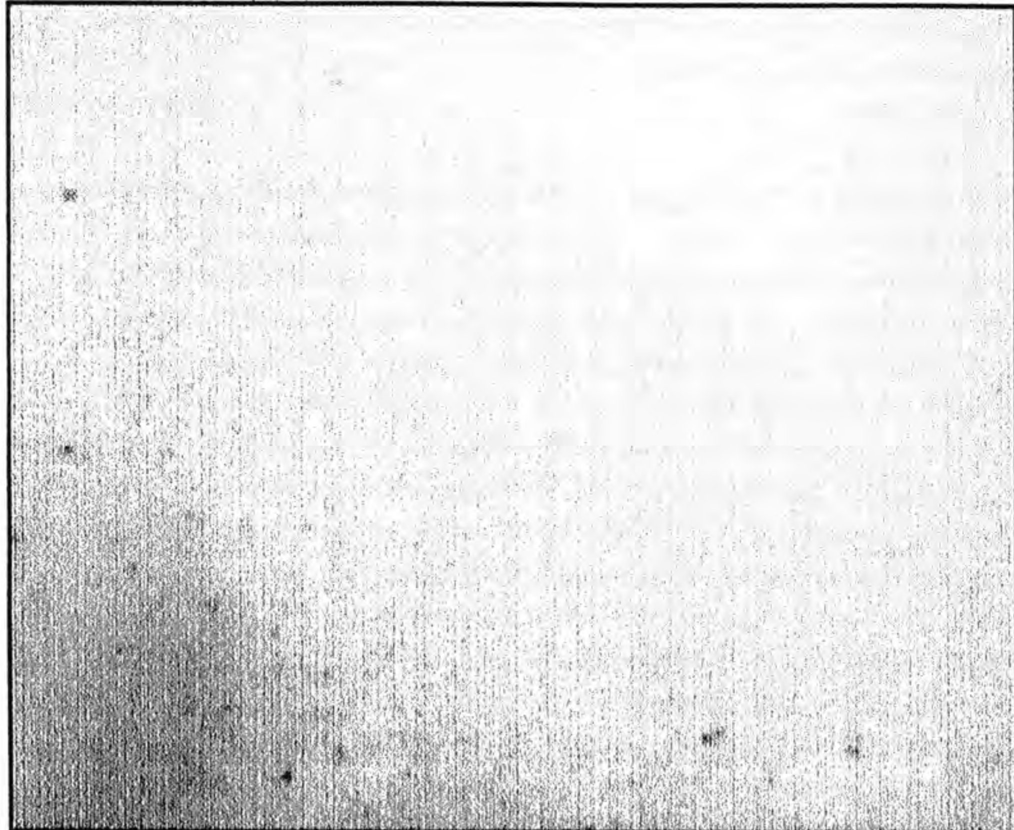

Figure 6.5(b). 10x optical image of a 2 mins hydrogen plasma treated spin coated layer of silver nitrate/palladium acetate on glass.

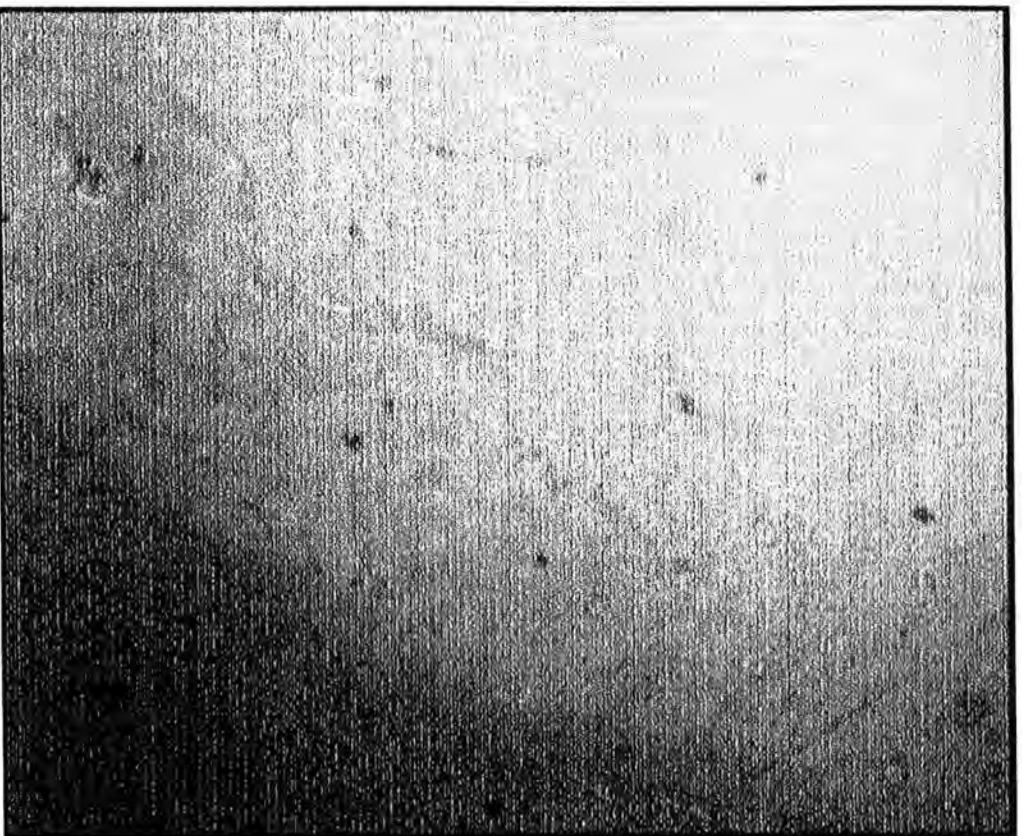

Figure 6.5(c). 10x optical image of a 30 mins hydrogen plasma treated spin coated layer of silver nitrate/palladium acetate on glass.

6.5 CONCLUSIONS

This chapter has shown that it is possible to reduce two metal salts on a surface simultaneously using a low temperature hydrogen plasma. Electrical resistance measurements have shown that reduction to the metallic state occurs very quickly, and that prolonged plasma treatment leads to an increase in resistance. This increase is due to cracking of the film, i.e. sintering has occurred. Due to the extremely thin resultant metal films it was not possible to perform XRD on them to prove alloy formation. The use of higher concentrations of precursor solution should allow the production of thicker film. However, this would require different metal precursors and/or solvents as the maximum solubility of palladium(II) acetate in acetonitrile was found to be only 3% wt/v.

XPS has shown that there is an enrichment of silver at the surface after plasma treatment, which would suggest that alloy formation has not taken place. However the silver enrichment at the surface seen here by XPS may only be due to the extremely thin nature of these films. Therefore it may still be possible to use this metallization technique for the production of thicker alloy films.

6.6 REFERENCES

1 J. Shu, B. P. A. Grandjean, A. Van Neste, S. Kaliaguine, *Can. J. Chem. Eng.* **1991**, *69*, 1036.

2 E. Feurer, H. Suhr, *Thin Solid Films* **1988**, *157*, 81.

3 J. E. Gozum, D. M. Pollina, J. A. Jensen, G. S. Girolami, *J. Am. Chem. Soc.* **1988**, *110*, 2688.

4 Z. Yuan, N. H. Dryden, J. J. Vittal, R. J. Puddephatt, *Chem. Mater.* **1995**, *7*, 1696.

5 Ch. J. Raub, *Platinum Metals Review* **1982**, *26*, 158.

6 V. Jayaraman, Y. S. Lin, M. Pakala, R. Y. Lin, *J. Membrane Sci.* **1995**, *99*, 89.

7 M. L. Chou, N. Manning, H. Chen, *Thin Solid Films* **1992**, *213*, 64.

8 S. E. Roark, K. L. Rowlen, *Anal. Chem.* **1994**, *66*, 261.

9 J. - D. Grunwaldt, F. Atamny, U. Göbel, A. Baiker, *Appl. Surf. Sci.* **1996**, *99*, 353.

10 Z. Y. Li, H. Maeda, K. Kusakabe, S. Morooka, H. Anzai, S. Akiyama, *J. Membrane Sci.* **1993**, *78*, 247.

11 J. F. Moulder, W. F. Stickle, P. E. Sobol, K. D. Bomben in *Handbook of X-ray Photoelectron Spectroscopy* (Ed. J. Chastain) Perkin Elmer Corporation, Minnesota, USA, **1992**, Chapter II.

12 *Pratical Surface Analysis Volume 2 - Ion and Neutral Spectroscopy* (Eds. D. Briggs, M. P. Seah) John Wiley and Sons, Great Britain, 2nd Edition, **1992**, Appendix 4.

13 *Handbook of Physics and Chemistry* (Ed. R. C. Weast) CRC Press, 63rd Edition, Florida, USA, **1982**, Section F-133.

14 F. K. McTaggart in *Plasma Chemistry in Electrical Discharges*, Elsevier Publishing Company, Amsterdam, **1967**, Chapter 6.

15 H. Turcicova, H. Arend, O. Jarolimek, *Solid State Comm.* **1995**, *93*, 979.

16 F. K. McTaggart, *Austr. J. Chem.* **1965**, *18*, 937.

17 F. K. McTaggart, *Austr. J. Chem.* **1965**, *18*, 949.

18 F. K. McTaggart, A. G. Turnbull, *Austr. J. Chem.* **1964**, *17*, 727.

19 R. Anton, H. Eggers, J. Veletas, *Thin Solid Films* **1993**, *226*, 39.

20 S. Ouannasser, J. Eugène, H. Dreyssé, C. Wolverton, D. de Fontaine, *Surf. Sci.* **1994**, *307*, 826.

CHAPTER 7

CONCLUSIONS

CHAPTER 7

CONCLUSIONS

7.1 CONCLUSIONS

This thesis has been primarily concerned with exploring the possibilities of using non-isothermal plasmas for the reduction of metal salts deposited on a substrate. It has been shown that this technique is viable for the production of thin films of various metals on different types of substrate.

Current methods for thin metal film formation all have drawbacks; the need for UHV conditions, copious solvent use, incapability of coating complex shaped objects, the use of high temperatures, or the need for complicated or expensive metallic precursor species. The technique described in this thesis for the production of metal films using a low temperature glow discharge does not need UHV conditions, high temperatures, expensive metal salts, or large amounts of solvent, and due to the nature of the plasma is capable of treating complex shaped objects.

Freshly prepared metal surfaces (other than gold) are susceptible to rapid oxidation on contact with the atmosphere. In order to analyse the surface composition of reduced metal films without exposure to air it was necessary to design and build a plasma chamber attached directly to a UHV chamber. This allowed XPS to be performed on the sample without it being exposed to the atmosphere.

The creation of a precursor film for the production of a gold layer presented its own difficulties; it was necessary to produce a gold(III) chloride layer that was stable in air. This was achieved by spin coating from a gold(III) chloride solution in acetonitirile on to a Nylon 66 substrate. This resulted in stable layers containing a mixture of the gold salt

and Nylon 66 chains. Plasma reduction of this supported film, using hydrogen, helium or argon as the feed gas, resulted in the formation of a thin gold film with greater than 95 % purity. The use of different feed gases for the production of gold films from the supported gold complex indicates that it is not only chemically active plasmas, i.e. hydrogen, that are responsible for the reduction process, but that reduction also occurs by the action of VUV and metastable species.

The production of silver and palladium films on glass from their corresponding salts has shown that this reduction phenomenon is not just peculiar to gold(III) chloride, or to metal salts deposited on polymers, and that this technique can be used to retain complex crystalline structures formed during the spin coating process. Also the production of a bi-salt layer consisting of silver and palladium has shown that it may be possible to use this technique for the deposition of alloy films.

This thesis has also been concerned with studying the effect of soft X-rays on supported gold(III) chloride layers. It has been shown that it is possible to use X-ray treatment for the production of gold rich films, whose electrical properties change over a period of time, although elucidation of the exact mechanism for the reduction process has not been achieved. This discovery could have impact in the areas of manufacture of IC's and for the production of intelligent packaging systems.

In summary this thesis has shown that non-isothermal plasma reduction of supported metal precursors is a viable method for the production of thin metal films on a wide variety of substrates. Also X-ray reduction of supported gold(III) chloride can be used for the creation of gold rich layers.

7.2 FUTURE WORK

The work presented here is just a small fraction of the potential of this area. This section outlines some of the future work that could be done to build upon this thesis.

7.2.1 Optimisation of Noble Gas Plasma Treatment Conditions

Noble gas plasma reduction of supported gold(III) chloride results in a layer of gold which has a higher purity than that seen for hydrogen plasma reduction. No attempt has

been made to optimise the powers used for this, or the time required for reduction of the gold salt.

7.2.2 X-ray Degradation of Other Metal Salts

The use of soft X-rays in the production of films of other metals should be addressed. Work carried out during the course of this thesis (although not reported herein) indicated that platinum(IV) chloride was also reduced by X-rays. This may mean that platinum rich films can be produced by the same method as for the X-ray reduction of supported gold(III) chloride.

7.2.3 Deposition of Plasma Polymer Layers to Enable Metallization of PTFE

The deposition of a plasma polymer interface layer on to low surface energy materials such as PTFE, would allow the coating of these materials with metal salt solutions. Subsequent reduction would provide a route to metallizing these materials.

APPENDIX

COLLOQUIA, SEMINARS, PRESENTATIONS AND LECTURE COURSES.

UNIVERSITY OF DURHAM

BOARD OF STUDIES IN CHEMISTRY

COLLOQUIA AND SEMINARS FROM INVITED SPEAKERS

1994

October 19	Prof. N. Bartlet, University of California
	Some Aspects of Ag(III) and Ag(III) Chemistry
October 26	Dr. G. Rumble, Imperial College
	Real or Imaginary 3rd Order Non-Linear Optical Materials
December 7	Prof. D. Briggs, ICI and University of Durham
	Surface Mass Spectrometry

1995

March 1	Dr. M. Rosseinsky, Oxford University
	Fullerene Intercalation Chemistry
April 26	Dr. M. Schroder, University of Edinburgh
	Redox Active Macrocyclic Complexes
May 3	Prof. E. W. Randall, Queen Mary & Westfield College
	New Perspectives in NMR Imaging
October 4	Prof. D. Tuck, University of Windsor, Ontario
	Electron Transfer Processes in Main Group Chemistry
October 11	Prof. P. Lugar, University of Berlin
	Low Temperature Crystallography

November 17	Prof. D. Bergbreiter, Texas A&M
	Design of Smart Catalysts, Substrates and Surfaces
November 22	Prof. I. Soutar, Lancaster University
	A Water of Glass? Luminescence Studies of Water Soluble Polymers
December 8	Prof. M. Reetz, Mullheim
	Size Selective Synthesis of Metal Clusters

1996

January 10	Dr. B. Henderson, Waikato University
	Electrospray Mass Spectrometry - A New Technique
January 17	Prof. J. W. Emsley, Southampton University
	Liquid Crystals: More than Meets the Eye
January 31	Dr. G. Penfold
	Soft Soap and Surfaces
February 14	Prof. R. Nolte
	Design Strategies for Supramolecular Architectures
March 6	Dr. R. Whitby, University of Southampton
	New Approaches to Chiral Catalysts
March 12	Prof. V. Balzani, University of Bologna
	Supramolecular Photochemistry

October 22	Prof. B. J. Tighe, Aston University
	Polymers for Biomedical Application
October 23	Prof. H. Ringsdorf, Johannes Gutenberg-Universitat
	Function Based on Organisation
November 6	Dr. K. Reid, Nottingham University
	Probing Dynamic Processes with Photoelectrons
November 18	Prof. G. Olah
	Crossing Conventional Lines in my Chemistry of the Elements
November 20	Prof. J. Earnshaw, Belfast University
	Surface Light Scattering: Ripples and Relaxation
December 4	Prof. K. Muller-Dethlefs, York University
	Very High Resolution ZEKE Spectroscopy

1997

February 6	Prof. P. Bartlet, Southampton University
	Integrated Chemical Systems
February 19	Brian E. Hayden
	Dynamics of Dissociation at Surfaces
March 3	Dr. M. Owen and Dr. D. Gravier, Dow Corning
	Siloxanes at Surfaces
March 6	Prof. K. Toth
	Advances in Scanning Electrochemical Microscopy

EXAMINED LECTURE COURSES

Oct. 1994 - Jan. 1995	General Laboratory Techniques (Dr. D. P. Hampshire)
	Electron Microscopy (Dr. K. Durose)
	Spectroscopy (Dr. D. P. Halliday)
Jan. - Mar. 1995	Synthetic Methodology in Organometallic and Co-ordination Chemistry (Prof. V. C. Gibson, Prof. D. Parker)